



LUND UNIVERSITY

Helical tomotherapy for total marrow and total skin irradiation

Optimisation, verification, and clinical results

Änghede Haraldsson, André

2021

Document Version:

Publisher's PDF, also known as Version of record

[Link to publication](#)

Citation for published version (APA):

Änghede Haraldsson, A. (2021). *Helical tomotherapy for total marrow and total skin irradiation: Optimisation, verification, and clinical results*. (1 ed.). Lund University.

Total number of authors:

1

Creative Commons License:

CC BY-NC-ND

General rights

Unless other specific re-use rights are stated the following general rights apply:

Copyright and moral rights for the publications made accessible in the public portal are retained by the authors and/or other copyright owners and it is a condition of accessing publications that users recognise and abide by the legal requirements associated with these rights.

- Users may download and print one copy of any publication from the public portal for the purpose of private study or research.
- You may not further distribute the material or use it for any profit-making activity or commercial gain
- You may freely distribute the URL identifying the publication in the public portal

Read more about Creative commons licenses: <https://creativecommons.org/licenses/>

Take down policy

If you believe that this document breaches copyright please contact us providing details, and we will remove access to the work immediately and investigate your claim.

LUND UNIVERSITY

PO Box 117
221 00 Lund
+46 46-222 00 00

Helical tomotherapy for total marrow and total skin irradiation

Optimisation, verification, and clinical results

ANDRÉ HARALDSSON

MEDICAL RADIATION PHYSICS | FACULTY OF SCIENCE | LUND UNIVERSITY



Helical tomotherapy for total marrow and total skin irradiation

Optimisation, verification, and clinical results

by André Haraldsson



LUND
UNIVERSITY

Doctoral dissertation

Thesis advisors: PhD. Per E Engström, Assoc. Prof. Sven Bäck,
MD Assoc. Prof. Jacob Engellau, Assoc. Prof. Sofie Ceberg,
MD. PhD. Silke Engelholm, Prof. Crister Ceberg
Faculty opponent: Assoc. Prof. Albert Siegbahn

To be presented, with the permission of the Faculty of Science of Lund University, for public criticism in the lecture hall Alwallsalen in Alwallhuset, Barngatan 2, at Skåne University Hospital in Lund, on Friday, the 15th of October 2021 at 09:00.

Organization LUND UNIVERSITY Medical Radiation Physics, Clinical Sciences Box 117 SE-221 00 LUND Sweden		Document name DOCTORAL DISSERTATION	
		Date of disputation 2021-10-15	
		Sponsoring organization	
Author(s) André Haraldsson			
Title and subtitle Helical tomotherapy for total marrow and total skin irradiation: Optimisation, verification, and clinical results			
Abstract <p>In modern cancer therapy, radiotherapy (RT) is a vital part of most treatments. Most RT treatments in Sweden are performed using intensity-modulated radiotherapy (IMRT) with fixed or dynamic arc delivery. The dose gradients outside the target are steep, the margins are small, and the treatment delivery is complicated. Complicated treatments increase the requirement for control of the uncertainties in planning and delivery. This requires robust treatments and mitigation of the various uncertainties. In addition, robust planning and rigorous quality assurance (QA) of the patient treatments that takes account of all types of uncertainties are essential.</p> <p>A TomoTherapy device (Accuray Inc., Madison, WI, USA) is an RT device with a linear accelerator mounted on a slip-ring construction, giving it the ability to irradiate while continuously rotating around the patient, very similar to a CT scanner but with megavoltage instead of X-ray energy generation. Since helical tomotherapy can entail long and complicated irradiations, new treatment types targeting RT to large parts of the body have emerged. These new techniques are challenging regarding the optimization and verification of the planning and treatment process.</p> <p>Recurring blood cancers (leukaemias) can be treated with RT and chemotherapy before stem cell transplantation. Traditionally, the patient is irradiated with whole-body irradiation using a conventional linac at a large distance. The treatment can be performed with helical tomotherapy to avoid organs at risks to a greater extent. Another emerging treatment with helical tomotherapy is irradiation of whole-body neoplastic skin lesions, such as mycosis fungoides. These patients were traditionally treated with electron irradiation in different positions, subsequently complemented with x-ray fields in 'hard-to-reach' sites. Delivering this treatment with photons is complex but opens the possibility for integrated boost treatments of lesions and simultaneously avoiding OAR and previously treated areas.</p> <p>The clinical follow-up illustrated the potential and usefulness of helical tomotherapy targeting the bone marrow, with more patients surviving without severe complications after one year, than with the previous technique. Further, we showed the possibility to implement irradiation of the entire skin with helical tomotherapy. Overall, we demonstrated the usefulness of helical tomotherapy, and solutions to overcome challenges in implementing large-target techniques.</p>			
Key words TSI, TMI, tomotherapy, radixact, surface, scanning, SGRT, ALL			
Classification system and/or index terms (if any)			
Supplementary bibliographical information		Language English	
ISSN and key title		ISBN 978-91-7895-979-2 (print) 978-91-7895-980-8 (pdf)	
Recipient's notes		Number of pages 153	Price
		Security classification	

I, the undersigned, being the copyright owner of the abstract of the above-mentioned dissertation, hereby grant to all reference sources the permission to publish and disseminate the abstract of the above-mentioned dissertation.

Signature



Date 2021-09-02

Helical tomotherapy for total marrow and total skin irradiation

Optimisation, verification, and clinical results

by André Haraldsson



LUND
UNIVERSITY

A doctoral thesis at a university in Sweden takes either the form of a single, cohesive research study (monograph) or a summary of research papers (compilation thesis), which the doctoral student has written alone or together with one or several other author(s).

In the latter case the thesis consists of two parts. An introductory text puts the research work into context and summarizes the main points of the papers. Then, the research publications themselves are reproduced, together with a description of the individual contributions of the authors. The research papers may either have been already published or are manuscripts at various stages (in press, submitted, or in draft).

Cover illustration front: TomoTherapy HD No. 414 at Skåne University Hospital in Lund

Cover illustration back: Schematic illustration of surface scanning with helical tomotherapy. Illustration by Per E. Engström.

Funding information: During this study, my department received funding from Accuray Inc.

© André Haraldsson 2021

Faculty of Science, Medical Radiation Physics, Clinical Sciences

ISBN: 978-91-7895-979-2 (print)

ISBN: 978-91-7895-980-8 (pdf)

Printed in Sweden by Media-Tryck, Lund University, Lund 2021



Dedicated to my family
Sara – Viggo – Noel

Contents

Summary	ii
List of publications	iii
Acknowledgements	v
Populärvetenskaplig sammanfattning på svenska	vi
Abbreviations	vii
Coordinate systems	ix
Helical tomotherapy for total marrow and total skin irradiation: Optimisation, verification, and clinical results	I
1 Introduction	I
2 Background and Theory	4
3 Optimisation of treatment plans for large targets in helical tomotherapy	28
4 Verification of complicated treatments	36
5 Clinical aspects	45
6 General discussion	55
7 References	58
Publications	73
Paper I: Implementing safe and robust Total Marrow Irradiation using Helical Tomotherapy - A practical guide.	75
Paper II: Helical tomotherapy as a robust low-dose treatment alternative for total skin irradiation	83
Paper III: Surface-guided tomotherapy improves positioning and reduces treatment time: A retrospective analysis of 16 835 treatment fractions	97
Paper IV: Organ sparing total marrow irradiation compared to total body irradiation prior to allogeneic stem cell transplantation	109
Appendix: Conference proceedings	129

List of Figures

1	Scematic view of coordinate systems	ix
2	Dose optimisation examples with treatment planning software	5
3	Schematic image of the TomoTherapy gantry	6
4	Image of a Multi Leave Collimator bank	8
5	Leaf open time histogram with binned opening times	9
6	Latency difference between gantry speed and machine type	10
7	MLC sinogram for helical tomotherapy	11
8	Dose ripple in helical tomotherapy	12
9	Comparison of dose ripple	13
10	Surface guided radiotherapy example	20
11	Immune system and RT in transplantation	27
12	Virtual bolus comparison	31
13	Directional blocking in helical tomotherapy	33
14	Mean doses to organs and target for phantom and patients in TSI	34
15	Doses to organs and targets for first patients treated with TMI	35
16	Junction dose in TMI	36
17	Film dosimetry in TSI	37
18	Daily image of TSI patient	40
19	Delivered DVH for CTV for TSI patient	41
20	Delivered DVH for TMI patient	41
21	Effect of optimal pitch	43
22	Correction vector length distribution for laser-based and SGRT-based setups	44
23	Thrombocyte count for TSI patient 1	48
24	Modelling platelet reconstitution after hematopoietic stem cell transplantation	51
25	Comparison of time to engraftment	52

List of publications

This thesis is based on the following publications, referred to by their Roman numerals:

- I **Implementing safe and robust Total Marrow Irradiation using Helical Tomotherapy - A practical guide.**
Haraldsson A, Engellau J, Lenhoff S, Engelholm S, Bäck S, Engström PE.
Phys Med. 2019;60:162-7
- II **Helical tomotherapy as a robust low-dose treatment alternative for total skin irradiation**
Haraldsson A, Engleson J, Bäck S, Engelholm S, Engström PE.
J Appl Clin Med Phys. 2019;20:44-54.
- III **Surface-guided tomotherapy improves positioning and reduces treatment time: A retrospective analysis of 16 835 treatment fractions**
Haraldsson A, Ceberg S, Ceberg C, Bäck S, Engelholm S, Engström PE.
J Appl Clin Med Phys. 2020;21:139-48.
- IV **Organ sparing total marrow irradiation compared to total body irradiation prior to allogeneic stem cell transplantation**
Haraldsson A, Wichert S, Engström PE, Lenhoff S, Turkiewicz D, Warsi S, Engelholm S, Bäck S, Engellau J.
Eur J Haematol. 2021; 00:1-15. <https://doi.org/10.1111/ejh.13675>. Online ahead of print.

The following published papers was not included in this thesis,

Residual positioning errors and uncertainties for pediatric craniospinal irradiation and the impact of image guidance

Gram D, Haraldsson A, Brodin P, Nysom K, Björk-Eriksson T, Munck af Rosenschöld P
Radiat Oncol. 2020;15:149

The HILUS-Trial—a Prospective Nordic Multicenter Phase 2 Study of Ultracentral Lung Tumors Treated With Stereotactic Body Radiotherapy

Lindberg K, Grozman V, Karlsson K, Lindberg S, Lax I, Wersall P, et al.
Radiotherapy. J Thorac Oncol. 2021;16:1200-10

A selection of presentations at international conference,

Dose-rate dependence in haematological recovery following total marrow irradiation compared to total body irradiation

Haraldsson A, Wichert S, Engellau J, Lenhoff S, Turkiewicz D, Warsi S, Engelholm S, Bäck S, Engström PE
Radiother Oncol. 2020;152:S489-S

OC-0461: Acute toxicity and recovery following total marrow irradiation compared to total body irradiation

Engellau J, Haraldsson A, Engström PE, et al.
Radiother Oncol. 2020;152(Supplement 1):S257

PO-1771: Significant lower dose to brain after implementation of new treatment protocol for brain metastasis

Haraldsson A, Engleson J, Wieslander E, Engström P, Abri A, Munck af Rosenschöld P
Radiother Oncol. 2020;152(Supplement 1):S986

PO-0990 Positioning uncertainties for pediatric craniospinal irradiation and the impact of image guidance

Gasic D, Haraldsson A, Brodin NP, Nysom K, Björk-Eriksson T, Rosenschöld PM
Radiol Oncol., 2019, p. S544-S545

PO-0978 Accurate positioning with decreased treatment time using surface guided tomotherapy

Haraldsson A, Ceberg S, Crister C, Engelholm S, Bäck S, Engström PE
Radiother Oncol. 2019;133:S534-S5

EP-2180: Total Skin Irradiation using helical tomotherapy: First experience

Haraldsson A, Engleson J, Engelholm S, Enström PE
Radiother Oncol. 2018;127:S1204-S5

EP-1735: Total skin irradiation with helical Tomotherapy: Planning and dosimetry feasibility aspects

Haraldsson A, Engström PE
Radiother Oncol. 2017;123:S954-S5

All papers are reproduced with permission of their respective publishers.

Acknowledgements

First, I want to thank my supervisors for their time and effort. You have all guided me through this journey of growth to become a better scientist. Per Engström, without your effort, support, dedication, vast knowledge, and humour, none of this would have been possible; I want to be more like you when I grow up. Sven Bäck, your irrefutable scientific knowledge and sharp mind have vastly improved this work and my education. Sofie Ceberg, your positive view, great knowledge in general and in research specifically, have improved this work and my understanding considerable. Jacob Engellau, your no-nonsense decision-making, clinical knowledge, and pedagogic skills have greatly improved my knowledge on the subject and this work, especially on the clinical side. Your driving force and calm have encouraged me greatly. Crister Ceberg, one of the smartest and most knowledgeable persons in radiotherapy science I know, the discussions with you was not only crucial for this work, but it was also a lot of fun. Thank you, Silke Engelholm, for your support, input, and providing an organisation for research. In addition, a big warm thank you to the people both at the institution and at the clinical department for collaboration on this work and to find flexible solutions unique to someone with a foot in both worlds.

A large thank you to all my co-authors. Stina Wichert, from the hematology department, worked tirelessly with our publication. In the process, I learned much about hematopoietic stem cell transplantation, hematological disease, and treatment, thanks to your expertise. Thank you to the high-energy doer Jens Engleson for great collaboration on Paper II, the help from such a sharp and knowledgeable physician made it easy to move the project forward. Thank you to everyone at Radiotherapy physics at Skåne university hospital in Lund, thank you for the input, help, and understanding of the difficulties with two different focus areas. Especially thank you to both former team leader Andrzej Tomaszewicz and current Sacha af Wetterstedt for the support. Further, I want to thank all the wonderful radiation treatment personnel (Radiotherapy department, Lund) that helped with the continuous improvement of the treatments in this thesis, everyone from the CT/immobilisation personnel and especially Carola Hagström, and of course all the wonderful personnel at the TomoTherapy, all of which makes sure every single treatment is world-class.

Thank you to Accuray Incorporated, who believed in this project and were available and helpful with expertise and input in the technical aspects. A special thank you to Lisa Goggin, Julien Gerard, Fabienne Hirigoyenberry and Nathalie Chadeau. Also, thank you to C-Rad for providing expertise on their products.

Without the support and love from my Sara I would not have made it this far – I love thee to the level of every day's. To my young boys Viggo and Noel, whose laugh and presence seems to wash all worry away and have taught me the joy of the moment.

Sincerely, André

Populärvetenskaplig sammanfattning på svenska

Strålbehandling är en viktig del i behandling av elakartade blod-, och tumörsjukdomar. Modern behandlingsteknik är i hög grad datoriserad där olika komponenter i behandlingen som strålkällans rörelse, strålfältets utformning, behandlingsbrietsens rörelse och patientens positionering koordineras. Resultatet är en väsentligt mer precis strålbehandling och möjlighet att undvika högre stråldoser till delar av kroppen i närheten av behandlingsområdet. En sådan komplex behandling måste vara noggrant kontrollerad så att den är robust med avseende på alla involverade osäkerheter. Ett sätt att kontrollera en patients position före och under behandling är genom att använda en kamera som skannar av positionen på patienten i relation till där maskinen ska stråla, och övervakar att patienten alltid ligger rätt.

Konventionell strålbehandling utförs genom att patienten ligger still och en strålbehandlingsarm roterar sedan runt brieten och strålar samtidigt. I denna avhandling har en så kallad TomoTherapy strålbehandlingsapparat använts och den skiljer sig från den konventionella konstruktionen i med att patienten ligger på en briet som sakta åker genom en öppning i en ring där strålgeneratoren roterar. Fördelen med TomoTherapy typ av behandlingar ("helisk tomoterapi") är att väldigt långa komplicerade områden kan strålbehandlas, vilket är svårt eller omöjligt med andra tekniker. En sådan behandling ställer stora krav i många avseenden, och att man i ännu högre grad har kontroll på system, maskin och patient. Ett exempel på behandling är när patienter med olika typer av blodcancer strålbehandlas innan transplantation av friska blodstamceller. Strålbehandlingen görs för att slå ut resterande tumörceller och hämma patientens immunförsvar så att den nya transplanterade benmärgen kan etableras. Strålbehandlingens fördel är att den når områden där annan behandling såsom cellgiftsbehandling inte kan nästla sig in. Konventionell strålbehandlingsteknik innebär att hela kroppen får väsentligen samma stråldos, även om de egentliga målen för behandling är benmärgen samt mjälten och för vissa leukemier även centrala nervsystemet och testiklar. Med kombinationen av denna helkroppstrålning och kemoterapi följer stor risk för allvarliga akuta och sena biverkningar från andra organ som inkluderats. Ett annat exempel på en omfattande behandling som ges är mot en typ av hudlymfom som kan engagera hela huden. Strålbehandling kan då vara aktuellt mot hela huden för att minska sjukdomens svåra symptom. Förutsättningen är dock att det går att stråla huden utan att skada andra delar av kroppen.

I detta arbete har vi utvecklat och utvärderat behandlingstekniker som strålar stora delar av kroppen med TomoTherapy. Vi har också undersökt vilka fördelar och hur säkert det är att använda en kamerabaserad ytskanner som avläser patientens position och föreslår positionsändringar för att patienten ska ligga så exakt som möjligt under strålbehandlingen. Slutligen så utvärderades resultatet av strålbehandlingar som sker innan stamcellstransplantation där huvudsakligen benmärgen strålas jämfört med den äldre helkroppstekniken. Sammanfattningsvis så är behandlingsteknikerna komplicerade men effektiva om de kombineras med

ett kamerabaserat positionssystem. Kliniska resultat av denna nya TomoTherapy-baserade strålbehandling inför stamcellstransplantation är mycket goda och patienter som nu får behandling överlever med färre allvarliga biverkningar jämfört med tidigare given strålbehandlingsteknik.

Abbreviations

3D-CRT	3-dimensional conformal radiotherapy
aGvHD	Acute graft-versus-host disease
ALL	Acute lymphocytic leukaemia
AML	Acute myeloid leukaemia
BED	Biologically effective dose
BMT	Bone marrow transplantation
CBCT	Cone-beam computer tomography
cGvHD	Chronic graft-versus-host disease
CML	Chronic myelogenous leukaemia
CNS	Central nervous system
CSF-1	Colony-stimulating factor 1
CSI	Craniospinal irradiation
CT	Computed tomography
CTV	Clinical target volume
DD	Dose difference
DICOM	Digital imaging and communications in medicine
DTA	Distance to agreement
DVH	Dose-volume histogram
FOV	Field of view
FWHM	Field width at half max
G-CSF	Granulocyte colony-stimulating factor
GM-CSF	granulocyte-macrophage colony-stimulating factor
GTV	Gross target volume
GvHD	Graft versus host disease
H&N	Head and neck
HLA	Human leukocyte antigen
HSC	Hematopoietic stem cell
HSCT	Hematopoietic stem cell transplantation
HT	Helical tomotherapy
IEC	International electrotechnical commission
IMRT	Intensity modulated therapy
IP	Interstitial pneumonitis
LFOF	Leaf fluence output factor
LOT	Leaf open times
LOTH	Leaf open time histogram
LQ	Linear-quadratic
MF	Modulation factor

MHC	Major histocompatibility complex
MLC	Multi leaf collimator
MU	Monitor unit
MUD	Matched unrelated donor
MVCT	Mega-voltage computer tomography
NAL	No action limit
OAR	Organs at-risk
OS	Overall survival
PBSCT	Peripheral blood stem cell transplantation
PTV	Planning target volume
QA	Quality assurance
QC	Quality control
RIC	Reduce intensity conditioning
RP	Radiation pneumonitis
RT	Radiotherapy
SDF-1	Stromal cell-derived factor-1
SGRT	Surface guided radiotherapy
SSD	Surface to skin distance
TBI	Total body irradiation
TERMA	Total energy release per unit mass
TMI	Total Marrow Irradiation
TMLI	Total marrow and lymph irradiation
TPS	Treatment planning systems
TSEBT	Total skin electron beam therapy
VMAT	Volumetric modulated arc therapy
VOD	Veno-occlusive disease

Coordinate systems

For reference, the patient coordinate system is visualized on a patient geometry in figure 1

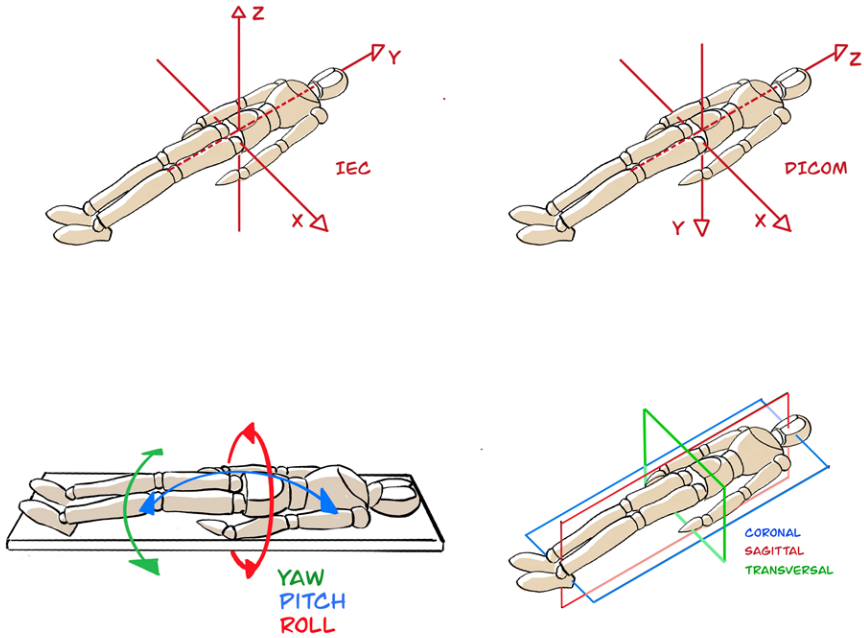


Figure 1: Patient-based coordinate system for the two most common used in RT: International Electrotechnical Commission (IEC) and Digital Imaging and Communications in Medicine (Dicom) with explanation of terminology for viewing planes and rotation around the different axis. Illustrations by Per E. Engström.

Helical tomotherapy for total marrow and total skin irradiation: Optimisation, verification, and clinical results

I Introduction

One in three persons in Sweden will develop cancer during their lifetime, and the most common types are prostate and breast cancer. The five-year survival rate has improved substantially: in 1970, 35% of men and 48% of women survived for five years, and today those proportions are 75% for men and 74% for women [1].

Blood cancers, or hematologic cancers, are a group of diseases that includes leukaemia, lymphoma, and multiple myeloma. In blood cancers, the disease spreads and acts in the bone marrow and/or lymphatic system in different cell types. In Sweden during 2016, 504 patients were diagnosed with leukaemia and 38 children were diagnosed with acute lymphocytic leukaemia (ALL), the most common type among children. These types of cancer are lethal; for example, in ALL, only 35–40% patients survive past five years [2].

The treatment commonly comprises of chemotherapy, and transplantation of blood stem cells with preceding chemotherapy and RT. Stem cell transplantation of bone marrow with RT has some advantages beneficial to the transplantation in terms of disease-free survival and also alters the patterns of acute toxicity[3]. Treating the entire body with RT is very toxic and can also be very difficult to implement with high certainty. Fortunately, technical advances in RT allow cancer sites to be targeted with low uncertainty over large areas. RT machines specialising in complicated delivery to long targets could potentially reduce the toxic effects of radiation and decrease treatment-related deaths, permitting increased doses for greater immunosuppression and cancer-killing effects. To achieve this, RT needs to be

delivered with high certainty to the patient's entire bone marrow. The patient setup, treatment delivery, treatment plan optimisation, and effects of treatment create a complicated system whose parts all contribute to successful RT treatment. Optimising and following up these large, complicated RT treatments was the overall aim of this work. The specific aim of this work was:

- Investigate a robust and efficient treatment with helical tomotherapy (HT) to condition the bone marrow prior to stem cell transplantation
- Develop a palliative RT treatment for mycosis fungoides treating the entire skin with HT
- Investigate the effect and impact of surface scanning on helical tomotherapy by means to deliver a precise treatment
- Follow up the results of the developed treatments implemented in the clinic

This thesis covers several treatments intended to deliver RT to large, complicated targets using HT, together with thorough control of the various uncertainties.

1.1 Outline

In this thesis, the four included published and peer-reviewed journal articles are presented in three main sub-sections. In dose planning, findings are presented and discussed regarding the RT treatment plan optimisation of large targets with HT. In verification, the complications and development of treatment plan QA and treatment delivery optimisation with regard to uncertainties are presented. In the final main subsection, clinical aspects and clinical findings, together with their relationships and potentials, are presented and discussed as a whole. These sections are preceded by background and theory and followed by a general discussion, conclusions, and final remarks. Each main section includes an introduction to the subject, followed by a material and methods section - where selected methods and materials are presented and/or discussed, followed by a results and discussion section.

I conducted this work from 2017 to 2021 as a PhD student affiliated with Lund University, while employed as a medical physicist at Skåne University Hospital, where 50% of the position was dedicated to PhD studies. During most of this period, the hospital department received funding from the RT device manufacturer Accuray Inc. (Madison, WI, USA).

1.2 Author contributions

Paper I: Implementing safe and robust Total Marrow Irradiation using Helical Tomotherapy - A practical guide.

I analysed all the data, collected new data, and performed new calculations based on robust junctions and treatment data. The drafts of the article were written solely by me with thorough input at each step from the other authors.

Paper II: Helical tomotherapy as a robust low-dose treatment alternative for total skin irradiation

The entire treatment method was developed with support from the literature by me with input from co-authors during development and clinical implementation. All analysis, data collection, and measurements were conducted by me. In addition, I wrote most of the paper, with input from the co-authors during each draft.

Paper III: Surface-guided tomotherapy improves positioning and reduces treatment time: A retrospective analysis of 16 835 treatment fractions

All data collection, method development, analysis, and writing were done by me with input from co-authors regarding statistics and methods. I wrote the vast majority of the article with input from supervisors/co-authors on each draft.

Paper IV: Organ sparing total marrow irradiation compared to total body irradiation prior to allogeneic stem cell transplantation

I conducted most of the data analysis and some of the data collection. Physicians responsible for treatment and care collected patient follow-up data. Furthermore, I wrote most of the article.

2 Background and Theory

2.1 Radiotherapy

Today, external RT is commonly administered using linear accelerators. Several configurations exist, with the dominant one being a c-arm configuration in which the radiation is administered via a large arm that directs the radiation to the patient. The arm rotates around the patient, who often lies prone on a couch, and the radiation beam can be modulated using built-in metal leaves and blocks. Other configurations have been developed that have specific advantages and disadvantages. A relatively widespread type of external RT device is the TomoTherapy device, in which the linac is mounted in a slip-ring construction that can rotate relatively quickly, and the patient's couch is translated through the slip-ring construction and the modulated beam. This configuration can administer complex dose delivery patterns to relatively long targets, such as the entire bone marrow or large parts of the skin.

Modern advanced RT treatments are often delivered as fractionated IMRT, i.e., on several occasions. IMRT is delivered from several angles in different shapes modulated by the built-in leaves and for different treatment times, intersecting at the target, thus creating overlapping beams in the tumour leading to a highly conformal dose in the tumour and a lower dose to OAR (figure 2). These advanced radiotherapies have been made possible by increasingly complex treatment planning systems (TPSs) together with motorised multi-leaf collimators (MLCs) and the ability to modulate the dose rate and gantry speed. The treatment plan is optimised by defining dose limits to targets and normal tissues to be fulfilled using complex algorithms, in contrast to the 'trial-and-error' process standard in three-dimensional conformal RT (3D-CRT). Volumetric modulated arc therapy (VMAT), in which the treatment is administered using a gantry and moving MLC, both simultaneously rotating, has replaced stepwise IMRT and features increased speed and improved plan quality [4].

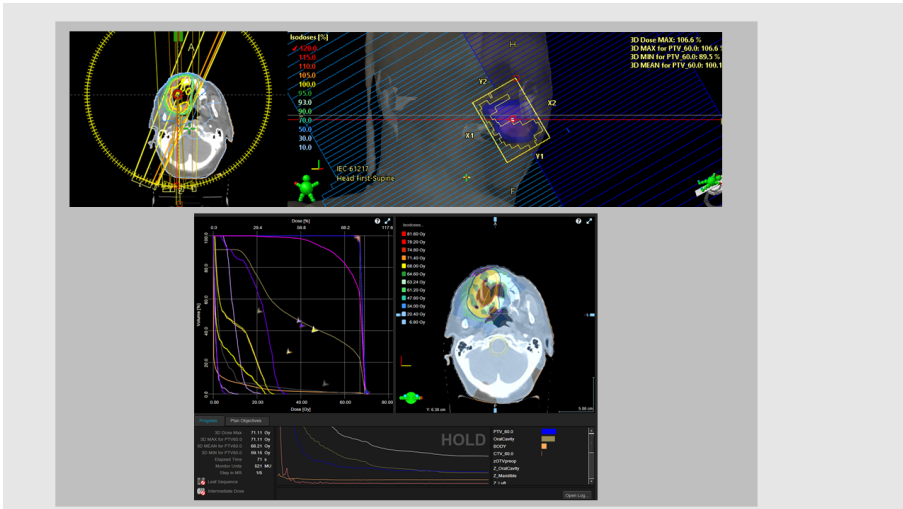


Figure 2: Example of volumetric modulated arc therapy (VMAT) optimisation and delivery on a patient receiving treatment in the head and neck region. VMAT treatment to the head and neck region showing an arc spanning a full rotation (top left). Multi-leaf collimator forming a subfield in the same patient (top left). Optimisation software showing user-defined constraints as small triangles and the dose-volume histogram for target and organs defined on the CT (bottom).

2.2 The TomoTherapy & Radixact System

The TomoTherapy

The TomoTherapy [5] was developed based on an idea from the late 1980s in which collimator jaws form a slit beam that would be translated and rotated, using multiple shaped fields and modulated using a fast MLC bank [6]. Today, the TomoTherapy takes the form of an RT device with a linear accelerator mounted on a slip-ring construction, similar to a CT device but with a much higher energy and dose rate. The patient couch is continuously translated through the gantry simultaneously as the linac is rotating, administering a helical treatment pattern to the patient; this irradiation method is usually referred to as helical tomotherapy (HT) (Figure 3). The first patient was treated with HT in 1994 [6]. In TomoTherapy, daily imaging is acquired using the treatment beam at lower energy, so the imaging and treatment isocentres coincide. On the other hand, the use of megavoltage energies results in lower imaging contrast and resolution than in comparable online kV imaging techniques such as cone-beam computer tomography (CBCT).

The MLC on a TomoTherapy device is driven by pneumatic controllers and has 64 interlacing leaves. The width of the MLC at the isocentre is 0.625 cm, and the linac target-to-isocentre distance is 85 cm. The pneumatic drivers enable the MLC to open or close the leaves in 20 ms. This technical advantage of the MLC and the helical delivery pattern enables extreme delivery modulation. The gantry's rotation speed ranges from 11.8 to

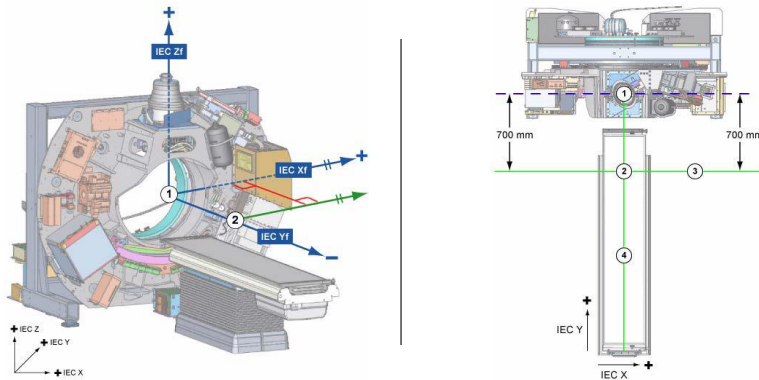


Figure 3: Schematic image of the TomoTherapy gantry (left) and top view (right) showing some of the beamline components, such as the linac (a), exit detector (b), and shielding. Also visible is the machine-specific coordinate system with +z in the vertical, +x to right when facing the machine, and +y inwards to the machine when facing the gantry. Virtual isocentre used for patient setup (2) and machine isocentre (1) separated by 700 mm. From patient positioning workflows 1059569.D RN764 (Accuray, Madison, WI, USA) [7]. Images used with permission from Accuray Incorporated.

60.0 s, but for treatment with 2 Gy per fraction, the rotation speed is usually 12–30 s with common rotation overlap. Simultaneously to the gantry rotation, the couch is translated through the gantry at a fixed speed. The couch speed-to-gantry speed relationship, called the pitch, is defined as the couch translation length as part of the width of the beam, per gantry rotation. A typical value for a pitch of 0.43 with a longitudinal beam opening of 5 cm is 2.15 cm of couch translation per gantry revolution. Thus, at a gantry speed of 20 s/rev, this translates to a couch speed of about 6.45 cm/min. The longitudinal beam width is 1.05, 2.50, or 5.02 cm at the isocentre, although the jaw can technically be set to more widths. In addition, with the dynamic jaw option, the collimator can dynamically collimate the penumbra longitudinally¹, minimising the dose to the patient outside the target, cranially-caudally². The couch translation on a TomoTherapy device can facilitate the irradiation of targets up to 140 cm³. These technical advances contribute to TomoTherapy’s ability to create highly modulated dose distributions in very long targets.

In addition, the TomoTherapy device can also deliver multiple fixed-beam-angle treatments with couch translation, a sort of fixed-angle IMRT. This technique is called TomoDirect and can be used when rotation therapy is not desired due to uncertainties, such as tangential

¹In the machine-specific coordinate system y-direction, i.e., cranially-caudally in the patient.

²In the machine-specific coordinate system y-direction, i.e., cranially-caudally in the patient

³Depends on the height and start position of the couch

breast cancer treatments or anterior–posterior treatment of medullar compression.

The TomoTherapy device has a movable positioning setup laser system (red) in all planes and one fixed laser system that defines the virtual isocentre (green) (see Figure 3). The patient is positioned 700 mm outside the bore.

The Radixact

The Radixact is the next-generation treatment unit from the manufacturer Accuray, based on the same concept as the TomoTherapy device but with several new functionalities. The machine has a higher (optional) dose rate and a couch catcher to prevent couch bending when the couch travels through the gantry. In addition, the machine can be fitted with a kV imaging unit on the slip ring, orthogonal to the linac. The kV imaging unit can be used for high-quality CT at 120 kV and intrafraction tracking of the target with fiducials or image features at high speed. A whole-scan-range CT scan of approximately 150 cm can be performed in about 1–2 min, 10 times faster than MVCT with the older TomoTherapy unit.

Basic principles of helical tomotherapy

In HT, the gantry rotates continuously during treatment. The optimisation, in turn, is performed to 51 discrete angles. The maximum dose rate at the isocentre with a fully open MLC and a 5-cm jaw opening is around 8.5 Gy/min. The dose is delivered on a time basis, in contrast to the more common monitor unit (MU) basis. A dose servo controls the dose rate, continuously adjusting the pulse amplitude control and injector/gun current. For practical reasons, the patient is set up outside the bore with the couch retracted. With the virtual isocentre defined at 700 mm longitudinal to the beam isocentre, the couch moves to the treatment position prior to treatment start. With the beam on, the couch translates through the gantry during irradiation at a constant velocity. The linac has a maximum energy of 6 MV, and both the jaws and the 64-leaf pneumatic MLC are oriented to open and close in the longitudinal⁴ direction (Figure 4).

The jaw has the options of 1.0-, 2.5-, and 5.0-cm longitudinal openings and additional dynamic openings at the target ends, cranially and caudally in the patient. The jaw is dynamic, i.e. the leading jaw closes with the end of the target in the longitudinal direction, minimising the penumbra. The MLC can open or close in approximately 20 ms. The opening times of the individual leaves are measured and stored in the beam model as MLC latencies in the TomoTherapy and in the machine translation instructions in the Radixact. The MLC is 40 cm wide at the isocentre. Opposite to the linac is an MVCT detector for imaging and

⁴In the machine-specific coordinate system, the couch translates longitudinal in the +y direction.

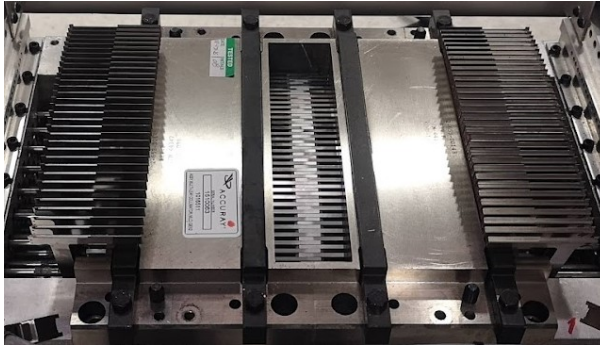


Figure 4: MLC with interlaced leaves in the MLC bank.

QA purposes, i.e., a 640-channel xenon-filled tungsten septal-plate detector with a field of view (FOV) of 39 cm. The primary collimator has up to 2–3 cm of tungsten in both the fixture and jaw. The machine has no flattening filter. Leaves are made of 10-cm-thick tungsten with a 6.25-mm isocentre width and are interlaced, meaning that every leaf on each side translates interchangeably over the entire opening. The pneumatic MLC sets the beam width, since both the jaw and MLC operate in the longitudinal direction. Thus, the jaw fixture sets the beamlet size for the MLC opening in the longitudinal direction. The gantry rotation speed is 11.8–60 s per revolution, and there is a constraint on the opening time⁵; one leaf can be completely closed, open, or modulated down to 2–10% of the optimisation angle.

The total opening time per optimisation angle is called the leaf open time (LOT) and is usually presented as a leaf open time histogram (LOTH) (Figure 5).

The TomoTherapy device works with ‘gold standard’ beam data, with the beam being tuned to match the universal beam data. A few factors are individual to each machine, and moving a treatment case between machines usually requires recalculation. The leaf opening latency is the time from signal to fully open leaf and is leaf dependent. One peculiarity of the beam model is the finite source size: the linac is so close to the MLC that the individual leaf output depends on the number of adjacent open leaves. The leaf fluence output factor (LFOF) is typically 1.05 if a neighbouring leaf is open. Thus, a highly modulated treatment has a disproportionately lower dose rate than a less modulated treatment. Since the field width at the half maximum (FWHM) opening time is 20 ms, and the time for one projection (i.e., angle time) can be as little as 230 ms, the latencies affect the delivery in different ways. Here, shorter opening times can be hard on the MLC and the pneumatic drivers, affecting the QA and delivery results⁶ (Figure 6).

⁵In the TomoTherapy/Precision planning system (Accuray, Madison, WI, USA).

⁶Due to differences in how the MLC latencies are compensated for, this effect is less prominent in a Radixact device.

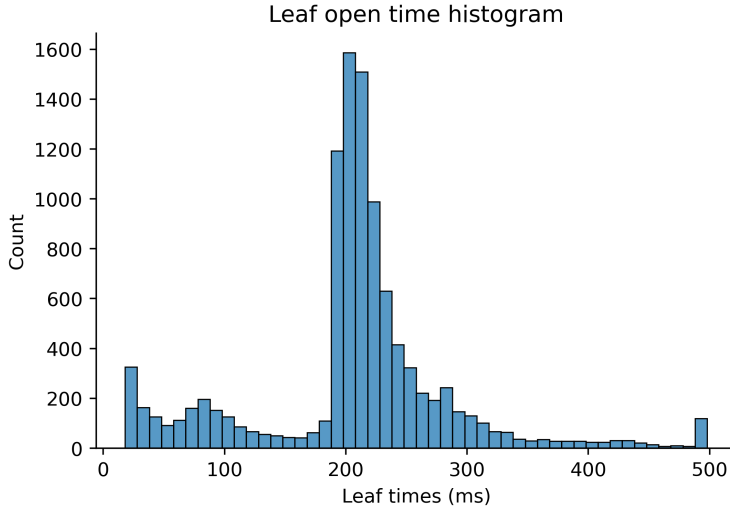


Figure 5: Leaf open time histogram, showing the binned open times for the MLC leaves on the x-axis for the entire treatment.

Optimisation of helical tomotherapy plans

Plan optimisation is performed in full-dose mode, which means that constraints derived from rotation times are applied during the final dose calculation. The optimisation beamlets are organised in a sinogram, which comprises the entire time-resolved openings of the MLC bank (Figure 7).

In full dose calculation, a time-resolved treatment is generated based on the number of fractions. The dose engine uses the total energy release per unit mass and a convolution kernel to calculate the dose, i.e., collapsed cone convolutions. The beamlet opening time is based on the energy fluence per ideal opening time, and the modifiers are the energy spectrum, beam profile, jaw size, and LFOF. Attenuation values other than water and bone are interpolated versus radiological depth.

The optimisation function⁷ is defined as follows:

$$F = \Sigma((DV_{prescribed} - DV_{actual})^2) \cdot \frac{I_{Importance}}{V_{ROI}} \cdot I_{penalty} \quad (1)$$

Here F is the optimisation function, $DV_{prescribed}$ is the prescribed dose-volume, DV_{actual} is the actual dose-volume, $I_{Importance}$ the importance function value set by the user, V_{ROI} is the volume of the structure and $I_{Penalty}$ the penalty function value set by the user.

⁷For helical tomotherapy planning in Precision.

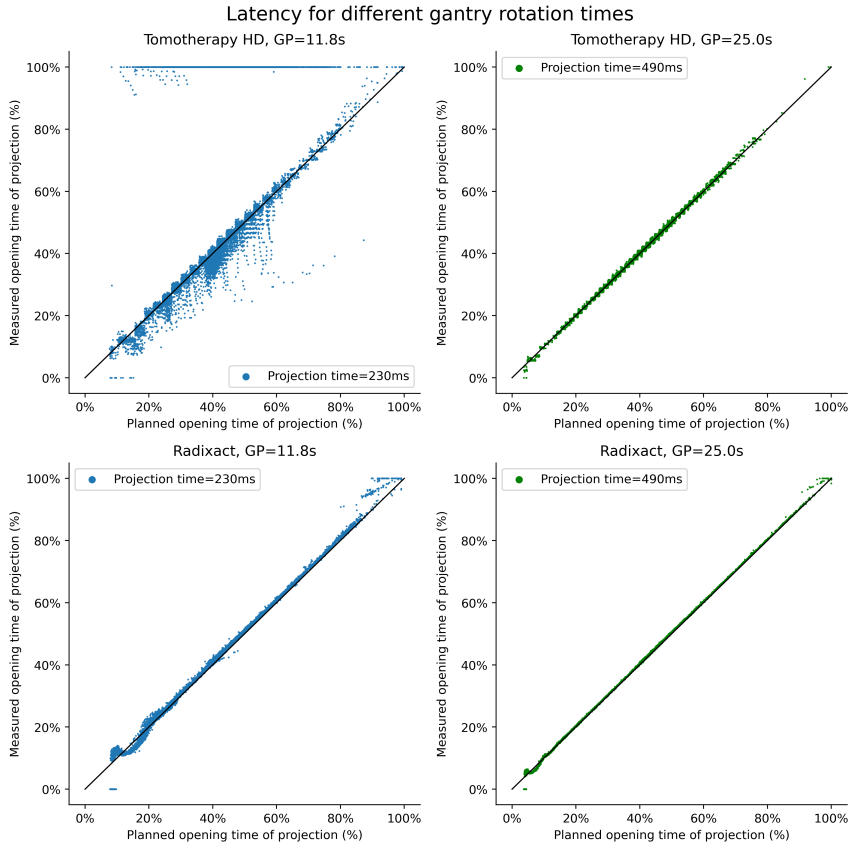


Figure 6: Difference in latency between a typical fast and a typical slow rotation of the Tomotherapy and Radixact as measured on the two systems at Skåne university hospital in Lund.

The optimisation of the dose plan is performed using a normalised objective function. The importance penalty is the overall factor for the entire volume and one Dose-Volume Histogram (DVH) penalty, normalised by the ROI volume (equation 1). The importance and penalty values are relative. The importance factor is applied to all voxels, but the penalty area is applied only to voxels that fail to meet the criteria. When the plan is optimised, the actual dose rate to the target depends on the number of open MLC leaves and other factors, such as off-axis position and depth. The fluence needed for each pass, and thus each gantry angle, is a combination of the overlap of each revolution, off-axis target position, fractional dose, and size and depth of target. Since the couch speed is constant, the longest opening time in any optimisation segment constrains the possible revolution speed together with the overlap, or rather pitch. To constrain the longest opening time and thus the total delivered time, and in part the delivery complexity, the ratio between the longest and average opening times can be capped, disregarding non-open leaves. This setting is defined as the modulation factor (MF). For example, an MF of 2.0 means that the longest opening

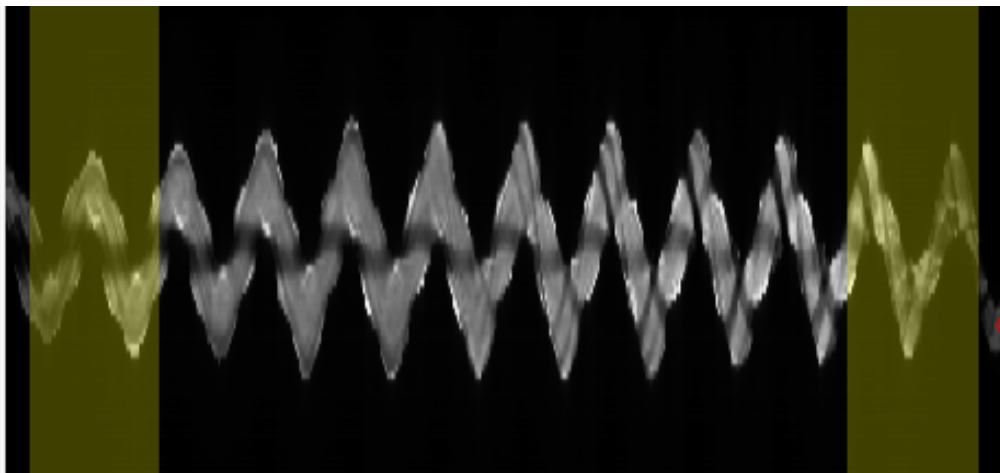


Figure 7: An MLC sinogram for a head and neck patient. The time-resolved openings of the MLC are shown as intensity black to white, when white is fully opened the entire segment. Each leaf is represented on the y-axis (top–bottom) with one projection per row on the x-axis (right–left). The yellow area represents the dynamic opening of the collimator.

time for any leaf/beamlet can be twice the mean opening time over the entire treatment. Furthermore, the final dose calculation removes short opening times in relation to physical constraints on the MLC. The number of leaf cycles per second is constrained to under 163 leaf cycles per second to avoid overburdening the MLC air supply.

Planning aspects of large targets

The optimisation of targets spanning large parts of or the entire body differs from regular HT dose planning. First, the target volumes are considerably larger than the volumes of the OAR. The optimisation volumes/regions of interest in use are normalised to total volume in the optimisation process, which is less than ideal when the targets are as large as 5000 cc. In addition, the treatment width opening of the MLC is limited to 40 cm, making it impossible to treat the entire width of an adult patient from every angle. The treatment time scales linearly with the MF, so it is essential to balance the MF against the plan quality for large treatments to avoid unacceptably long treatment times. One approach recommended by experienced users is to start with a reasonably high MF and then slowly lower it stepwise, optimising at least 20–50 iterations after each step until an acceptable target coverage-to-treatment time ratio is achieved. Leaf opening times that deviate more than the MF from the mean opening time will be removed at optimisation. The constraint on the number of leaf cycles can cause problems in large-volume irradiations, and a lower MF will also help regulate this – most importantly – as will a slower gantry period. More overlap per revolution is thus easier to modulate for optimisation purposes, but this generates a faster gantry rotation speed. The field width (FW) is directly and linearly correlated to the treatment

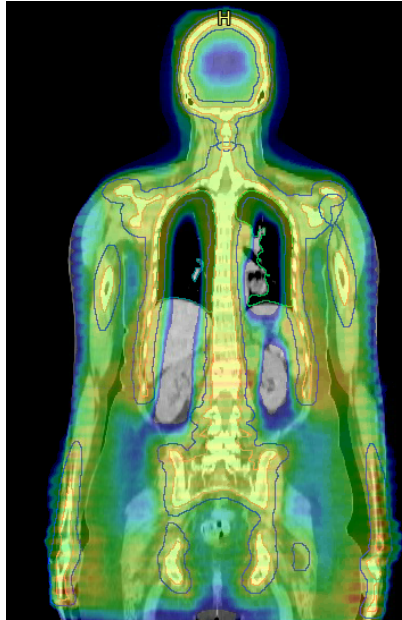


Figure 8: Ripple in the longitudinal direction in total marrow irradiation with helical tomotherapy in which treatment was planned with a suboptimal pitch. As seen in the image, the ripple is more prominent farther from the treatment isoaxis.

time. In publications, the FW has generally been set to 5 cm for whole-body plans due to long treatment times [8, 9].

The beam divergence in fan beam geometry is quite complex. The helical delivery results in a small-dose delivery pattern that, when unmodulated, looks like a ripple effect (Figure 8) [10]. This effect comes from several inert properties of the HT delivery. The absence of a flattening filter creates a cone-shaped profile; this dose profile will overlap unevenly outside the central axis due to reducing intensity, width change, and, as mentioned, the cone beam [11]. This effect is small on the isocentre axis and for small targets. This is seen as a ripple or oscillating dose pattern in the longitudinal direction for large and off-axis targets. The effect can be minimised in the optimisation process but can strain the MLC when the optimiser compensates for this effect. The threading effect is pitch and MF dependent and can be minimised by choosing an optimal pitch value (Figure 9). A higher pitch will generally slow the gantry rotation, allowing more modulation with relatively short segments; this will reduce the influence of leaf latency and create more robust plans with a generally higher gamma pass rate for plan verification.

Delivery time in helical tomotherapy

The gantry period can be estimated from the following:

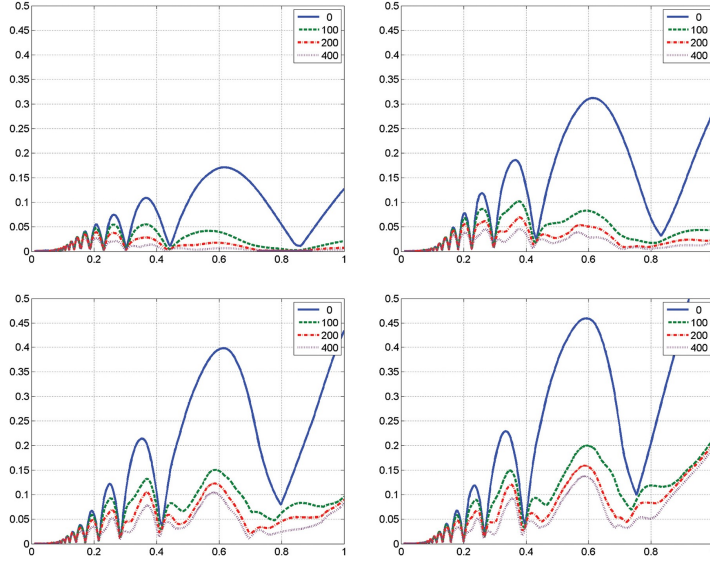


Figure 9: Different ripple amplitudes in the longitudinal direction at four different off-isocentre axis distances, i.e., 5, 10, 15, and 20 cm, performed for different number of iterations. This illustrates that the ripple effect can to some extent be compensated for through modulation/optimisation, but not that effectively and at the expense of longer treatment times (from Chen et al. [11]). Displayed is pitch on x-axis and ripple amplitude on y-axis.

$$GP = MF \cdot PITCH \cdot \left(1 - \frac{BLOCK}{100}\right) \cdot \frac{d}{\dot{D}} \cdot 60 [s] \quad (2)$$

Here, GP is the gantry period, MF is the modulation factor, $PITCH$ is the actual pitch after optimisation, $BLOCK$ is the blocked part as a percentage of the gantry period, d is the fractional dose in Gy, and \dot{D} is the dose rate to the target, which for estimation can be set to 4–5 Gy/min. The total treatment time can then be approximated as follows:

$$T = \frac{L}{(PITCH \cdot FW)} \cdot GP [s] \quad (3)$$

Here, T is total treatment time, L is the treatment length in the longitudinal direction, and FW is the field width in cm. The gantry period is fixed, and as such the segment with the highest demand for fluency and thus delivery time determines the rotation time and total treatment time.

2.3 Uncertainties in external radiotherapy

Numerous factors contribute to uncertainties in dose determination in RT. The dose delivery from the linac to the intended target in the patient includes positional uncertainties

stemming from day-to-day variation in anatomy and patient positioning. In addition, movement during irradiation, such as breathing, intestinal movements, and heart contractions, can influence the uncertainties of treatment delivery. Generally, there are two types of uncertainties in RT, random and systematic [12]. Random uncertainties could stem from random motion during treatment and random components of the patient setup. In contrast, systematic uncertainties, such as machine-dependent geometrical offsets and misalignments during reference CT, influence the entire treatment in the same direction and magnitude. In addition, since the treatments are usually administered in several fractions, random uncertainties have less influence on the derived treatment margins than do systematic uncertainties due to daily variation in the random components throughout the treatment. However, the true randomness of most such random uncertainties is debatable. To remedy such uncertainties, margin strategies have been adopted based on the theory that the uncertainties follow a Gaussian distribution. The target is defined as a point, and the dose distribution moves rigidly with the deviation [13, 14]. This approach is a simplification, even more so in IMRT and HT.

Example of uncertainties in RT:

- Target delineation error – **systematic** uncertainties in definition of the Gross Tumour Volume (GTV), Clinical Tumour Volume (CTV), and Planning Target Volume (PTV)
- Target position and shape – the difference in anatomy between that acquired in the planning CT and treatment and between treatment fractions, **systematic** and **random**
- Phantom transfer error – reference imaging versus treatment system, position between image isocentre versus treatment isocentre including calculation, and geometric error (also image resolution and structure polygon-to-voxel calculation), typical **systematic** uncertainties
- Patient daily setup error – **random** variation in patient position, shape, and size, such as weight loss, including day-to-day organ variation
- Intrafraction uncertainties – **random**/cyclic movement during treatment, for example, breathing

Uncertainties that are not mitigated with imaging are compensated for with margins around targets or OAR. In addition, imaging can be performed on a non-daily basis to reduce total treatment time; the increased uncertainty that follows is compensated for with additional margins. An extended no action limit (NAL) [15] protocol is used when the initial N-times position is adjusted for systematic error by moving the initial patient setup position

to compensate for systematic uncertainty. Several images are initially acquired, the average translation adjustment is calculated, and the patient setup is adjusted accordingly. NAL is a suitable method if the random component is small and systematic errors are not introduced during treatment [12].

2.4 Systems for dosimetric verification

A reliable dose measurement system that is also a viable alternative for mass measurements is essential for implementing complicated treatments. Here, we analyse complicated systems whose parts are known and form an intricate whole. For whole-body IMRT treatment, each part needs to be analysed, and QA of the parts is followed by QA of the complete system in order to understand both the parts and the entire system.

Delta4 phantom

The Delta4 Phantom (ScandiDos, Uppsala, Sweden) is a 2×2 D detector with two orthogonal diode arrays situated in a PMMA cylindrical phantom. Each diode is sampled on a beam pulse basis such that the dose can be evaluated per segment. There are 1069 p-type diodes with a 1-cm interval and at 5 mm on each plane's central $6 \times 6\text{-cm}^2$ area. The total area covered is $20 \times 20\text{ cm}^2$. The Delta4 can be used with an ion chamber insert for QA and calibration purposes. The treatment plan to be measured is imported into the Delta4 software for comparison with the measured dose distribution. The dose can be compared using a gamma criterion [16], in which either the point-wise dose difference (DD) or the distance to agreement (DTA) is within tolerance. The typical DD is 3% and the DTA is 2 mm, with a threshold under which no dose is evaluated (e.g., 15%). The number of points within the tolerance is summed, and the percentage of approved points is evaluated. Still, even with a high gamma pass, the measured dose should be evaluated for difference from the planned dose, since a pass rate of 99% does not exclude a hot spot of twice the prescribed dose, or a cold spot. The Delta4 software can calculate a 3D dose distribution using the built-in algorithm. The dose from each beam is rescaled along the ray lines from the source to each detector. This is done for all beams or segments to get a 3D dose distribution. The angular direction dependence is adjusted automatically [17]. The Delta4 Phantom+ is a newer version with wireless operation and a less complicated calibration procedure.

Film dosimetry

Radiochromatic films such as Gafchromic EBT3 (Ashland Advanced Materials, Bridgewater, NJ, USA) have a high spatial resolution and reasonably low spectral sensitivity [18]. EBT3 has a single active layer, 30 μm thick, between two polystyrene sheets. The effective

measurement depth is 0.153 mm. After irradiation, separate colour channels can be used for read-out. Red is often used for contrast, but all channels (i.e., red, blue, and green) can ensure a stable response. The proper procedure includes scanning and irradiation in the same direction and only using the calibrated surface of the scanner.

With HT, it is possible to deliver precise treatment to superficial targets. However, the surface dose is generally overestimated in the TPS [19]. The problem is twofold: overestimation of the surface dose, and optimisation effects in the build-up region, as previously mentioned. A reliable surface dose measurement system is needed to test the consistency of the dose distribution from the TPS.

For radiochromatic film, there is very little volumetric averaging: it has an isotropic response and can be irradiated in any position. There are some uncertainties in film dosimetry, homogeneity, manipulation, irradiation, digitalisation, and response to absorbed dose. After correcting for all this uncertainty, film dosimetry can be done with an accuracy of 1.0–1.8% [20, 21, 22, 23].

Snir et al. [24] tested EBT₂ for surface dose measurements and found that it was similar in response to semi-conductor (MOSFET) and optically stimulated luminescence (OSL) detectors. One of the most challenging parts of film dosimetry *in vivo* is to determine the position of the measurement point in the TPS dose, and thus the expected dose to the detector. This can be alleviated by using radio-opaque markers, but they can distort the dose reading. The film has been found to be acceptable for surface dose measurements, but proper calibration was needed for the first few millimetres of build-up [25, 19]. A correction of up to 15% of the response has been found in good agreement with Monte Carlo simulations and other measurements [25].

2.5 Commissioning of robust treatments

The commissioning of a new treatment follows the verification and implementation of any new technique and depends on the treatment complexity. Modern RT involves many agents and is a complicated system of imaging, contouring, target definition planning, and treatment planning, with RT being one of many treatment options. Similar to multi-institutional QA of trials, the audit should be used to ‘see through’ the process from a different perspective [26]. QA and QC are significant for the implementation of new treatments. For example, the Pediatric Oncology Group’s study of Ewing’s sarcoma (POG 8346) found that patients who received the RT-treated per-volume protocol had an advantage in local control compared with those that did not adhere to the protocol, i.e., 80% versus 16% [27]. Other investigations have obtained similar results, such as the German Hodgkin study group trial, HD₄, in which local control was 82% versus 70% with or without protocol violations [28].

As stated in ISO 9001 [29], understanding and managing a process as a whole system improves effectiveness and efficiency.

Risk-based thinking is about carrying out preventive action that eliminates potential non-conformities and analysing such nonconformities that do occur, and taking appropriate action to prevent recurrent events at the level of the nonconformities. Actions should be implemented that address risks and opportunities. Risks arise from uncertainties, which can have both positive and negative effects. A proper quality management system determines the inputs and outputs required, the sequence of interactions, the criteria and methods used, and the resources needed; it assigns responsibilities, addresses risks and opportunities, evaluates the processes, and implements changes to ensure that the processes achieve the intended results.

Risk-based thinking: Actions should be planned to address risk as a preventive tool

Unfortunately, the RT protocols in studies are often vague, minimal, or inconsistent with current procedures used at treatment centres, despite published recommendations and templates for RT protocols [30]. This can create problems when centres try to implement techniques from studies. Typically, when a centre participates in a trial, the centre needs to adhere to a benchmark test or case representing the typical treatment of the disease. This should be similar when a new treatment is implemented from the literature. This verifies that the treatment plan has been performed according to the guidelines from the protocol and that the personnel involved are knowledgeable about the study, having conducted a dry run [31].

Notably, many studies are careful with the dose prescription but differ or are vague regarding the dose specification. It is common to use the average or medium dose to target as the prescribed dose, and dose-volume coverage criteria are common, such as 95% of the prescribed dose to 95% of the target volume, or 75% of the prescribed dose to 100% of the volume in stereotactic RT.

Anthropomorphic phantoms can be used for dosimetry and electronic data submission. Treatment plans are assessed for compliance with the specifications of the protocol and treatment chart to confirm that the prescribed dose is delivered. Other criteria are whether the plan is actually implemented as planned, with the physicist's role being to program start-up, conduct routine QA, and supply protocol-specific support. For example, thermoluminescent dosimeter (TLD) dosimetry is used when participating in NCI-sponsored trials.

A credential is widely used to evaluate treatment planning and execution. The credential was originally used to verify that the dose was uniform between treatment units and that

planning could be performed as set out in the study guidelines [26].

Knowledge assessment is a tool that requires critical reading and answers questions about subjects such as dose prescription, treatment techniques, and required data. Dry run and benchmark testing cases is excellent for practice delineation, defining target volumes, test treatment planning, compliance, and phantom irradiation study. The dosimetric aspect is institution/machine specific, but delineation is individual. Should we credential specific individual clinicians and dose planners?

In summary, a good implementation of a new treatment contains:

1. Protocol knowledge assessment
2. Benchmark case
3. Protocol-specific benchmark
4. End-to-end test
5. Image guidance study
6. Pre-treatment clinical or dosimetry review
7. Follow-up of treated patients

Examples of specific matters to be considered when implementing new treatments:

- The immobilisation needed to achieve the best possible level of accuracy
- Target and OAR - toxicity and margins
- Treatment planning - training of treatment planning and analysis of margin, including robust planning, i.e., analysis of delivered dose given assumed movement
- Delivery commission - can the RT device deliver the planned distribution?
- In vivo preparation - can the plan be delivered to the patient as measured on an anthropomorphic phantom?
- Necessary imaging technique for the treatment
- Coordination with other actors - usually RT is only one of many treatments
- Peer review of the process
- Multidisciplinary - all actors are involved from the start

Specifically, in complicated treatments, it is important to involve all actors in the treatment to properly assess the chain of events from immobilisation to the last treatment.

2.6 Surface guided radiotherapy

Today, there are several systems that can aid in the delivery of accurate RT. Surface scanners are usually fitted with either a laser-type or camera-type scanner that aids in the positioning and/or the monitoring and management of motion uncertainties by means of direct feedback to users and optional beam control [32].

The most common RT schedule is daily treatment for 1–39 days, depending on the type of cancer and intent of treatment. A standard workflow for the patient setup at radiation treatment start includes aligning the room lasers to laser markers (i.e., point or lines) on the patient, complemented with imaging depending on the specific patient imaging protocol. The image is registered to a reference, and couch translation can directly compensate for the deviation. The TomoTherapy can also compensate for roll deviation by adjusting the start angle.

Positioning verification with built-in imaging can be time consuming, contributing to additional integral dose. Surface-guided radiotherapy (SGRT) scanning may facilitate the initial setup process of patient positioning and allows for motion monitoring. The patient's surface is scanned with an optical- or laser-based system that compares the daily setup with a reference surface. Some systems have live feedback on the patient with a coloured map to improve the interactivity of the patient positioning. Surface scanning can expedite positioning and make daily imaging redundant. However, SGRT needs a correct surface-to-target position correlation to be accurate. How well the surface can represent the target position has been investigated [33, 34, 35, 36]. Usually, the surface correlation with the target position is verified with the built-in CBCT for the first few fractions, following weekly or other intervals of standard imaging. Using SGRT has several advantages in HT. The FOV of the technique is unique and can incorporate the complete treatment volume (140 cm). The long imaging volume of the total marrow irradiation (TMI) or total skin irradiation (TSI) patient requires up to 15–20 min with mega-voltage computer tomography (MVCT), and any large deviations require adjustment of the patient and a subsequent rescan. SGRT can remedy this with high certainty by adjusting the patient to a reference surface. Relatedly, the FOV of MVCT on TomoTherapy and Radixact devices is limited to 40 cm, which often excludes parts of the shoulders and entire arms for adult patients. SGRT can be used for the setup and verification of areas outside the FOV of the treatment machine (Figure 10). In addition, surface scanning can monitor the patient during treatment to verify that the patient's position conforms to the reference throughout the treatment, which is especially important during long treatment times.

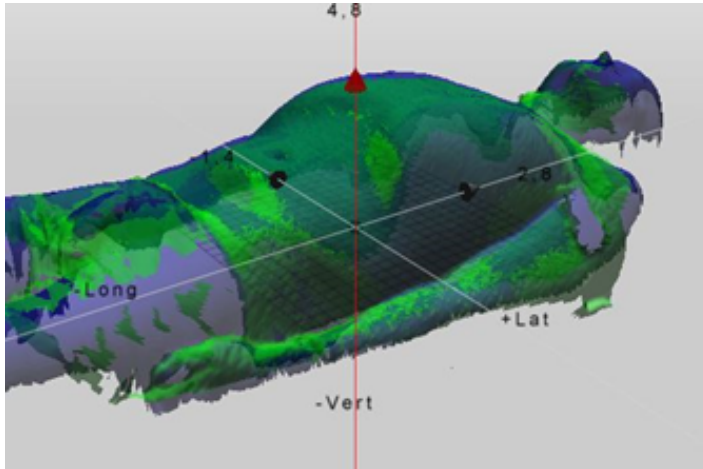


Figure 10: Example of a whole upper body surface scanning image of a patient using the Catalyst system (C-RAD Positioning AB, Uppsala, Sweden). The colour map represents the reference position (blue) and daily position (green); the colour map can also be projected onto the patient to aid setup.

2.7 Basic radiobiology

The energy deposited by radiation is measured as absorbed dose in RT. However, the effect of the absorbed dose depends on numerous factors, such as RT interval, tissue-specific factors, and the amount of deposited dose on each occasion.

RT fractionation is based on the linear-quadratic (LQ) response for sparsely ionising radiation. This radiation produces oxygen-derived free radicals or ionises the DNA directly [37], mainly via Compton electrons. The DNA damage caused by these interactions is divided into single-strand and double-strand breaks. The cell repairs single-strand breaks under normal circumstances, with covalent bonding to the DNA by agents present in the cell. Double-strand breaks sever the entire DNA chain; however, they can be repaired depending on the cell cycle and other factors, using, for example, homologous repair in which the duplicate chromosome coil is a basis for the repair process. A break in DNA can be fixated to become a lethal break if the free end is bonded to a free radical. This effect makes the abundance of oxygen a vital part of the RT response. These theories led to the LQ model and the biologically effective dose (BED) model [38, 39, 40, 41]:

$$S = e^{-\alpha D - \beta D^2} \quad (4)$$

where S is the LQ survival response to radiation from the total dose, D , and to the cell/tissue-specific radiosensitivity constants α and β .

$$BED = D \cdot \left(1 + \frac{d}{\alpha/\beta}\right) - \frac{\ln 2 \cdot (T - T_k)}{\alpha \cdot T_p} Gy_{\alpha/\beta} \quad (5)$$

where D is the total dose, d is the dose per fraction, is the fractionation sensitivity, T and T_k are the treatment time and kick-off time to when the cell repair accelerates, respectively, and T_p is the potential doubling time. The time factor adjusts for the repopulation. The dose rate modifies the quadratic component, i.e., the repair of the strand breaks if the cells repair some of the total damage during irradiation:

$$BED = D \cdot \left(1 + G \cdot \frac{d}{\alpha/\beta}\right) Gy_{\alpha/\beta} \quad (6)$$

where G is the dose rate factor for the intracellular repair of radiation lesions called the Lea-Catcheside G factor.

Dose rate effects are of importance for TMI treatment. Older total body irradiation (TBI) treatment was administered with the patient in an extended surface-to-skin distance (SSD) position of up to 4.5 m. This reduces the dose rate, and the difference in dose rate from that in a TomoTherapy device, which is 10–15 fold, can affect the treatment results, for example, for radiation pneumonitis (RP) in TBI [42]. Lately, other radiobiology factors have emerged in radiobiology. Research on cancer stem cells, cytokine signalling, intra-tumour signalling, and immunotherapy has led to insight into cancer and tissue response to RT [43, 44].

2.8 Mycosis fungoides

Mycosis fungoides is a cutaneous T-cell lymphoma, generally affecting the skin with symptoms such as rash, plaque, ulceration, and skin tumours. It is an uncommon disease occurring in 0.3 of 100,000 persons worldwide [45]. The patient is usually a long-term survivor with a median survival time of 15–30 years if the disease does not engage deep-seated visceral organs, and the treatment is usually seen as long-term palliative. There are numerous available treatments, such as UV(B), steroids, chemotherapy, and RT, with fractionated RT commonly being administered with electrons to a total dose of 12–36 Gy. The target in RT is the epidermis and the underlying cutaneous tissues.

2.9 Leukemia

Leukaemia is a bone marrow-derived clonal malignancy that produces an uncontrolled mass of immature, immune-incompetent white blood cells or blasts. In Sweden, there are approximately 700 new cases of leukaemia each year [2]. In acute leukaemia, the malignant

cells consist of early-stage blasts normally destined to form lymphocytes (in ALL) or myeloid cells (in acute myeloid leukaemia [AML]). The disease often has a rapid onset and early life-threatening symptoms of bone marrow failure (due to the abundance of leukemic cells present), severe infections, and bleeding. A quarter of patients with ALL are children. In chronic leukaemia, both chronic myelogenous leukaemia and chronic lymphocytic leukaemia, the malignant cells are later-stage or nearly mature white blood cells, still abnormal and with compromised immune competence. Symptom progression is often slower and less dramatic, and the course of the disease may span decades. Multiple myeloma is a malignant disease that stems from cells destined to be antibody-producing plasma cells.

2.10 Treatment of blood cancers

Common blood cancer diseases that are treated with RT are aggressive leukaemias and lymphomas, such as ALL, including younger patients with AML and extramedullary disease. Hematopoietic stem cell transplantation (HSCT) is often the only curative treatment option for patients with recurring or high-risk haematological malignancies, and it always includes a preceding conditioning regime with chemotherapy and optional RT. The objective of such full conditioning regimes is to eradicate possible remaining subclinical leukaemia cells and, importantly, to enable immunological suppression for the allogeneic stem cell transplant to become established in the recipient patient's bone marrow.

A comprehensive description of the treatment of leukaemias is beyond the scope of this presentation, but the treatment will be briefly summarised. Overall, chronic leukaemias occur in older patients; the disease may be kept at bay with relatively low-toxicity treatments, and recently also with disease-specific targeted therapy. The diseases are chronic, rarely completely curable, and, due to age and co-morbidities, the patients are rarely candidates for intensive chemotherapy treatment or stem cell transplantation.

Acute leukaemias, when occurring in young-to-middle-aged patients, are treated with intent to cure. Schematically, treatment consists of intense chemotherapy to induce remission, followed by consolidating courses of chemotherapy to reinforce the leukaemia-free remission. A cure is attainable, but depending on the presence of high-risk factors such as how the leukaemia was present at diagnosis, involvement of sanctuary sites such as the central nervous system (CNS), and molecular variants known to carry a high risk of subsequent recurrent disease, some patients may be identified as at increased risk of relapse. Such high-risk patients and patients with recurring acute leukaemias are candidates for allogeneic, or non-self-derived, HSCT in order to improve the chance of cure.

Human leukocyte antigen

Human leukocyte antigen (HLA) is the human version of the major histocompatibility complex (MHC) that encodes surface proteins. These surface proteins regulate the immune system and, as such, are essential in stem cell transplantation. Any cell with HLA types other than those of the immune cell is seen as non-self by immune cells, causing them to attack the cell. This means that transplanted immune cells can attack the host if there is an HLA mismatch, which is the most common cause of graft-versus-host disease (GvHD). Allogeneic transplantation became feasible after HLA was identified. The HLA complex is linked to chromosome 6, and this complex and chromosome are inherited together from a single parent; two siblings have a one-in-four probability of being HLA identical and thus avoiding rejection of the allograft. In matching siblings, this is the most favourable donor–recipient combination. However, improved knowledge of the complexity of the immune system has led to unrelated donor–recipient pairing also being common, albeit incurring a higher risk of GvHD. New technology has increased the speed and certainty of donor–recipient matching, as have centralised donor registries, and the World Marrow Donor Association (WMDA) currently has 39,224,035 registered donors [46].

T cells

T cells, or T lymphocytes, are a family of immune cell types derived from stem cells in the bone marrow that mature in the thymus and play a paramount role in the cell-mediated immune response. As such, the patient's T cells may put the donor HSCs at risk of an attack by the recipient, particularly in allogeneic transplantation with a non-sibling donor. T cells present in the donor hematopoietic cell population may also increase the risk of an attack on the recipient patient's tissues. Therefore, patients with unrelated donors generally have anti-T cell antibody treatments included in the pre-transplantation conditioning regime, and the donor cells are T-cell depleted. Depletion of T cells in the graft reduces this effect but increases the relapse rate, illustrating the donor T cells' role in the graft-versus-leukaemia (GvL) effect; it has been suggested that most acute GvHD (aGvHD) is mediated by cytokine dysregulation, which harms the healthy tissue. In addition, these effects can be seen in the mismatch between HLA-identical siblings who differ in proteins encoded by genes not part of the MHC. The T cells play an essential part in the GvL effect and are an essential part of the treatment when HSCT is used as a treatment alternative.

Cytokines

Cytokines are soluble proteins used in cell-to-cell communication. They are used in differentiation, inflammatory, and anti-inflammatory signalling between cells. They often

respond to stimuli and have a short half-life with few exceptions, most notably haematopoietic growth factors. The intended cell target of the cytokine has receptors that the cytokine binds to, triggering signalling within the cell and modifying the gene transcription (i.e., how the DNA is copied to RNA). Hence, they alter the differentiation and proliferation of the cell and induce or modify the function of the cell. Different cytokines work in synergy or antagonism in the same cell, which has the correct receptors, and their function can depend on the concentration and timing of different cytokines.

Some cytokines regulate or inhibit tumour cell growth, having anti-proliferative effects or pitting the immune cells against the tumour cells. This discovery led to research on cancer therapy with cytokines. For example, two different cytokines, interleukin (IL)-2 and (interferon-alpha) IFN- α , have FDA approval for cancer therapy, in which they activate the patients' immune system to be cytotoxic against the cancer cells. However, these therapies are highly toxic and have a low response rate. Nowadays, regulators combined with immune checkpoint inhibitors that remove the cancer cells' defence against T cells are being researched.

Relevant cytokines are granulocyte-macrophage colony-stimulating factor (GM-CSF) and granulocyte colony-stimulating factor (G-CSF); they stimulate the bone marrow causing blood cell growth, of granulocytes and stem cells, respectively. Here, GM-CSF helps stimulate myeloid reconstitution after bone marrow transplantation. Colony-stimulating factor 1 (CSF-1) causes HSCs to differentiate into macrophages and related cell types. Stromal cell-derived factor-1 (SDF-1) with its cognate receptor, CXCR4, is expressed in many cell types. It activates leukocytes and may be induced by proinflammatory activity and creates signals that regulate HSC trafficking in the bone marrow. SDF-1 is produced in the bone marrow and can act as an attractor of blood stem cells, regulating cell survival and cell cycle status. Its function is vital in the adult bone marrow; together with a specific antagonist of CXCR4, it induces rapid and robust HSC mobilisation. In preclinical trials of human AML engraftment, the addition of SDF-1 antibodies and a few other antibodies caused the homing of tumour cells to the bone marrow to be blocked [47]. Also, studies have shown that the SDF-1/CXCR4 axis affects the intratumoral immune cell subsets and the immune response to tumour cells [43].

The HSC population gives rise to all parts of the immune system. Undifferentiated, it usually resides in the bone marrow. The binding to the CXCR4 receptor of SDF-1 provided by the bone marrow promotes survival. Ionising radiation has been shown to stimulate HIF-1 and SDF-1/CXCR4 signalling by means of several processes, directly or indirectly via radiation-induced cell killing and the resulting hypoxia [48, 49]. Bone marrow stem cells can be recruited to a site of radiation injury in a regulated process modulated by several agents such as G-CSF.

Hematopoietic stem cell transplantation

There are two main types of transplantation, allogeneic and autologous, with autologous transplantation only being used in bone marrow rescue and not in combination with RT. When the patient receives stem cells from another person, it is called allogeneic transplantation. Autologous transplantation is when the patient's own stem cells are transplanted after treatment.

In the case of allogeneic HSCT, treatment is usually administered in several stages. Having identified a transplant donor on the basis of compatibility with the recipient, both patient and donor undergo a series of examinations to identify any medical conditions influencing the probability of surviving the subsequent intensive treatment (for the recipient) and safely going through with the donation procedure (for the donor). Prior to the HSCT itself, a conditioning regime is administered to the patient to eradicate any possibly remaining subclinical leukemic cells and suppress the patient's immune system, preventing rejection of transplanted stem cells. These pre-transplantation regimes may be based on chemotherapy or a combination of chemotherapy and RT. Myeloablative conditioning (MAC) regimes are highly toxic and generally reserved for young patients. In contrast, reduced-intensity conditioning (RIC) regimes are less intense and intended more for GvL/immunological effects in fragile patients. Commonly, the indications for RT are:

- Lymphatic malignancies such as ALL, lymphoma, and selected young high-risk myeloma
- Leukaemia with involvement of the CNS and/or testis, or a high risk thereof
- HSCT indicated for younger patients under 40 years old
- Particular forms of leukaemia with involvement of viscera, lymph nodes, or tissues
- Extramedullary disease

Deviations from these indications is not uncommon, for example, HSCT have been used as treatment alternative for patient over 40. For many high-risk patients, the only curative option is HCST, which remains the most effective way to cure high-risk refractory leukaemia [50]. The patient can receive donated marrow from either a sibling or a registered matched unrelated donor. Today, with modern sequencing techniques, mutations can be detected and distinguished and patient treatment can be customised based on this information, since different mutations are associated with different level of success, especially in chemotherapy.

Specifically, HSCT is used when leukaemia is not responding to chemotherapy, recurs after standard treatment, and the patient is relatively young, i.e., under 40 years old. The stem

cells are either collected from the blood as in peripheral blood stem cell transplantation (PBSCT) or bone marrow transplantation (BMT) is conducted. Stem cells split into either daughter cells that retain stem cell properties or progenitor cells that can differentiate into other types of blood cells. Here, the cell surface CD34+ is used as a marker to estimate the number of blood cells collected and transplanted.

Bone marrow cells continuously detach from the bone marrow and can be harvested from the blood, eliminating the need to harvest them from the bone marrow. The donor receives granulocyte colony-stimulating factor (G-CSF) to increase the detachment from the bone marrow. In contrast to bone marrow-collected stem cells, the peripherally collected stem cells result in more rapid haematopoietic recovery, since they contain more mature mononuclear T cells. Peripherally collected stem cells increase the incidence of chronic GvHD [51] but induce a faster GvL effect.

Chemotherapy and RT are used as immunosuppression measures to permit engraftment. Specifically, whole-body RT is used since it is not cross-resistant with chemotherapy and can reach sites that chemotherapy cannot. Some cancer cells even survive the RT before stem cell transplantation but are killed by the immunological active donor cells/lymphocytes. Fractionation reduces toxicity in RT, which is well known. A higher total dose in RT correlates to lower relapse but does not increase overall survival, probably due to toxicity [52]. For a schematic presentation of RT in HSCT see figure 11.

Graft-versus-host-disease

GvHD is divided into acute and chronic forms and can occur after allogeneic (i.e., from foreign donor) stem cell transplantation. It occurs when immune cells in the donor tissue, the graft, attack the host's tissue and cause several complications. The risk of GvHD can be 20–80%, depending on how close the match is between donor and recipient (i.e., host). Acute GvHD (aGvHD) is defined as graft-versus-host events occurring within 100 days of transplantation, whereas chronic GvHD (cGvHD) is defined as graft-versus-host events occurring up to a year after transplantation. Typical complications are dermatitis (skin inflammation), hepatitis (liver inflammation), enteritis (bowel inflammation, including diarrhoea), and vomiting. Acute GvHD increases the risk of developing cGvHD. Severe GvHD is associated with reduced long-term survival in the form of treatment-related mortality (TRM)[53], since severe GvHD requires more immunosuppression, which increases the risk of infections and is followed by TRM.

About 40% of leukaemia patients undergoing HSCT die from complications or relapse [54]. Today, TRM occurs in about 4% of HSCT patients at Skåne University Hospital. Cytokines are critical to GvHD development, exerting an influence through genetic variations, with HLA grade matches being the most critical factor. Trials of the inactivation of

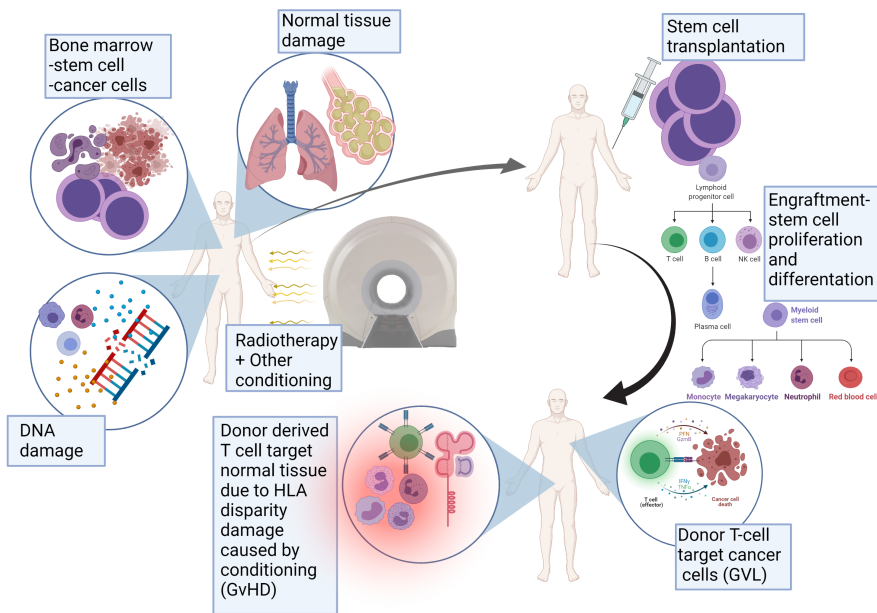


Figure 11: Immune system and RT in transplantation. The radiotherapy causes DNA damage, which, if extensive, can cause acute and chronic tissue toxicity; the goal is to deplete the bone marrow of stem cells and kill the remaining leukaemia cells. The stem cell transplantation is performed on the last day of RT after the last dose of RT. The donor stem cells adhere to the bone marrow, proliferating and differentiating into different blood and immune cells. The donor T cells can kill the remaining cancer cells and target the patient's own tissue due to the difference in HLA, which the immune cells wrongly interpret as foreign cells, in what is called graft-versus-host disease (GvHD). Created with BioRender.com.

relevant genes in mice have eliminated death from GvHD in mice [55].

T cells play an essential part in GvHD. The process begins when the T cells act on incompatibilities in the recipient cells and antigens. This reaction can lead to a plethora of host tissue injuries of minor or greater severity. The severity of the manifestation depends on the degree of the difference in HLA antigens and on the graft alloreactivity, i.e., the T cells' ability to react to differences in the MHC. In HSCT, the allogeneic graft causes the recipient's immune system to react to the compatibility of the recipient's and donor's immune systems, i.e., the HLA match of the host's T-cells may recognize the donor stem cells as foreign and reject the graft, although the risk of graft rejection with TMI/TBI is rare. In the inverse T-cell reactivity, donor T-cells may recognize the host environment as foreign and cause GvHD, albeit a tempered such reaction is wanted as a corollary as a graft-versus leukaemia effect [56], but graft rejection is rare.

Matched recipient HLA improves engraftment and lowers the severity and occurrence of GvHD. A large part of the clinical manifestation of GvHD in HSCT comes from the host tissue activating T cells derived from donor cells that respond to differences in the MHC. Here, the conditioning regimes have a significant impact on how GvHD occurs [53]. TBI

and other conditioning regimes are used to reduce underlying disease and suppress the host immune system defence in order to prevent donor graft rejection. However, this can cause damage to host tissue when cells from the damaged tissue activate inflammatory cytokines. Here, increased expression of antigens may increase the likelihood that T cells will discover incompatibilities in the MHC. The donor-derived T cells attach to host cells in the developing phase of GvHD and start releasing inflammatory cytokines, depending on the mismatch in MHC, which activates more T cells or other immune response cell types, such as NK cells [53].

Milgrom et al. [57] quantified patients who had undergone allogeneic SCT and later received RT. GvHD in this setting is relatively uncommon (5%), but offers an interesting perspective on the pathways involved. The radiation-related inflammation caused the grafted immune cells to attack the patients' healthy cells upon radiation injury, although the study design hinders us from deriving a causal relationship between RT and GvHD. Thus, RT potentially triggers GvHD via local damage and the subsequent induction of pro-inflammatory pathways.

Transplant-related mortality (TRM) and GvHD remain prominent complications in HSCT, so reducing toxicity is vital to increasing survival [58]. Clift et al. [59] showed that the probability of moderate to severe aGvHD was 0.21 for a 12.0-Gy group and 0.48 for a 15.75-Gy group ($P = .02$) in a randomised trial with TBI, i.e., no sparing of normal tissue. Patients exposed to the higher irradiation dose had a higher incidence of aGvHD. The increased dose of TBI significantly reduced the probability of relapse but did not improve survival because of increased mortality from causes other than relapse. In a large Japanese study, Naksone et al. [60] analysed 6848 patients who had received HSCT with both myeloablative conditioning (MAC) and RIC with TBI. Both were associated with aGvHD in older patients; the high-dose regime with TBI had an adverse impact only in HLA-matched HSCT. This is similar to previous findings concluding that conditioning intensity, TBI, and graft source affect aGvHD [61].

3 Optimisation of treatment plans for large targets in helical tomotherapy

In this section, selected dose planning and treatment optimisation aspects will be presented from papers I and II. Planning targets that span the entire patient length entail several unique challenges in HT that were addressed similarly in both publications, albeit with some variations.

3.1 Background

Mycosis fungoides is a rare form of non-Hodgkin T-cell lymphoma mainly affecting the cutaneous tissue, occurring in around 3 per 1,000,000 person-years in Sweden. Total skin electron beam therapy (TSEBT) is considered the standard treatment today. TSEBT is administered with the patient standing on a rotating platform or in several fixed positions at an extended SSD of 3–8 meters and offers good short-term remission and few reported cases of severe toxicity [62]. However, not all cutaneous tissue can be irradiated using this technique, and patch fields with x-rays are needed for areas not reached with the electron treatment. Furthermore, if any part of the patient must be avoided, lead shielding is needed, which is common for the genitals, eyes, and lips; this makes the technique cumbersome. Alternatively, the patient can be treated in two parts (i.e., upper and lower body) using HT with the patient prone on the couch, and OAR and previously irradiated areas can be avoided.

TBI is used in conditioning regimes to suppress the immune system and eradicate tumour cells before HSCT. The lower relapse rate when patients are treated with RT and chemotherapy versus chemotherapy alone [63, 64] validates its use. The treatment is primarily given to younger high-risk patients with haematological malignancies. The technique is robust and straightforward and can be performed on almost any linac accelerator. However, the entire patient is irradiated, so no organs are avoided unless shielded with lead blocks. Commonly, the lungs are shielded, but this creates considerable dose heterogeneity and can still cause pulmonary toxicity. Toxicity has ruled out any further dose escalation in TBI. RT targeting the bone marrow, such as HT TMI, can be used to avoid OAR and increase dose homogeneity in the targeted bone marrow, lowering toxicity, increasing engraftment, and improving outcome. TBI before HSCT has been administered to patients since the 1960s [65] and the first publication with successful allogenic SCT was published in 1977 [66]. In some treatment centres, TBI has been replaced with IMRT to target the bone marrow while sparing normal tissue [8]. The implementation of this technique with HT is the focus of Paper 1, which focuses on how to plan, verify, and deliver robust TMI.

The most commonly prescribed dose for TMI is 12 Gy [67], although it is administered in different fractionations (often in six fractions). However, the actual dose to the PTV differs between studies due to differences in normalisation. The planned normalised dose varies between the median and prescribed doses, reaching up to 95% coverage, and this lack of consensus hampers the comparison of treatments. Often, 95% volume of 95% dose coverage is deemed good enough for TMI plans. Pneumonitis correlates with TRM [52], which constrains the average lung dose to being under 9.4 Gy [68] or under 8 Gy [69]. Several dose planning parameters face similar challenges in both TSI and TMI. Pitch and other optimisation parameters and how to optimise the junction between the dose plans for the upper and lower body are addressed analogously.

In IMRT optimisation, a superficial PTV causes the TPS to increase the photon fluence in regions with low electron build-up, which can create over-optimisation and, in turn, lead to high-dose spots, primarily when daily setup deviations are incorporated. To mitigate this effect, a virtual bolus has been suggested [70]. The virtual bolus is an optimisation structure with a defined density in the planning software other than 0 g/cm^3 outside the external structure of the patient. This increases or decreases the dose to the superficial target in setup errors, but can increase the overall dose since the additional fluence is administered to the patient when the virtual bolus is not present during the treatment.

3.2 Materials & Methods

General dose planning aspects

In Paper II, we developed an IMRT treatment technique to treat the entire skin for mycosis fungoides. In addition, our focus was on uncertainties in setup and delivery and on the novel use of surface scanning. For any RT, immobilisation mitigates effects that stem from uncertainties in day-to-day variation in the setup before irradiation and from movement during irradiation. This effect is critical in large-body irradiation due to the large target and long treatment times. Dose planning of TSI was performed with predefined pitch, the largest FW, and over 500 iterations. In large-target optimisation it is generally helpful to split the target into several sub-volumes, to use several aiding structures, such as concentric rings around the targets, and to subtract the OAR overlapping the target with a margin of a few mm. The treatment planning aim was a prescribed dose of 60% to PTV with 95% of the prescribed dose to 95% of the volume of the targeted PTV. The internal part of the patient was blocked against beamlets traversing the patient to a depth of 2–3 cm, creating tangential irradiation of the skin.

Pitch is the fractional beam overlap per rotation. The cone-beam and other effects in HT can create ripples in the longitudinal direction if optimisation is not done correctly due to inherent machine properties, especially for lateral targets. In addition, too short or too long an overlap between revolutions can strain the MLC or create sub-optimal plans due to too fast or too slow gantry rotation.

In whole-body tomotherapy, junction plans are needed to keep the dose close to the prescribed level over the area where the upper body plan stops and the lower body plan starts on the patient; the patient is repositioned between the plans, so uncertainties regarding the position between the plans need to be addressed to avoid over- or underdosage to the target. There are several different ways to create a junction and treat the lower body in TMI, as described in the literature [71, 72, 9]. The lower body can be treated using a conventional linac, TomoDirect, or HT. Small children <140 cm tall may be treated with one field/treatment run. When treating the junction with a linac, the beam penumbra caud-

ally/cranially is matched with the penumbra of the HT treatment. When optimising with HT and TomoDirect, the treatment time and conformity can be similar, using natural fall-off or optimisation volumes. Zeverino et al. [9] used optimisation volumes, but as their technique relied on altering the metadata in the treatment files, it may be not feasible in many clinics. Generally, added optimisation volumes over a longer part of the junction translate to improved optimisation and a more robust junction but prolong the treatment time somewhat. The natural fall-off cranially/caudally in HT can be used, but achieving an excellent homogenous overlap region using this technique is not easy. Generally, two plans with different CT sets cannot be matched in the TomoTherapy or Precision system and need to be transferred to an external system.

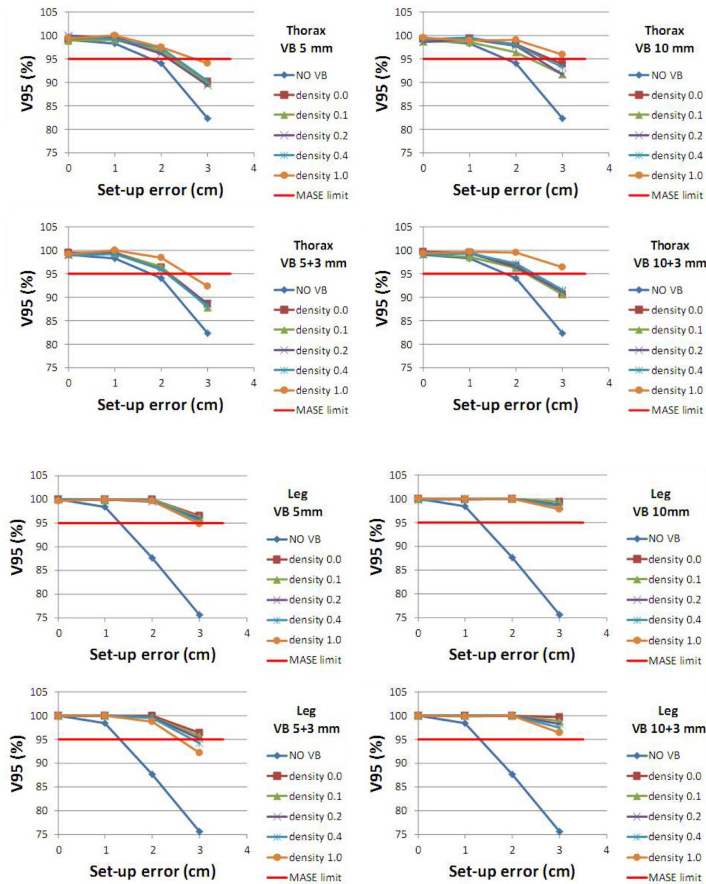


Figure 12: Illustration of the virtual bolus (VB) according to Moliner et al. [70], where the difference in V95% to the PTV is measured in terms of different VB thicknesses and densities, different margin extensions outside the body, and different extra bolus outside the PTV.

Bolus in large target helical tomotherapy

The use of a bolus in HT treatment for TSI has been debated. Serfahni et al. [73] used no bolus, whereas other treatment centres [74], including ours, have used a bolus for TSI as described in Paper II. In our case, a virtual bolus of 0.4 g/cm^3 was used with a physical whole-body, neoprene skin bolus to balance the different aspects.

The optimal density for the bolus depends on the situation. When a small part of the target is superficial, a water-equivalent density might be prudent, but this may cause an extra dose to be delivered to the patient, far beyond the prescribed whole-body skin treatment. Moliner et al. [70] investigated different margins and densities with setup errors (Figure 12). They found that a virtual bolus with a density of 0.4 g/cm^3 and a thickness of 8 mm was a good compromise between bolus thickness and peak effect/setup accuracy for the targets used in their study.

3.3 Results & Discussion

General dose planning aspects

From experience, we learned that in dose planning for TSI, immobilisation is essential and should optimally keep the patient's back in as close to a cylindrical shape as possible, with the arms tight to the chest wall. Also, too large a patient can be difficult to impossible to handle – the largest patient handled in Paper II was 190 cm tall and weighed 90 kg at treatment. This limitations depends on the 40-cm width of the treatment beam, limiting the number of angles with which a wide patient can be treated. The planning is performed with the skin as the target and is optimised using blocking structures to prevent beams from deeply penetrating the patient's body (Figure 13). The blocking structure needs to be experimentally determined depending on the patient, usually 3–4 cm from the external structure of the body and adjusted at the shoulders. This ensures tangential irradiation of the skin to prevent direct irradiation straight through the patient. Unfortunately, this also creates ineffective irradiation due to the limited range of the opened leaves. In general, doses to OAR and target were satisfactory (Figure 14).

In Paper I, we published a TMI technique using surface scanning and strove to reduce uncertainty by conducting robust calculations and measurements. Dose planning of TMI is, as in TSI, a complicated procedure that takes time and practice to achieve good results. Other publications have shown a 30–70% reduction in the dose absorbed by selected organs as compared with TBI, which is consistent with our results in Paper I. In general, we achieved good results in the dose sparing of normal tissue and the dose coverage of the target in patients covered in Paper I (Figure 15). However, the treatment was hampered by a long beam-on time and long image acquisition time of approximately 18–22 minutes in

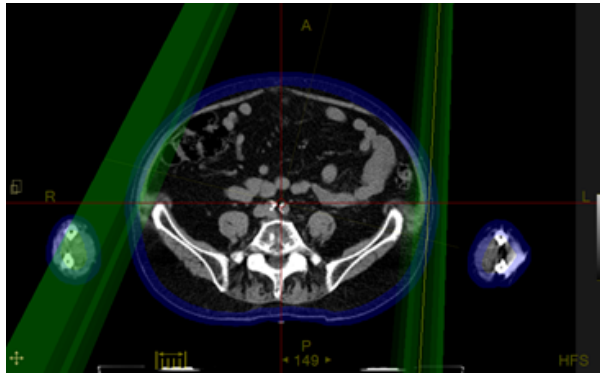


Figure 13: Illustration of the opening of the MLC (green) at one gantry angle for total skin irradiation, with the inside of the patient being blocked to prevent irradiation directly penetrating the patient.

HT, and by complex delivery, but this problem has been significantly reduced thanks to our implementation of SGRT. Our publication expands on current knowledge and presents a technique to account for uncertainties and machine constraints.

Choosing optimal planning parameters such as pitch, MF, and FW is a similar challenge in both TSI and TMI, but for patients who receive TSI, it was even more complex to reach peripheral parts of the target. If the patient is too wide, this problem could be partly mitigated by tightly immobilising the patient in a vacuum bag.

We used an FW of 5.02 cm in our publications to reduce the treatment time. The FW scales linearly with time, making the treatment time cumbersome for a full-grown adult using a 2.5-cm FW. For children treated under sedation, an FW of 2.5 cm is possible.

The actual MF directly scales with beam-on time. For TMI, several factors are proposed in the literature [75, 76, 77, 72, 9] and consensus is lacking. A higher MF reduces the dose to OAR and increases the dose homogeneity in the target. The MF should be determined based on the complexity and planning goals versus treatment time trade-off. We used an initial MF of 2.5–3.0 for both TSI and TMI, where the actual MF was usually 0.2–0.5 lower after the final calculation. This was followed by optimisation by gradually lowering the MF and optimising 20–50 iterations before lowering the next step until a good trade-off is achieved, as recommended in the literature [78]. A reduced MF of 1.5 has been used for lower body optimisation, which considerably reduces treatment time but was possible due to the uncomplicated target shape and relative lack of dose-sensitive OAR in the lower extremities.

Takahashi et al. [79] investigated the effect of dose ripple amplitude for large targets at a pitch of 0.430. They found the ripple to be 9.2% at 20 cm off axis, but it decreased to under 2% at a pitch of 0.200; the maximum ripple amplitude was seen at a pitch of 0.556. Their findings were verified with EBT₃ film dosimetry. The pitch value recommended by Kissick

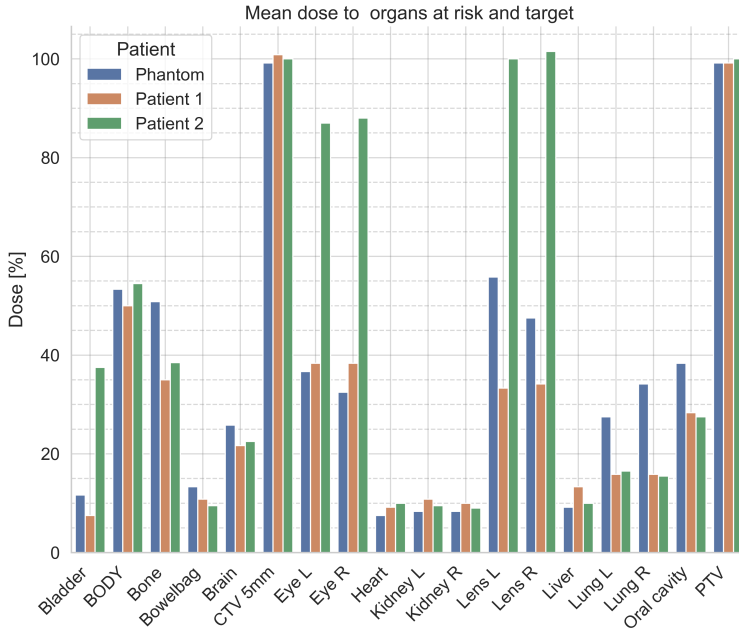


Figure 14: Mean doses to organs at risk and to the target for the phantom study and the first two patients optimised for TSI treatment.

et al. [10] of $0.86/n$ seems to be suboptimal off axis and only valid at the isocentre axis. A low-ripple pitch allows more time for the MLC to modulate the dose. Chen et al. [11] theorised that the pitch ripple effect depends on several factors, including the cone effect, source to target per angle, and off-axis distance and FW. They derived an equation and calculated optimal pitch for different off-isocenter-axis positions and FWs, simulated in a cylindrical phantom. A faster gantry speed, which can be offset by a lower pitch, prevents higher-intensity modulation, resulting in a trade-off between dose modulation and thread amplitude reduction. As stated by Chen et al., the ripple can be smeared out by ‘blurring’ the dose using robust calculation or optimisation. Thus, the optimal pitch is dependent on the width of the target. A good start was to follow the pitch as recommended by Chen et al., but to reduce the gantry speed by lowering the pitch to ease the burden on the air supply.

For the junction of treatment plans, in Paper I we explored a technique using a natural fall-off, but that technique was soon changed. In Paper IV, we conducted a retrospective follow-up; by then, many of the junctions were being optimised using at least four fall-off regions as optimisation structures. The robustness of this junction method regarding translational setup uncertainties has been evaluated for up to 1 cm with good results. We conducted a thorough test by shifting the isocentres of both the upper and lower body plans 5 mm in each direction relative to each other and recalculating a total of 48 plans.

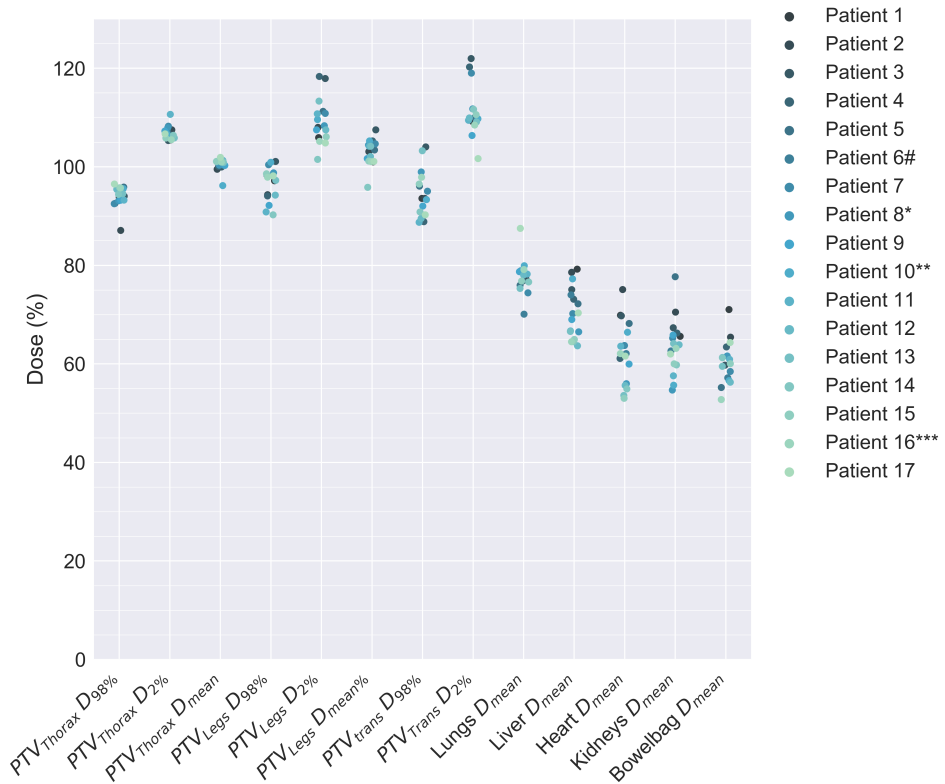


Figure 15: Mean dose (Dmean) to organs at risk, near maximum dose (D2%), and near minimum dose (D98%) to the target with lower body and upper body plans summed but excluding any boost treatment. Doses are normalised to the prescribed dose and patients are numbered consecutively. PTVThorax extends from the vertex to upper thigh, including the dose from the lower body plan above the junction. PTVLegs extends from the toes to upper thigh, including the dose from the upper body plan below the junction. The transition volume (PTVTrans) extends 1 cm cranially-caudally (a total of 2 cm) across the junction. # Patient 6: missing data for PTVLegs and PTVTrans due to corrupt data file. Patient 8: prescribed dose of 8 Gy/4 F. **Patient 10: prescribed dose of 6 Gy/3 F. ** Patient 16: prescribed dose of 11 Gy/4 F. Data from paper 1.

The junction volume was defined as 2 cm in each direction cranially-caudally from the junction marker on the thigh (Figure 16). In later work, Sresty et al. [80] investigated the junction volumes after an optimisation of the junction from 10% to 90% of the prescribed dose over 10 cm, similarly concluding that an optimised junction yields the correct dose coverage over the junction volume.

Bolus

There are a few arguments in Paper 11 for the use of a bolus in TSI. If no virtual bolus is used, over-optimisation in the build-up region will overdose parts of the patient by as much as 30% over the prescribed dose if the patient is not precisely positioned during treatment.

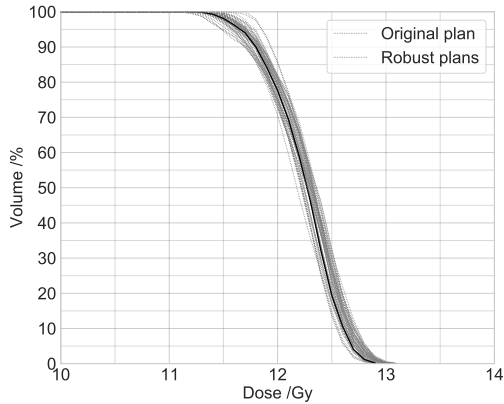


Figure 16: Robust test of the junction in TMI treatment. A 4-cm long part of the PTV over the junction was evaluated. Each plan was shifted ± 5 mm.

Using only a virtual bolus, the skin in the build-up region will be underdosed, and an overly dense virtual bolus will result in an extra dose to the patient beyond the target depth. In Paper II, we used a combination of a virtual and physical bolus to mitigate movement, setup uncertainties, and inherent optimisation effects for the robust planning of the whole-body irradiation of the skin. In vivo measurements with film were used for the first 1 or 2 fractions for each patient to verify the use of the bolus and setup. The resulting measurement showed generally good agreement with the planned dose. The actual point dose from the TPS was hard to verify, but the measured value was close to the prescription dose, i.e., with a mean difference from TPS of 5.3% (SD = 11.9%) and 1.5% (SD = 9.0%) for patient 1 and 2 that received TSI. A comparison of measured versus planned dose is seen in figure 17 for patient 1.

4 Verification of complicated treatments

In this section, selected aspects of the subject verification of the delivery of complicated HT treatments will be presented and discussed.

4.1 Background

Modern RT involves many agents and is a complicated system of imaging, contouring, target definition, planning, and treatment delivery. RT is one of many treatment options and thus lends itself to a multidisciplinary approach for best effect.

Accurate, robust, and reproducible dosimetry is essential for the verification of large HT

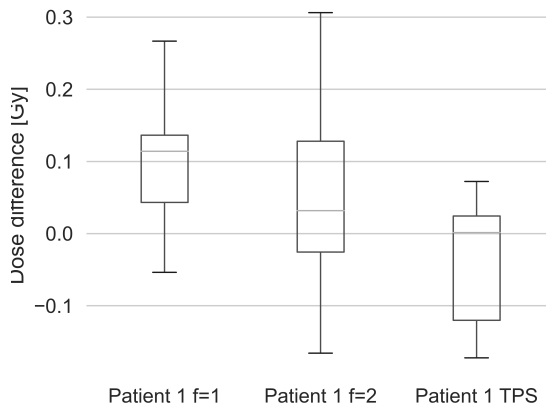


Figure 17: Comparison of in vivo measurements versus a random sample of the TPS dose to target equal to the number of measurement points. For fraction 1 ($f=1$), and fraction 2 ($f=2$) and planned dose (TPS).

treatments. In our papers, we used a combination of a 2D-3D diode array phantom, film dosimetry, and other phantoms to verify the deliverability of the treatments.

The accurate, reproducible, and fast setup of the patient is important for successful RT treatment, especially in large-target HT. The treatment margins are calculated based on the uncertainties associated with the treatment. Thus, in Paper III, we evaluated the significance of surface scanning in HT over a pure laser-based setup. In addition, time gain with the use of surface scanning over a laser-based setup was evaluated. Treatment time can affect the uncertainties associated with the treatment due to how patient intrafraction movement tends to increase with time, which has a dosimetric impact [81].

4.2 Materials & Methods

Multidisciplinary development and implementation of new treatment techniques

In papers I and II, we illustrated and discussed difficulties, pitfalls, and solutions for the entire treatment chain when implementing TSI and TMI. We described forming a multidisciplinary group consisting of all personnel involved in the treatment and presented our analysis of that treatment, end to end: determination of the conditioning regimen for RT, patient immobilisation, computed tomography (CT), target and OAR delineation, treatment planning, QC, setup and imaging, treatment, and backup planning. The entire RT treatment chain was described, extending from immobilisation to backup planning. Specifically, the multidisciplinary approach helped in the process, including the time man-

agement of the treatment, which is essential for increasing efficiency.

There were several issues to address during clinical implementation. The patients were immobilised in a vacuum bag (thermoplastic, five-point mask), immobilising the head and shoulders and keeping the arms close to the body. A whole-body 7-mm neoprene suit was used for the bolus. The patients were scanned and treated in two parts, the upper and lower body, with a junction over the thigh. The CTV was defined to a depth of 5 mm beneath the skin surface, and the PTV was a 5-mm isotropic expansion of the CTV. Later, we adjusted the PTV for the hands, feet, and stomach to address anatomical and setup problems as well as daily variation. Optimisation was challenging, but planning on an anthropomorphic phantom was a helpful learning experience since problems such as dose delivery to the back and arms of the patient had already been investigated. We optimised with a 0.4 g/cm^3 , 8-mm virtual bolus.

Dosimetry

For all our measurements in Paper II, an Epson 1000 XL was used, with 48-bit transmission settings using filmQA software (Ashland Advanced Materials, Bridgewater, NJ, USA) in papers I and II. The raw pixel value depends on the dose and film pixel position, especially in the transverse scanning direction. To account for exposure polymerisation, we allowed for a 12–24-h pause, or simultaneously irradiated a film from the same sheet and batch with a known dose to account for inhomogeneity and polymerisation. Intra-sheet and intra-batch homogeneity need to be examined at a dose of zero before use, or separate calibration curves should be used. We used triple-channel evaluation, since it has been found to be better than single-channel evaluation [21].

For Delta4 measurements, the gamma pass rate was evaluated using a 3% DD and a 2-mm DTA from the global dose, with a dose under 15% as the threshold.

Surface scanning in helical tomotherapy

In total, 16,835 treatment fractions were analysed in Paper III. The difference between the laser-based and surface-based setups was compared, using the built-in MVCT as the ‘gold standard’ for the setup. The residual deviation between the two deviations and the image-to-beam on-time difference were evaluated.

4.3 Results & Discussion

Multidisciplinary development and implementation of new treatment techniques

Generally, good immobilisation was crucial for TSI dose planning, especially keeping the back rounded and the arms very tight to the body, since the patients were generally wider than the transverse beam size of 40 cm. The arms and shoulders are only irradiated from limited angles, requiring higher MF values and thus longer beam-on times. Today, a typical setup of patients with long targets can involve a combination of surface scanning and MVCT covering only a few centimetres after 2 or 3 fractions with full-target daily imaging. Discussing daily imaging with all relevant professions present helped in the development of setup and immobilisation management; nurses, the physician, and the physicist were present during imaging, and the physicist was present with treatment personnel for immobilisation during the reference CT, the creation of the immobilisation setup, and the first fractions of the treatment, creating a feedback loop in this important step.

The target volumes in TSI were defined as the cutaneous tissue, to a depth of 3–5 mm from the external skin surface. The PTV margin in Paper II was an estimate of the geometric uncertainties, which amounted to 5 mm from the CTV. Hsieh et al. [74] did not find a 5-mm PTV margin sufficient and therefore extended the margins on the shoulders and chest to 8 mm and 1 cm, respectively. Similarly, we found a need to adjust the PTV margins around the stomach and feet on several treated patients due to setup uncertainties, weight loss, and patterns of diaphragm breathing or tension.

The first patients treated at our clinic with TSI were pre-positioned using surface scanning and verified using daily imaging MVCT (Figure 18). The resulting registration was applied and used in treatment. After treatment, the daily image was recalculated to verify good target coverage. Daily CTV coverage was satisfactory for patient 1 calculated using re-delineated CTV on the daily images for all fractions (Figure 19), and verified using film dosimetry (Figure 17).

Verification is necessary for TSI treatments due to the complexity of irradiation. In Paper II, we verified the treatment using several of the above-mentioned systems and in vivo measurements of the first fraction with consistent results, but acted on doses to regions parallel to the beam, such as the skin of the sole, and areas varying greatly during treatment and between fractions, such as the abdomen.

Our verification demonstrates that we have developed a robust technique for TSI treatment. Moreover, the process described can be used for implementing other complicated treatments. Few publications address TSI using HT. In a short work, Guerts et al. [82] investigated TSI using film, a TomoPhantom, and an anthropomorphic phantom with some shifts for uncertainty analysis. Later, Serfehnia et al. investigated and treated a patient [73]

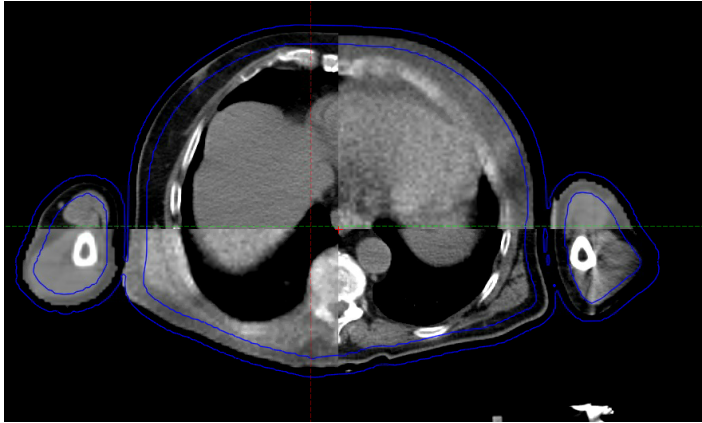


Figure 18: Daily image of the first patient treated with TSI at our clinic, shown with a split window where the daily MVCT has more noise and less contrast. Generally, with a good match between reference and daily image.

with TSI. They verified using film in a phantom and reported the setup, other treatment-related events, and, as in our study, uncertainties in the abdominal area and similar or higher doses to OAR. We did not encounter similar problems with the setup as Serfehnia et al. did, perhaps due to more experience with full-body treatments, differences in immobilisation, and our use of surface scanning equipment. The same treatment centre later reported a patient who received TSI with 40 Gy in 30 fractions [74], avoiding a previously treated area on the patient's side. As in our study, they used a 5-mm PTV, which was expanded to 1 cm in the chest and abdomen. They used a wetsuit type bolus and a virtual bolus but without reporting the bolus density. They reported in vivo film measurements with up to 40% deviation from the prescribed dose.

Similarly, the TMI treatment was developed and iteratively improved through a multidisciplinary approach and by evaluating the results. The first 15 TMI patients were evaluated by registering their daily images to reference CTs, re-contouring the CTV to the daily image, and recalculating the plan for all fractions; the result for an example TMI patient receiving 12 Gy in six fractions is shown in figure 20. The daily delivered dose to the CTV can be evaluated by summing all fractions in a total DVH, called a dose-coverage histogram (DCH). As reported in Paper 1, for patients calculated with DCHs, 98% of the prescribed dose to at least 93% of the target volume was achieved for 100% of the planned fractions and 90% of the delivered fractions.

Zuro et al. [83] reported on the accuracy of setups in TMI patients and the impact on dose delivery in a multi-institutional trial. Unsurprisingly, they concluded that a high registration mismatch correlated to a greatly affected fractional dose and, when comparing partial registration with full-body registration, that full-body registration lowered the uncertainty in dose delivery, which was dependent on patient immobilisation, the pre-treatment ima-

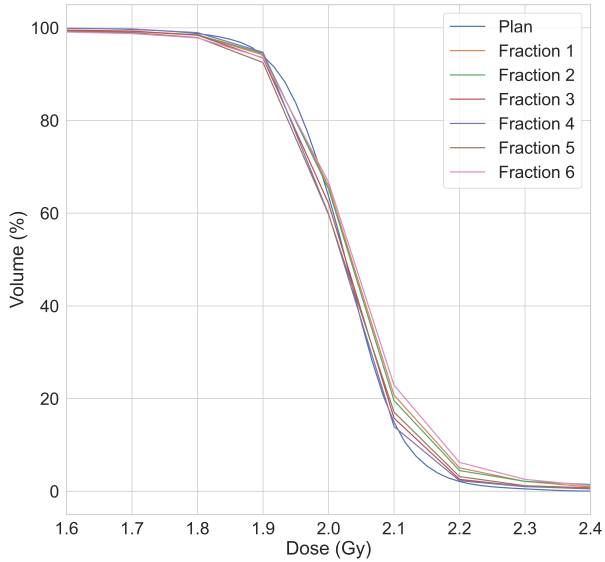


Figure 19: DVH for fractions 1–6 of TSI patient 1 and planned dose showing CTV coverage as calculated on the daily image using the target structure registered and transferred to the MVCT.

Delivered versus planned dose for example patient

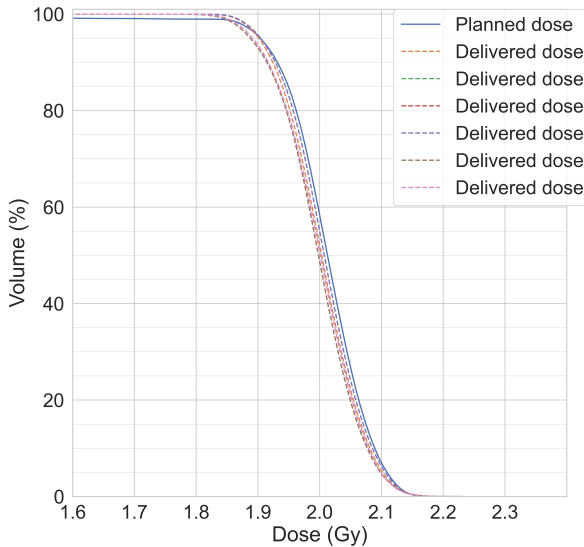


Figure 20: Evaluation of daily dose coverage for the CTV on a TMI patient. The daily image was registered to the reference CT, and the CTV was contoured on the daily image. The plan was recalculated with the daily image and evaluated.

ging protocol, and PTV margins. They evaluated the DD of the 90% dose between several structures, among others, the planned PTV to delivered CTV volume. The 95% confid-

ence interval was over 15% in two treatment centres for the skeleton as target. Comparison with our study is hampered, since the evaluations are for different volumes and doses, but their result emphasises the importance of evaluating the delivered dose, correct imaging, and the immobilisation protocol, as concluded in the article. Similar to their discussion, we conclude that for large-volume targets as in TMI (and TSI), seemingly small percentage deviations can amount to relatively large absolute underdosage volumes, which could in turn potentially affect the outcome if the underdosage hampers the immunosuppression or if more leukaemia cancer cells remain.

Dosimetry

Radiochromatic film was consistently used for the development as pre-treatment QA in Paper II and in vivo measurements for TSI patients. Each batch was calibrated separately, and a relative dose measurement from each sheet was used with a known dose as a reference.

In an earlier conference proceeding [84], we measured the ripple effect using the Delta4 external measurement system [84] (Figure 21). The results indicate that a plan-specific pitch value based on FW, MF, and the target's lateral localisation can affect the delivery quality of the treatment plan and should be compensated for during dose planning.

One disadvantage of the current dosimetry systems used is the limited volume of measurements. Large-target HT entails complicated delivery and complete patient-specific QA is essential. QA using the built-in detector array has been researched and applied in several publications [85, 86, 87, 88, 89, 90]. In a recent publication, Thiyagarajan et al. investigated the use of LOT for pre-treatment QA in TMI treatment plans. They concluded that the method was accurate and best suited for large treatment plans, and recommended specific plan parameters for optimal dose distribution, but only compared two pitch values quantitatively, 0.43 and 0.3, which weakens their recommendation. For HT on a TomoTherapy device, optimal parameters are still needed for good planning to ensure delivery consistency, and different dosimetry systems serve different purposes. To more easily find optimal parameters for deliverability on the TomoTherapy, a 3D array system or further development of the use of built-in detector arrays seems prudent. The applicability of these parameters and any possible variation in deliverability to the Radixact device has yet to be investigated. The Radixact uses a different method to compensate for the MLC latencies from version 2.0, for example, and this has an effect on the latency in fast treatment delivery. Hence, the Radixact may be more suitable for large-target HT.

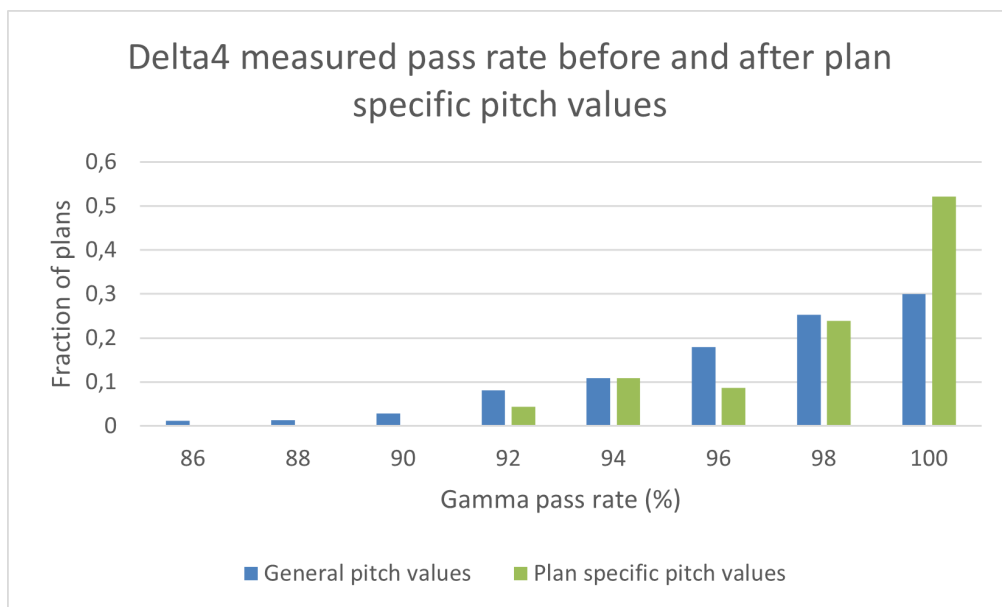


Figure 21: The Delta4-measured gamma pass rate: DD 3%, DTA 2 mm, threshold 15%, global dose. We measured clinical plans with and without plan-specific pitch values.

Surface scanning in helical tomotherapy

In Paper III we found that for patients immobilised with a three- or five-point mask, only 1.7% of the fractions positioned with surface scanning had a residual error larger than 5 mm, compared with positioning with a laser-based setup, in which 27.5% of the fractions had a residual error larger than 5 mm (Figure 22). With an NAL protocol, the laser-based setup can be corrected for the first three fractions; with that technique, 11.5% of the laser-based setups' residual errors were larger than 5 mm. The time saving was 3.8–5.0 min depending on the treatment site. Surface scanning of large targets differs somewhat from a conventional surface scanning setup on a TomoTherapy device. First, the limited FOV of the built-in MVCT rules out any daily imaging of arms, which is an integral part of the treatment and perhaps the hardest part to reproduce in the setup. In addition, due to the large target and few treatment fractions, surface scanning has benefits when used as a time-saving means to avoid rescanning due to patient re-setup. Also, the imaging techniques can be combined, such as an initial surface-based setup with a short MVCT imaging volume for verification. Using a more straightforward setup and omitting MVCT on the lower extremities are, in contrast, uncomplicated thanks to the rigid surface-to-target coherence. In papers I and II, we used surface scanning to position patients with large targets, reducing uncertainties and creating more robust delivery.

SGRT has many advantages in tomotherapy. In breast cancer tomotherapy, Crop et al.

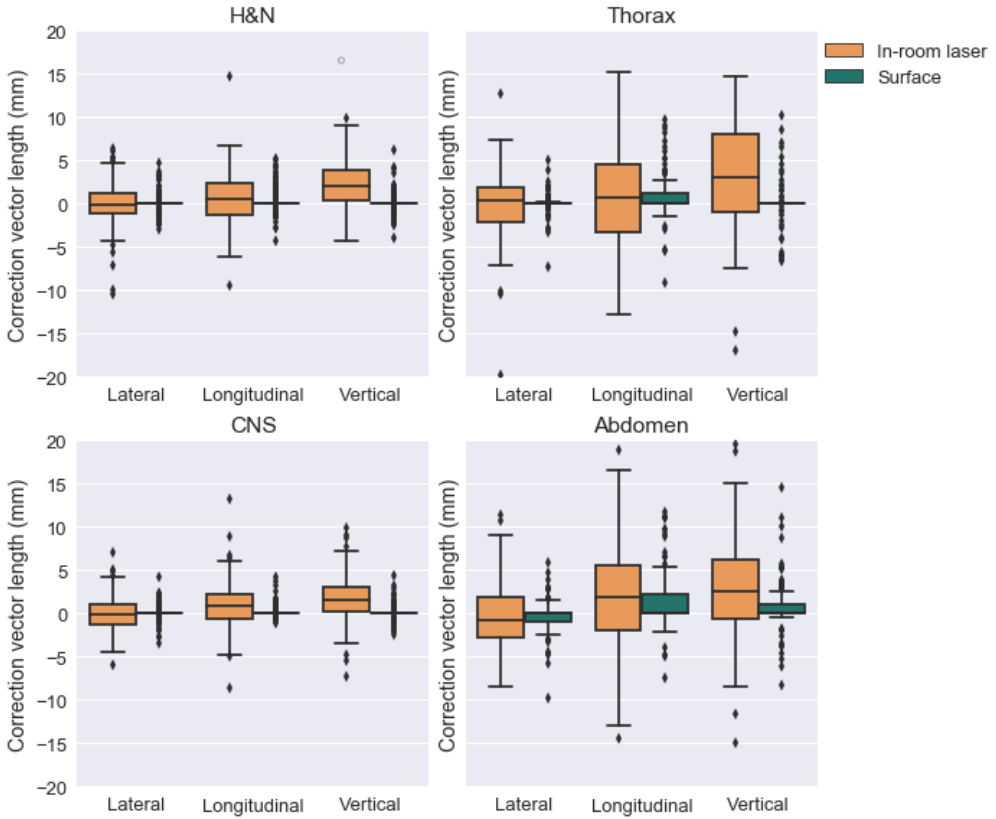


Figure 22: Correction vector length distribution for laser-based and SGRT-based setups, for four large treatment sites. From paper 111, with permission from the publisher.

[91] found that SGRT increased the efficiency and accuracy of positioning and generally in RT in other publications [32, 92]. The development of a closed-bore gantry surface scanning system has been tested [93]. Now, the TomoTherapy and Radixact devices have a system for the synchronisation of the breathing pattern, Synchrony. There are several key differences between the Catalyst SGRT system and Synchrony. Synchrony can alter the MLC pattern, follow the motion, and use both the breathing pattern and kV imaging. In contrast, the latest Catalyst HD system uses a three-camera setup and motion management, which improves efficiency in the positioning and sees the entire patient thanks to the three angles of projection, whereas MVCT has a limited FOV. In addition, SGRT could be used for breath-hold gating and has the advantage of separating the target from OAR such as the heart in, for example, breast cancer RT. Daily imaging with a fast kVCT image acquisition with a 50cm FOV could potentially change some of these advantages. However, SGRT will probably still be an effective way to set up the patient and reduce problems with rotation and positioning, especially outside the FOV of the daily imaging system.

5 Clinical aspects

This section will present and discuss a summary of clinical follow-up and outcome results from papers I, II, and IV.

5.1 Background

Mycosis fungoides has been treated with RT since the 1960s [94], and the standard treatment today is a technique using TSEBT [45]. Traditionally, a prescribed dose of 30–36 Gy over 6–10 weeks has been recommended [45], but lately, doses as low as 10–12 Gy have been used as step-wise short-term palliation [62]. The advantages of lower-dose regimes are several: the treatment time is shorter, good remission is maintained, it permits retreatment several times, and toxicity is lower. TSEBT is administered with the patient either on a rotating platform or in several fixed positions at an extended SSD of 3–8 meters to reach all parts of the skin. The technique has good short-term remission prospects and results in few reported cases of severe toxicity [45]. However, not all cutaneous tissue is irradiated with this technique and many patched fields are needed to cover the feet, hands, scalp, and other areas, raising questions regarding junction doses, and the technique is somewhat cumbersome due to the need for shielding.

An alternative treatment is total skin irradiation with HT. This complex RT can be more accurately planned, skin folds and areas difficult to reach with electrons can be adequately covered, and sensitive sites, such as eyelids and lips, can be avoided [95, 73].

In total body irradiation (TBI), the entire body is irradiated, but sometimes the lungs are partly shielded. The main targets are the red bone marrow, where the leukaemia resides and the stem cells are located, and usually the spleen; in cases of ALL, the leukaemia sanctuary sites, i.e., CNS and testicles, are also targeted. Primary OARs are the lungs, kidney, liver, spleen, and heart. RT is administered as fractionated RT with 2–3 Gy per fraction once or twice daily up to the equivalent of 12 Gy in 2 Gy per fraction [9, 67, 96]. The dose specification point varies, but usually is the mid-point dose at the thorax or stomach. The lungs can be shielded to reduce the risk of severe lung complications, which can be fatal [68]. In addition to tumour-cell kill, TBI is immunosuppressive to prevent the rejection of donor haematopoietic cells [42].

Alternatively, the treatment can be administered with HT as TMI, avoiding organs at risk such as lungs, stomach and liver.

A concern when changing treatment modality and technique in RT is that dose-rate-related response can affect treatment depending on the type of lesion and type of delivery; this has been addressed to a large extent in other works, and it is put into context here. A smaller

work on the subject is presented. Pulmonary toxicity is highly associated with TRM [97], and a higher dose rate has been found to be associated with a higher incidence of RP [98]. Pulmonary complications of allogeneic HSCT can be severe, accounting for up to roughly 25% of transplant-related deaths in some studies [14, 99]. Shinde et al. evaluated a dose rate range of 5.6–20.9 cGy/min with TBI and reported a dose rate of 200 cGy/min for their HT TMI treatments, which is a reasonable assumption regarding dose rate based on target depth. Since the treatment is administered in a helical overlapping pattern, the question is how to assess the dose-rate effect.

Joiner et al. [100] examined the effect of IMRT and dose rate on human cancer cell lines when treatment times were extended to 5–45 min; the loss of effect was 5.6–11.7% for single fractions. However, this effect is probably mitigated in HT since the radiation deposition is very heterogeneous in each revolution and subfield, and for cancers, the effect can be diminished by re-oxygenation in vivo and due to fractionation.

Similarly, the rate and quality of engraftment are dependent on the conditioning prior to HSCT and thus, in large part, prior to RT. That a switch from TBI to TMI affects engraftment is possible but complex to determine. The differences in dose coverage of the target and in the volume of tissue irradiated could potentially affect the following transplantation and engraftment.

5.2 Materials & Methods

Treatment of mycosis fungoides lesions on the skin

In Paper II, we developed a novel tomotherapy TSI technique and determined its feasibility, deliverability, and robustness regarding uncertainties with our verification systems. The technique was successfully delivered to two patients and later (not reported here) to a third. It has also been used clinically for partial-skin irradiation.

Total marrow irradiation

We developed and verified a technique in Paper I, helical tomotherapy to the bone marrow, TMI. In contrast to TBI, the only parts irradiated to the prescribed full dose in TMI are the bone marrow compartments and spleen due to the haematological buffer there, and for ALL patients also the CNS and, in males, also the testicles. The delivery of TMI was set up not to increase the complications and to keep the prescribed dose to the targeted bone marrow, similar to treatment with TBI.

In Paper IV, we followed the patients regarding the outcome in terms of adverse events and

the side effects of the pre-transplantation conditioning, development of GvHD, and TRM. A total of 37 TMI patients and 33 TBI patients were analysed in our follow-up.

Dose rate and dose volume effects

We retrospectively evaluated the dose-rate-dependent differences in haematological recovery and engraftment after allogeneic stem-cell transplantation in a shorter work. Subsequently, we adapted a compartment model from Ward et al. [101], Getto et al. [102], Marciniak-Czochra [103], and Stiehl et al. [102, 104] that was developed for HSC differentiation, according to:

$$\frac{dc_1}{dt} = (2a_{1,max}s - 1)p_1c_1 - d_1c_1 \quad (7)$$

...

$$\frac{dc_i}{dt} = (2a_{i,max}s - 1)p_i c_i + 2(1 - a_{i-1,max}s)p_{i-1}c_{i-1} - d_i c_i \quad (8)$$

$$\frac{dc_n}{dt} = 2(1 - a_{n-1,max}s)p_{n-1}c_{n-1} - d_n c_n \quad (9)$$

and,

$$s = \frac{1}{1 + kc_n} \quad (10)$$

where $c(t)$ is the population cell density at time t for compartment i to n , $s(t)$ is the signalling molecules, $p(t)$ is the proliferation rate at time t , and $a(t)$ is the fraction of daughter cells that stay undifferentiated; the death rate is denoted by $d(t)$ and k is the cytokine signalling at the constant rate through which the signalling decays in relation to the presence of mature stem cells.

5.3 Results & Discussion

Treatment of mycosis fungoides lesions on the skin

The strength of TSI is its versatility: it can be used for a simultaneous integrated boost (SIB) for plaque or to avoid previously irradiated skin areas or OAR. Its disadvantages include time-consuming optimisation, cumbersome positioning, especially with a bolus, and that the additional radiation scattered in the patient to the bone marrow affects its production of blood cells. The last issue demands careful monitoring of the blood cell count, particularly the radiation-sensitive and rapidly affected level of blood platelets and white blood cells, as

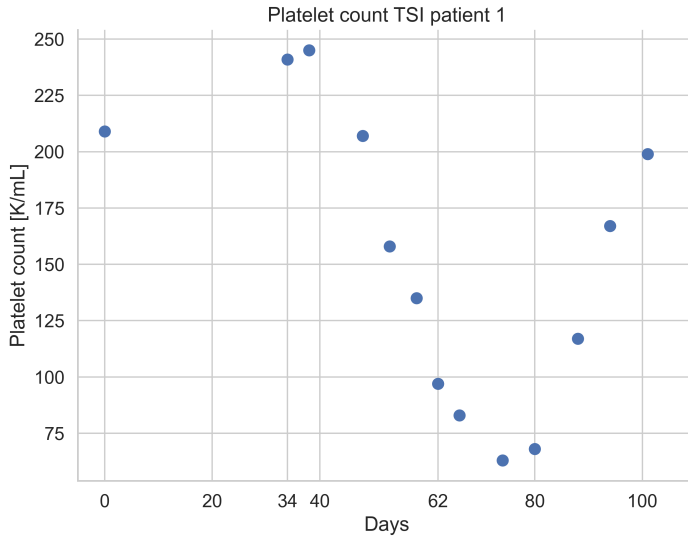


Figure 23: Thrombocyte count during TSI of patient 1 ($K/\mu L$). The patient started RT on day 34 and ended on day 62, with an average dose to the bone marrow of 0.6 Gy/fr, with the pelvic bone and spine receiving <0.3 Gy and <0.2 Gy per fraction, respectively

in our patient 1 (Figure 23). The first patient was a 72-year-old, 190-cm tall male diagnosed with mycosis fungoides in 2003. He had previously received RT via kilovoltage X-ray on several occasions and had also been treated with PUVA plus Methotrexate, Neotigason, and Targretin. At the time of TSI, he had patches and plaques covering more than 10% of his body surface. The patient handled the treatment well, but exhibited mild symptoms such as pain on the soles of his feet and under his chin. The patient was prescribed a mild sedative to handle the long treatment time.

There have been reports of grade V leukopenia events with higher doses (20 Gy) of photon treatment in partial TSI when some patients had previously undergone TSEBT [105].

Serfehnia et al. reported that their patient needed supportive care in the form of hematopoietic colony-stimulating factors (CSF), steroids, antioxidants, oral glutamine, and yeast-derived 1,3/1,6 glucopolysaccharide, but reported complete response. They concluded that haematology response/side effects need to be addressed in high-dose TSI.

In contrast to previous findings, our low-dose (12 Gy) treatment in six fractions was feasible without severe complications. We have reported a thorough analysis of the effects of the uncertainties on the setup and delivery of the technique, analysing the effects of the virtual bolus, physical bolus, setup uncertainty effect on target dose, and junction doses throughout the treatment with several different QA systems. In addition, our use of large-body surface scanning for setup has been shown to be effective for these types of treatments.

Total marrow irradiation

In Paper IV, we followed the patients regarding the outcome in terms of adverse events and side effects of the pre-transplantation conditioning, including the development of GvHD, TRM, and other side effects and outcome results. Most importantly, the one-year graft-versus-host-free survival (GRFS) was 67.5% for TMI and 39.4% for TBI with a Hazard Ratio (HR) of 0.45 ($p = .027$), and for a patient with matched unrelated donors, the GRFS was 80.5% and 42.3% with an HR of 0.24 ($p = .003$) for TMI and TBI, respectively.

Looking forward, it should be possible to use the innate ability of intensity-modulated therapy to alter the dose distribution and target less or more of the patient, depending on conclusions drawn from our and others' research. The dose distribution in HT with lower doses to OAR may affect GvHD, as presented in Paper IV. This is interesting for several reasons. GvHD is affected by the conditioning regime preceding the HSCT. The acute tissue damage due to RT is generally repaired but creates an inflammatory response that the grafted immune cells react to [106]. However, since the prescribed dose is generally low, the occurrence that stems directly from RT damage is perhaps not dominant. The altering of the immunoresponse is of interest in connection with RT's direct cancer-killing effect (i.e., the radiation's ability to create a niche in the bone marrow for the transplanted CD34+) and the transplanted T cells' effect on leukaemia. Thus, how the RT fractionation affects these parameters merits further investigation.

Other normal tissue toxicity occurrences were minor compared with other adverse events in the patients, such as GvHD. There was only one serious liver complication (i.e., veno-occlusive disease) and two pulmonary events, probably only one of which was RP. We demonstrated a significant difference in renal toxicity between the two RT types. However, the difference was not clinically large to the extent that it would affect the patient, and the renal toxicity was generally not high. In addition, there was no general decline in FEV₁ in any patient group after irradiation and HSCT. Oral mucositis can be quite severe after RT when the oral cavity is included, and therefore also occurs in HSCT with RT and chemotherapy. Direct mucosal basal cell injury can lead to atrophy, ulcerations, and local infections that can become systemic. All followed-up patients experienced mucositis, and the vast majority had grade \geq III mucositis, consistent with other studies [107]. Generally, our experience with normal tissue toxicity is in line with a recent study that specifically followed up 142 patients [69] who had received TMI prior to HSCT. They reported a 1/142 incidence of RP, no renal toxicity, 6% hypothyroidism, and 7% cataract formation. They concluded that a mean lung dose of 8 Gy or less was associated with fewer pulmonary complications.

Dose rate and dose volume effects

In Paper IV, engraftment measured as the recovery of blood cell concentration was significantly faster in terms of the restored platelet count in patients treated with TMI than TBI. However, the result was not robust since the effect was not significant in terms of days to reach a neutrophil count of 1.0 and 0.5 (K/ μ L). Of note, Hui et al. compared TBI with TMI in rodents [44]. They hypothesised that the lower radiation dose to the surrounding tissue resulted in a chemokine stromal-derived factor-1 (SDF-1) gradient, altering the engraftment rate. The effect could also be a consequence of the better irradiation targeting and more homogenous dose to the bone marrow niche creating more robust engraftment. We found that in patients receiving PBSCT, the mean time to engraftment as measured in terms of thrombocytes over 50 (K/ μ L) in TBI and TMI, respectively, differed significantly, with the stem cell source as a covariate (HR = 1.9; 95% CI = 1.1–3.2, $p = .02$). A Cox proportional model revealed the impact of the number of transplanted CD34+ cells, RT type, donor age, and stem cell source.

In addition, the dose rate could also affect the response and toxicity in RT treatment. Here, the local dose rate refers to the instantaneous dose rate to the targeted beam-on volume. This dose rate was increased approximately 30-fold in tomotherapy-delivered TMI compared with our previous TBI technique. The increase was due to the SAD of 85 cm in the tomotherapy and the dose rate of about 850 cGy/min, versus the dose rate of about 400–600 MU/min and the source-to-patient position of about 4.5 m in TBI. On the other hand, the global or overall dose rate to the target and patient decreased, since the beam-on time increased in TMI compared with TBI. For each revolution, the couch is moved 0.2–0.4 times the width of the beam at the isocentre, which is not necessarily spread evenly over each revolution. In addition, the dose coverage, mainly to the rib cage, changed between the treatment techniques, which could affect the result.

In a short publication [108], we used six compartments to model hematopoietic stem cell to platelet progression, with megakaryocytes splitting up to produce an average of 3500 platelets each. The cell dose (i.e., CD34 infusion), transplantation type, and RT type were modelled as the difference in initial uptake in the bone marrow of the infused CD34 cells, and the difference in dose rate was modelled as a scaled difference from the log cell kill of 1.9%, according to Fowler et al. [37]. In addition, a random component was added to the initial uptake of transplanted cells. An example of modelled versus measured platelet reconstitution in a patient is seen in Figure 24.

Our short work on modelling the dose rate does not shed light on the difference seen in our clinical follow-up. Our model was adapted to TMI patients, and the model correctly predicted the distribution of engraftment in the cohort, apart from one outlier (Figure 25). The model did not predict the difference in engraftment between RT types; on the contrary, the higher average CD34+ cell dose in the TBI cohort would suggest slightly faster

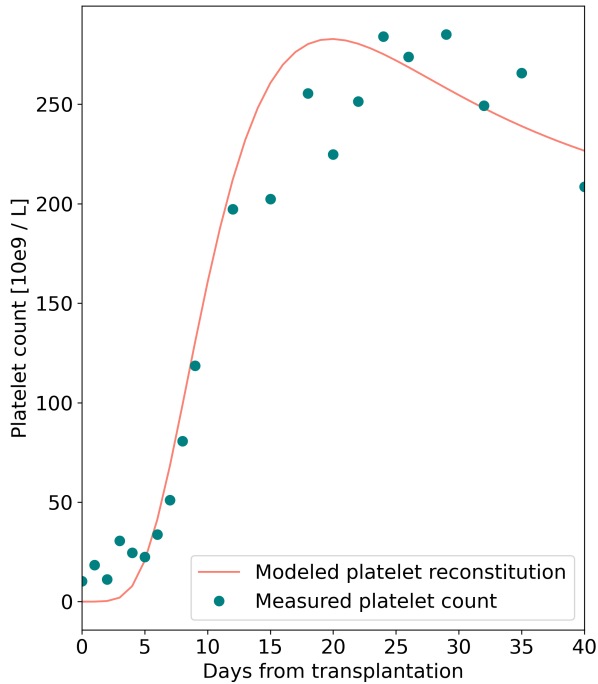


Figure 24: Platelet reconstitution after hematopoietic stem cell transplantation (HSCT) and radiotherapy in one patient who received total marrow irradiation prior to HSC. The model correctly depicts the initial recovery and maximum platelet count. The level of engraftment is 50×10^9 platelets per litre of blood, which makes the model sufficient for the current problem. Adapted from [108].

engraftment than TMI despite the 2% lower dose rate effect.

Dose rate and normal tissue toxicity

In Paper iv, there was no large reduction in mean lung dose compared with TBI; despite that, and in conjunction with a large difference in dose rate, no increase in RP was found. No general conclusions can be drawn regarding dose rate effects, due to the low incidence of toxicity related to dose rate effects. We delivered TMI with a dose rate to the lungs of approximately 200 cGy/min, but with the fractional dose divided over several gantry revolutions. The treatment was generally administered with a mean lung dose of under 9 Gy. Whether this is an effect in which the increased dose rate is cancelled by the helical pattern of the treatment administered is of interest if treatment centres want to implement TMI using VMAT. Then the treatment would be divided into several subarcs, with perhaps only one or two subarcs over the lungs administered over a few minutes. Since we are probably in a region of increased response to the dose rate when increasing from 10–20 cGy/min to 200–850 cGy/min, this could increase the risk of RP if the mean lung dose is

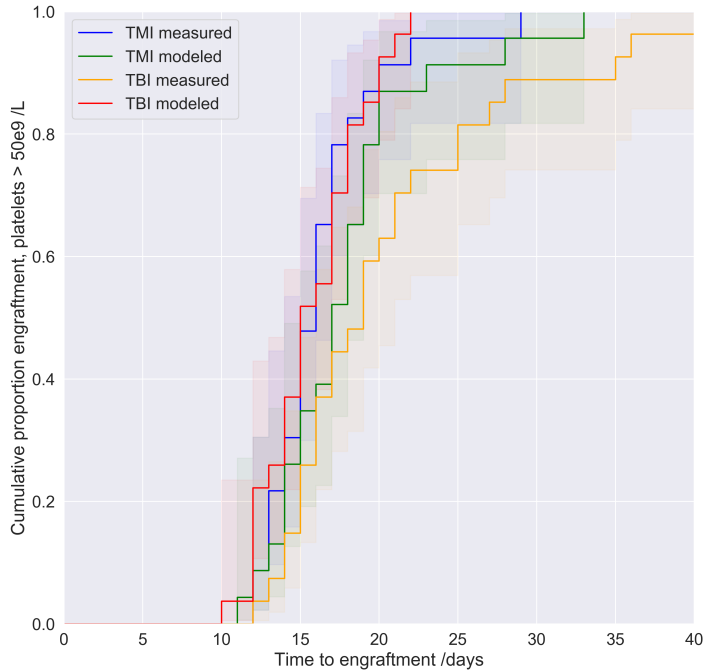


Figure 25: Time to engraftment for total marrow irradiation (TMI) and total body irradiation (TBI) as measured by a platelet count over 50×10^9 per litre of blood. The platelet reconstitution was modelled with a compartment model and varied with the transplanted CD34 cell dose count, transplantation type, and normally distributed random noise. The model parameters were adapted to one patient and applied to the cohorts with the difference in dose rate scaled to log cell kill being immunosuppressive, i.e., less initial uptake of transplanted CD34 cells. First published in [108].

not further lowered. Another explanatory model would be that high fractionation mitigates the dose rate effect, as reported in preclinical studies of bone marrow and lethality after TBI [109], where the authors concluded: ‘Once fractionated regimens were used, there was very little dose rate effect’. In addition, they concluded that BM effects were consistent, but that leukaemia radiation response displayed greater variation. Interestingly, in their study, fractionation did not spare BM much, but the lethal dose for 50% of population (LD₅₀) was significantly lowered to 120 cGy thrice daily, as used in their murine model study. As discussed in another publication [110], it can be hard to separate the effects of dose rate, fractionation, and differences in and lowering of normal tissue doses on the outcome and toxicity of the dose rate.

Sampath et al. [111] reported that the α/β value of the LQ model was estimated to be 2.8 Gy for the lungs. For interstitial pneumonitis (IP) as an endpoint, the D₅₀ was found to be 8.8Gy for TBI with 120 mg/kg of cyclophosphamide and 10.6 Gy without chemotherapy. Of note, no dose-rate effect was observed. Busulfan was found to be equivalent to RT with 14.8 Gy in four fractions with 50% transmission blocks shielding the lungs. Also, in a TMI treatment with HT, the dose to the lungs is extremely heterogeneous, being close to 1–2 Gy

at the centre of the lungs but closer to the prescribed dose on the edge of the lungs. If an optimised heterogeneous dose would cause a higher or a lower probability of IP or GvHD then an even irradiation is uncertain.

Dose-volume effects

It is not unlikely that the difference in engraftment effects between TBI and TMI seen in Paper IV, if associated with RT, stems from differences in irradiation accuracy and dose homogeneity to the target due not only to the optimised TMI treatment but also to the lead shields used in TBI at our treatment centre. These effects and possibly better medical treatments and dose-rate and dose-volume effects are hard to distinguish in a general clinical follow-up.

Since the dose rate effect might not be involved in the difference in engraftment response in GvHD, the explanation might be found in the difference in the size of the volume treated with RT or the difference in dose-volume coverage. The effect of the inflammatory response has been observed in rodents when comparing TBI and TMI [44]. A larger SDF-1 cytokine gradient in organs/BM was seen in TBI than in TMI, which was perhaps a reason for faster engraftment in TMI. Also, the levels of the GvHD-related tissue repair factor, i.e., epidermal growth factor (EGF), were significantly different in the intestine, specifically in the crypt cells. The EGF levels in TMI did not differ significantly from those in controls. The mechanistic role of SDF-1 in TMI is still somewhat uncharted, and there are many unanswered questions. The dissonance in the immunoresponse of the immune cells from the grafted bone marrow has been seen in a preclinical trial [112]. The authors showed that irradiation of the subject increased the SDF-1 expression in kidneys almost four-fold after the 40-Gy irradiation of zebra fish. Herberg et al. [113] found increased expression levels linked to SDF-1 in BM cells from irradiated subjects; this suggests spatial differences in the BM where SDF-1 differs in signalling and not only in the immediate cell surface microenvironment. The authors concluded that more studies are needed to assess the biological events following TBI that regulate the success of the HSCT, to better understand the alteration of the 'biological fingerprints' of the BM site and the preconditioning process.

Radiotherapy fractionation in HSCT

An important finding is that the intensity of the RT causes higher TRM and GvHD. The increased dose caused a higher immunoreactive gradient and increased T cell response intensity, causing severe reactions and inflammations in irradiated tissue. The lower relapse is in line with current knowledge of the effects of conditioning intensity in HSCT. The higher dose of irradiation increases the suppression of the host's immune system and stem

cells, and any remaining malignant cells. It thus increases the likelihood of engraftment by means of a larger gradient to the BM niche as well as the potentially greater anti-tumour activation of donor T cells. A view of this as an immunological therapy that relies on the graft-versus-leukaemia effect has been presented earlier [114] and is now seen as part of the treatment effect in HSCT. The dose-response properties of TBI in HSCT are known [115, 116]; specifically, a higher biologically effective dose in TBI was found to increase overall survival (OS) and disease-free survival and to decrease the incidence of relapse.

This opens discussion of the optimal fractionation scheme and the intended target in RT when introducing tomotherapy-delivered TMI. Irradiation causes inflammation and, in turn, GvHD from recipient-derived T-lymphocytes, and the effect is RT-intensity dependent. Normal tissue irradiation probably causes a cytokine gradient that attracts CD34+ stem cells and can alter the engraftment. In turn, irradiation creates room in the BM niche and adds anti-tumour-cell effects to other parts of the conditioning and to the anti-cancer effect of the donor immune system/T cells.

Thus, the bone marrow must be adequately irradiated at as high an intensity as possible. Relapse is the most common cause of death in this patient group. The fractionation should be chosen to be effective in tumour cell killing and bone marrow depleting. The intensity and fractionation should cause as little damage as possible, including inflammation/activation of the normal tissue's immune system. Finally, the irradiation timing should minimise the repopulation of the BM and tumour cells, and the timing of the stem cell transplantation after RT should maximise and minimise the influence of the negative and positive effects, respectively, of chemokine gradients by means of inflammation and attraction to the BM niche. Thus, the question arises of whether the known fractionation for early and late normal tissue effects is similar to the optimal fractionation for altering the immune system's inflammation response that causes T-cell homing and GvHD. Is there a dose-volume effect, and does it differ when creating chemokine gradients in the normal tissue that alter the homing of the transplanted CD34+ stem cells, and what is the dose-response effect? Does tomotherapy-delivered TMI lower the normal tissue toxicity and influence the development of GvHD, creating possibilities for increased RT intensity? How should such an increased intensity fractionation scheme be implemented? There are a few alternatives. First, the dose per fraction could be increased, keeping the total number of fractions and the irradiation time constant. The dose increases with either a higher prescribed dose or a higher intensity inside the BM than in the surrounding bony cortex (which lacks tissue). Two, the number of fractions could be increased jointly with the total treatment time, preferably without going over a weekend before transplantation to minimise the repopulation after/during irradiation; for example, our 2Gy/twice daily could be increased to 12 Gy with up to three additional fractions to a total of 18 Gy without irradiation during weekends. Third, further hyperfractionation could facilitate increased intensity without prolonged treatment time but with added work during late hours, with 1.5–2 Gy per frac-

tion three times a day. From what we know, bone marrow is highly radiosensitive, but blood cancers have a range of α/β values from 1.49 to 3.12 Gy [117]. Of course, from what we know, care should be taken when reducing the dose per fraction, but it could potentially reduce the GvHD and perhaps increase the stem cell homing to the BM in a hyperfractionation schedule if combined with dose escalation. Several dose escalation studies have been conducted. Escalation from 12–20 Gy with a fractional dose of 1.5–2.0 Gy over 4–5 days in ALL/AML patients [118] and 12–15 Gy in 1.5-Gy fractions [119] twice daily have produced encouraging outcomes in TMI. In addition, the technical feasibility of fractional doses of up to 8 Gy in TMI has been investigated with the BED kept below 12/2Gy in TMI treatments [120]. In 2017, Hui et al. [121] investigated 15 Gy and 18 Gy TMI dose escalation given with 3Gy/fraction together with cyclophosphamide (Cy) and fludarabine, to patients with refractory leukaemia or minimal residual disease. Three of six patient at 18Gy experienced TRM, for the 15Gy dose level the incidence of Grade III-IV acute GvHD was 25% and the 1-year OS was 42%. In contrast, Wong et al. [122] performed a split trail where group 1 combined VP16/Cy with RT and group 2 combined Busulfan with RT both groups were dose escalated using TMI with 1.5Gy/fraction to 12 Gy, 13.5 Gy and 15 Gy total dose. In group 2 dose limiting toxicities were seen at 13.5 Gy (stomatitis and hepatotoxicity), but no such events were recorded in group 1 where 1/12 experienced acute GvHD Grade III-IV. The authors concluded that dose escalation with the regime used in group 1 is feasible to at least 15 Gy total dose.

6 General discussion

TSI with HT has its limitations, but the technique's strengths can be used to develop a targeted technique in which only areas needing irradiation are targeted. The idea of 'total' irradiation of the skin comes from electron treatments that offered no alternative, as parts of the patient could not be easily shielded. TSI could also be viable in combination with irradiation of lymph nodes or other therapies (e.g., in combination with stem cell transplantation, which has been tested [123]). Similar to other complicated RT techniques with daily variations in setup, online adaptation would benefit the treatment. The optimisation and contouring could also be improved with AI-assisted tools. Similar to the conclusions of Buglione et al. [124], TSI with HT lends itself to easy modulation of the target, and thus is more suitable for limited irradiation of the skin and, additionally, for treatment centres not equipped for total skin electron treatment.

Zuro et al. [83] investigated margins in TMI and found that whole-body imaging was associated with lower setup deviations, but they did not include surface scanning as a tool in their study. SGRT can improve the efficiency and safety of total irradiation with HT, as discussed by Batista et al. [125]. Like all new techniques, the tool requires training for functional implementation. However, the efficiency it adds to total irradiation is evident

in Paper I, since it bridges the gap between the limited FOV and daily imaging time. In addition, motion monitoring would be beneficial for the treatment, since long treatment times cause increased patient movement [126, 127].

The technical development of HT continues. As stated by Wong et al. 2020 [110], ‘The exact role of total marrow irradiation or total marrow and lymphoid irradiation in new conditioning regimens seems dependent on its technological implementation, aiming to make the whole procedure less time consuming, more streamlined, and easier to integrate into the clinical workflow’. In part, papers I –III have aimed to implement this through surface scanning and clinical work with feedback. A few time-consuming obstacles are manual contouring, reported to require up to 12–16 h [71], and optimisation and related activities such as QA that can take 20 h. Moving forward, a few major recent technological advances could be implemented to increase effectiveness. Deep learning for auto-contouring has reached a point where implementation in the clinic is already viable [128, 129]. Scripting and Pareto-optimisation or other auto-planning capabilities are available from some vendors, which would increase effectiveness. QA can further be undertaken using built-in capabilities such as delivery analysis [130] to aid pre-treatment QA. The latest record and verify and planning system from Accuray IDMS/Precision, the Raystation planning system from Raysearch, and Radixact with Synchrony and ClearRT are the latest innovations. In turn, ClearRT is a kV tube fitted on the gantry orthogonal to the linac. Synchrony enables the tracking of tumour movement with or without fiducials, and Raystation can be used for scripting and machine learning planning. In addition, Precision software can utilise adaptive planning for the offline verification of dose delivery based on the recalculation on kV imaging.

To increase the accuracy, Synchrony-type tracking of target as developed by the TomoTherapy/Radixact manufacturer Accuray over the rib cage could be used as motion management with the new built-in kV CT. This could potentially increase the accuracy and efficiency of the treatments, thanks to imaging times shortened from 15 min to <1.5 min. The kV imaging and the possibility of adaptive planning lend themselves to offline adaptive planning based on daily imaging if the patient differs significantly in anatomy and setup from the reference CT. However, this offline re-planning will affect the following fraction, when the patients’ anatomy might have further changed. The actual implications for short treatments such as TMI are small unless particular circumstances such as a larger systematic deviation severely affect the treatment. However, the actual impact of the difference in dose can be recalculated daily and during setup thanks to the vast decrease in imaging time with ClearRT.

Online adaptive planning, i.e., adapting the plan to the daily anatomy between imaging and treatment, would considerably benefit the TMI treatment and probably significantly affect the outcome by substantially decreasing the irradiated volume. To implement this, the re-planning process for large targets such as upper body TMI should be shortened to under

20–30 min depending on the patient’s ability to lie supine for prolonged times. The dose to OAR and normal tissue could be decreased with this technique, so the improvement should be actively researched. For example, the margins used in our studies could be lowered to under 2–3 mm from the bone marrow in specific areas and to 3–5 mm for the extremities and ribs; in papers I and II, we generally used 10 mm for the body and 7 mm for the head and neck. Online adaptive planning would reduce the irradiated volume from 22,000 cc in an example adult patient to 13,600 cc with a 2–3-mm margin, a 40% decrease in the volume of irradiated tissue. Furthermore, using 4D-CT for margin calculation could improve the accuracy if applied to, for example, the rib cage, a vital part of the irradiation due to the dose-response to IP to outcome relationship.

6.1 Future perspectives

Today, there is a plethora of fractionations for use in TBI and TMI. The most commonly recommended fractionation is 2-Gy fractions once or twice daily, but 3-Gy fractions have also been used for historical and logistical reasons, but are associated with a higher rate of normal tissue complications, especially in the lungs, where two-sided RP can be fatal [68]. Interestingly, since the immunoresponse seems to contribute to the positive effects of RT, conventional radiobiology calculations of fractionation perhaps need revision. A new radiobiological practice or primer in which the fractionation is related to GvHD and haematological reconstitution would benefit the treatment. This could be investigated in more preclinical research or in a prospective clinical trial in which specific markers are followed during RT.

Due to the toxic nature of irradiation of the entire body, further research should focus on planning studies to increase the dose to BM without increasing the dose to normal tissue, especially those at risk of GvHD, such as the gut, oesophagus, mucosa, skin, and organs such as the liver, kidneys, and lungs. In addition, reducing planning margins and heterogeneous doses over the target could help improve the immunosuppression and killing of remaining tumour cells without increased toxicity. A reduced dose per fraction should be considered with conservative calculations of leukaemia fractionation sensitivity due to the wide range of α/β results in the literature. However, this could potentially mitigate the toxic RT effect on normal tissue while maintaining the immunosuppressive properties and cancer killing, as discussed in a preclinical study [109]. An increase in the total dose either through prolonged total treatment time or, preferably, while maintaining the same total treatment time should, in turn, be investigated. Any increase in total dose to normal tissue is expected to increase the risk of GvHD and probably the TRM compared with the same RT modality with reduced intensity unless the fractional dose is lowered. Thus, future research should focus on:

- Motion management for large-body HT using built-in surface scanning and other capabilities
- SIB or uneven irradiation of the skin with TSI for adaptive palliative treatment
- Increasing efficiency with AI-assisted tools, specifically auto planning and deep learning contouring
- Planning studies of heterogeneous irradiation and other techniques for delivering higher intensity to BM without increased dose to normal tissue
- Increased RT intensity with hyperfractionation

6.2 Conclusions

Papers I and II examined the deliverability, potential, and robustness of two different techniques, TMI and TSI. Paper III explored positioning in treatment on the TomoTherapy device with the help of surface scanning, as compared with laser-aided setup and daily imaging. This was put into perspective with the time gain of each imaging protocol. Finally, patients treated with TMI were followed regarding acute toxicity and haematological recovery in Paper IV.

Thus, treatment that is robust to uncertainties such as positioning uncertainty and daily variation was investigated, and conditioning on multi-person collaboration and iterative SGRT made the treatment more effective during clinical implementation. Furthermore, total skin irradiation was developed that was feasible, safe, and addressed difficulties in delivery and implementation regarding uncertainties in treatment delivery and effectiveness. Additionally, surface scanning and its use and time gain were investigated and evaluated through analysing a large number of patients. The clinical follow-up illustrated the potential and usefulness of TMI, with more patients surviving without severe complications after one year than was previously the case. Overall, the complications of large-target irradiation with HT were evaluated, and we demonstrated the usefulness of HT despite the difficulty of implementing large-target techniques.

7 References

- [1] O Bergman. *Cancer i siffror 2018 : populärvetenskapliga fakta om cancer*. Socialstyrelsen, 2018.
- [2] Cancerfonden. Cancerfonden.se. <https://www.cancerfonden.se/om-cancer/cancersjukdomar/blodcancer>, 2021. Accessed: 2021-08-21.

- [3] X Shi-Xia, T Xian-Hua, X Hai-Qin, F Bo, and T Xiang-Feng. Total body irradiation plus cyclophosphamide versus busulphan with cyclophosphamide as conditioning regimen for patients with leukemia undergoing allogeneic stem cell transplantation: a meta-analysis. *Leukemia & Lymphoma*, 51(1):50–60, 2010.
- [4] E. M. Quan, X. Li, Y. Li, X. Wang, R. J. Kudchadker, J. L. Johnson, D. A. Kuban, A. K. Lee, and X. Zhang. A comprehensive comparison of imrt and vmat plan quality for prostate cancer treatment. *Int J Radiat Oncol Biol Phys*, 83(4):1169–78, 2012.
- [5] T R Mackie, T Holmes, S Swerdloff, P Reckwerdt, J O Deasy, J Yang, B Paliwal, and T Kinsella. Tomotherapy: a new concept for the delivery of dynamic conformal radiotherapy. *Medical physics*, 20(6):1709–19, 1993.
- [6] T. R. Mackie. History of tomotherapy. *Phys Med Biol*, 51(13):R427–53, 2006.
- [7] Accuray Inc. Patient positioning workflows 1059569.d. Unpublished work, 2020.
- [8] SK. Hui, J Kapatoes, J Fowler, D Henderson, G Olivera, RR Manon, B Gerbi, T. R. Mackie, and JS Welsh. Feasibility study of helical tomotherapy for total body or total marrow irradiation. *Medical Physics*, 32(10):3214–3224, 2005.
- [9] M. Zeverino, S. Agostinelli, G. Taccini, F. Cavagnetto, S. Garelli, M. Gusinu, S. Vagge, S. Barra, and R. Corvo. Advances in the implementation of helical tomotherapy-based total marrow irradiation with a novel field junction technique. *Med Dosim*, 37(3):314–20, 2012.
- [10] M. W. Kissick, J. Fenwick, J. A. James, R. Jeraj, J. M. Kapatoes, H. Keller, T. R. Mackie, G. Olivera, and E. T. Soisson. The helical tomotherapy thread effect. *Medical Physics*, 32(5):1414–23, 2005.
- [11] Mi Chen, Y C, Q Chen, and W Lu. Theoretical analysis of the thread effect in helical tomotherapy. *Medical physics*, 38(11):5945–60, 2011.
- [12] P Hoskin, T Greener, M Kirby, H McNair, M Powell, D Routsis, and D Tait. *On Target: ensuring geometric accuracy in radiotherapy*. The Royal College of Radiologists, 2008.
- [13] M. van Herk. Errors and margins in radiotherapy. *Semin Radiat Oncol*, 14(1):52–64, 2004.
- [14] M van Herk, P Remeijer, C Rasch, and JV Lebesque. The probability of correct target dosage: dose-population histograms for deriving treatment margins in radiotherapy. *International Journal of Radiation Oncology*Biophysics*, 47(4):1121–1135, 2000.

- [15] H Boer and B. Heijmen. enal: An extension of the nal setup correction protocol for effective use of weekly follow-up measurements. *International journal of radiation oncology, biology, physics*, 67:1586–95, 2007.
- [16] D. A. Low and J. F. Dempsey. Evaluation of the gamma dose distribution comparison method. *Med Phys*, 30(9):2455–64, 2003.
- [17] R Sadagopan, JA Bencomo, RL Martin, G Nilsson, T Matzen, and PA Balter. Characterization and clinical evaluation of a novel imrt quality assurance system. *Journal of applied clinical medical physics*, 10(2):2928–2928, 2009.
- [18] Ugur Akbas, Nazmiye Donmez Kesen, Canan Koksall, and Hatice Bilge. Surface and buildup region dose measurements with markus parallel-plate ionization chamber, gafchromic ebt3 film, and mosfet detector for high-energy photon beams. *Advances in High Energy Physics*, 2016:1–10, 2016.
- [19] C. R. Ramsey, R. M. Seibert, B. Robison, and M. Mitchell. Helical tomotherapy superficial dose measurements. *Med Phys*, 34(8):3286–93, 2007.
- [20] IJ Das. *Radiochromic film : role and applications in radiation dosimetry*. CRC Press, 1st edition, 2017.
- [21] M. Mathot, S. Sobczak, and M. T. Hoornaert. Gafchromic film dosimetry: four years experience using filmqa pro software and epson flatbed scanners. *Phys Med*, 30(8):871–7, 2014.
- [22] L. Richley, A. C. John, H. Coomber, and S. Fletcher. Evaluation and optimization of the new ebt2 radiochromic film dosimetry system for patient dose verification in radiotherapy. *Phys Med Biol*, 55(9):2601–17, 2010.
- [23] J. Sorriaux, A. Kacperek, S. Rossomme, J. A. Lee, D. Bertrand, S. Vynckier, and E. Sterpin. Evaluation of gafchromic(r) ebt3 films characteristics in therapy photon, electron and proton beams. *Phys Med*, 29(6):599–606, 2013.
- [24] J. A. Snir, H. Mosalaei, K. Jordan, and S. Yartsev. Surface dose measurement for helical tomotherapy. *Med Phys*, 38(6):3104–7, 2011.
- [25] S. Devic, J. Seuntjens, W. Abdel-Rahman, M. Evans, M. Olivares, E. B. Podgorsak, T. Vuong, and C. G. Soares. Accurate skin dose measurements using radiochromic film in clinical applications. *Med Phys*, 33(4):1116–24, 2006.
- [26] J. E. Bekelman, J. A. Deye, B. Vikram, S. M. Bentzen, D. Bruner, Jr. Curran, W. J., J. Dignam, J. A. Efstathiou, T. J. FitzGerald, C. Hurkmans, G. S. Ibbott, J. J. Lee, T. E. Merchant, J. Michalski, J. R. Palta, R. Simon, R. K. Ten Haken, R. Timmerman, S. Tunis, C. N. Coleman, and J. Purdy. Redesigning radiotherapy quality

- assurance: opportunities to develop an efficient, evidence-based system to support clinical trials—report of the national cancer institute work group on radiotherapy quality assurance. *Int J Radiat Oncol Biol Phys*, 83(3):782–90, 2012.
- [27] S. S. Donaldson, M. Torrey, M. P. Link, A. Glicksman, L. Gilula, F. Laurie, J. Manning, J. Neff, W. Reinus, E. Thompson, and J. J. Shuster. A multidisciplinary study investigating radiotherapy in ewing’s sarcoma: end results of pog #8346. pediatric oncology group. *Int J Radiat Oncol Biol Phys*, 42(1):125–35, 1998.
- [28] E Dühmke, V Diehl, M Loeffler, RP Mueller, U Ruehl, N Willich, A Georgii, S Roth, D Matthaei, S Sehlen, O Brosteanu, D Hasenclever, R Wilkowski, and K Becker. Randomized trial with early-stage hodgkin’s disease testing 30 gy vs. 40 gy extended field radiotherapy alone. *Intl J Rad Onc Bio Phys*, 36(2):305–310, 1996.
- [29] International Organization for Standardization (ISO). Iso 9001:2015 quality management systems. Report, International Organization for Standardization, 2015.
- [30] P Nilsson, C Ceberg, E Kjellén, G Gagliardi, K Blomgren, S Nilsson, M Johansson, and B Glimelius. A template for writing radiotherapy protocols. *Acta Oncologica*, 54(2):275–279, 2015.
- [31] American Association of Physicists in Medicine (AAPM). Report no. 086 - quality assurance for clinical trials: A primer for physicists. Report 86, American Association of Physicists in Medicine (AAPM), 2004.
- [32] M Kügele, A Edvardsson, L Berg, S Alkner, C Andersson Ljus, and S Ceberg. Dosimetric effects of intrafractional isocenter variation during deep inspiration breath-hold for breast cancer patients using surface-guided radiotherapy. *Journal of Applied Clinical Medical Physics*, 19(1):25–38, 2018.
- [33] G. Carl, D. Reitz, S. Schönecker, M. Pazos, P. Freislederer, M. Reiner, F. Alongi, M. Niyazi, U. Ganswindt, C. Belka, and S. Corradini. Optical surface scanning for patient positioning in radiation therapy: A prospective analysis of 1902 fractions. *Technology in cancer research & treatment*, 17:1533033818806002–1533033818806002, 2018.
- [34] T. Moser, G. Habl, M. Uhl, K. Schubert, G. Sroka-Perez, J. Debus, K. Herfarth, and C. P. Karger. Clinical evaluation of a laser surface scanning system in 120 patients for improving daily setup accuracy in fractionated radiation therapy. *Int J Radiat Oncol Biol Phys*, 85(3):846–53, 2013.
- [35] M. Sharma, T. Dos Santos, N. P. Papanikolopoulos, and S. K. Hui. Feasibility of intrafraction whole-body motion tracking for total marrow irradiation. *J Biomed Opt*, 16(5):058002, 2011.

- [36] F. Walter, P. Freisleder, C. Belka, C. Heinz, M. Sohn, and F. Roeder. Evaluation of daily patient positioning for radiotherapy with a commercial 3d surface-imaging system (catalyst). *Radiat Oncol*, 11(1):154, 2016.
- [37] J. F. Fowler. 21 years of biologically effective dose. *Br J Radiol*, 83(991):554–68, 2010.
- [38] J. F. Fowler. The linear-quadratic formula and progress in fractionated radiotherapy. *Br J Radiol*, 62(740):679–94, 1989.
- [39] R. G. Dale. The application of the linear-quadratic dose-effect equation to fractionated and protracted radiotherapy. *Br J Radiol*, 58(690):515–28, 1985.
- [40] B. G. Douglas and J. F. Fowler. Letter: Fractionation schedules and a quadratic dose-effect relationship. *Br J Radiol*, 48(570):502–4, 1975.
- [41] S. B. Curtis. Lethal and potentially lethal lesions induced by radiation—a unified repair model. *Radiat Res*, 106(2):252–70, 1986.
- [42] JA Brochstein, NA Kernan, S Groshen, C Cirrincione, B Shank, D Emanuel, J Laver, and RJ O’Reilly. Allogeneic bone marrow transplantation after hyperfractionated total-body irradiation and cyclophosphamide in children with acute leukemia. *New England Journal of Medicine*, 317(26):1618–1624, 1987.
- [43] F Eckert, K Schilbach, L Klumpp, L Bardoscia, EC Sezgin, M Schwab, D Zips, and SM Huber. Potential role of cxcr4 targeting in the context of radiotherapy and immunotherapy of cancer. *Frontiers in Immunology*, 9(3018), 2018.
- [44] S. Hui, Y. Takahashi, S. G. Holtan, R. Azimi, D. Seelig, M. Yagi, J. Ingvalson, P. Alaei, L. Sharkey, B. Kodal, N. Peterson, C. Meyer, L. Godin, M. Ehrhardt, G. Storme, D. Zhou, and A. Panoskaltsis-Mortari. Early assessment of dosimetric and biological differences of total marrow irradiation versus total body irradiation in rodents. *Radiother Oncol*, 124(3):468–474, 2017.
- [45] GW Jones, BM Kacinski, LD Wilson, R Willemze, M Spittle, G Hohenberg, L Handl-Zeller, F Trautinger, and R Knobler. Total skin electron radiation in the management of mycosis fungoides: Consensus of the european organization for research and treatment of cancer (eortc) cutaneous lymphoma project group. *Journal of the American Academy of Dermatology*, 47(3):364–370, 2002.
- [46] World Marrow Donor Association. Wmda.info. <https://wmda.info/>, 2021.
- [47] S. Tavor, I. Petit, S. Porozov, A. Avigdor, A. Dar, L. Leider-Trejo, N. Shemtov, V. Deutsch, E. Naparstek, A. Nagler, and T. Lapidot. Cxcr4 regulates migration and development of human acute myelogenous leukemia stem cells in transplanted nod/scid mice. *Cancer Res*, 64(8):2817–24, 2004.

- [48] OZ Lerman, MR Greives, SP Singh, VD Thanik, CC Chang, N Seiser, DJ Brown, D Knobel, RJ Schneider, SC Formenti, PB Saadeh, and JP Levine. Low-dose radiation augments vasculogenesis signaling through hif-1–dependent and –independent sdf-1 induction. *Blood*, 116(18):3669–3676, 2010.
- [49] BJ Moeller, Y Cao, CY Li, and MW Dewhirst. Radiation activates hif-1 to regulate vascular radiosensitivity in tumors: Role of reoxygenation, free radicals, and stress granules. *Cancer Cell*, 5(5):429–441, 2004.
- [50] AH Bazarbachi, R Al Hamed, M Labopin, B Afanasyev, RM Hamladji, D Beelen, M Eder, C Scheid, D Wu, D Bunjes, P Stepensky, J Tischer, N Kröger, Z Peric, M Aljurf, S Giebel, A Nagler, and M Mohty. Allogeneic stem-cell transplantation with sequential conditioning in adult patients with refractory or relapsed acute lymphoblastic leukemia: a report from the ebmt acute leukemia working party. *Bone Marrow Transplantation*, 55(3):595–602, 2020.
- [51] D. Anderson, T. DeFor, L. Burns, P. McGlave, J. Miller, J. Wagner, and D. Weisdorf. A comparison of related donor peripheral blood and bone marrow transplants: importance of late-onset chronic graft-versus-host disease and infections. *Biol Blood Marrow Transplant*, 9(1):52–9, 2003.
- [52] J. Y. Wong, S. Forman, G. Somlo, J. Rosenthal, A. Liu, T. Schultheiss, E. Radany, J. Palmer, and A. Stein. Dose escalation of total marrow irradiation with concurrent chemotherapy in patients with advanced acute leukemia undergoing allogeneic hematopoietic cell transplantation. *International Journal of Radiation Oncology, Biology, Physics*, 85(1):148–56, 2013.
- [53] J. L. Ferrara, R. Levy, and N. J. Chao. Pathophysiologic mechanisms of acute graft-vs.-host disease. *Biol Blood Marrow Transplant*, 5(6):347–56, 1999.
- [54] E. A. Copelan, A. Chojecki, H. M. Lazarus, and B. R. Avalos. Allogeneic hematopoietic cell transplantation; the current renaissance. *Blood Rev*, 34:34–44, 2019.
- [55] Y Zhao, Q Liu, Li Yang, D He, L Wang, J Tian, Y Li, F Zi, H Bao, Y Yang, Y Zheng, J Shi, X Xue, and Z Cai. Tlr4 inactivation protects from graft-versus-host disease after allogeneic hematopoietic stem cell transplantation. *Cellular & Molecular Immunology*, 10(2):165–175, 2013.
- [56] J. B. Langenhorst, C. van Kesteren, E. M. van Maarseveen, T. P. C. Dorlo, S. Nierkens, C. A. Lindemans, M. A. de Witte, A. van Rhenen, R. Raijmakers, M. Bierings, J. Kuball, A. D. R. Huitema, and J. J. Boelens. Fludarabine exposure in the conditioning prior to allogeneic hematopoietic cell transplantation predicts outcomes. *Blood Advances*, 3(14):2179–2187, 2019.

- [57] S. Milgrom, Y Nieto, CC Pinnix, GL Smith, CF Wogan, G Rondon, LJ Medeiros, P Kebriyai, and BS Dabaja. Graft-versus-host disease after radiation therapy in patients who have undergone allogeneic stem cell transplantation: two case reports. *Journal of Medical Case Reports*, 10(1):209, 2016.
- [58] H Goker, IC Haznedaroglu, and NJ Chao. Acute graft-vs-host disease: Pathobiology and management. *Experimental Hematology*, 29(3):259–277, 2001.
- [59] R A Clift, C D Buckner, F R Appelbaum, E Bryant, S I Bearman, F B Petersen, L D Fisher, C Anasetti, P Beatty, and W I Bensinger. Allogeneic marrow transplantation in patients with chronic myeloid leukemia in the chronic phase: a randomized trial of two irradiation regimens. *Blood*, 8:1660–5, April 15 1991.
- [60] H. Nakasone, T. Fukuda, J. Kanda, T. Mori, S. Yano, T. Kobayashi, K. Miyamura, T. Eto, H. Kanamori, K. Iwato, N. Uchida, S. Mori, T. Nagamura-Inoue, T. Ichinohe, Y. Atsuta, T. Teshima, and M. Murata. Impact of conditioning intensity and tbi on acute gvhd after hematopoietic cell transplantation. *Bone Marrow Transplant*, 50(4):559–65, 2015.
- [61] M. Jagasia, M. Arora, M. E. Flowers, N. J. Chao, P. L. McCarthy, C. S. Cutler, A. Urbano-Ispizua, S. Z. Pavletic, M. D. Haagenson, M. J. Zhang, J. H. Antin, B. J. Bolwell, C. Bredeson, J. Y. Cahn, M. Cairo, R. P. Gale, V. Gupta, S. J. Lee, M. Litzow, D. J. Weisdorf, M. M. Horowitz, and T. Hahn. Risk factors for acute gvhd and survival after hematopoietic cell transplantation. *Blood*, 119(1):296–307, 2012.
- [62] R. T. Hoppe, C. Harrison, M. Tavallae, S. Bashey, U. Sundram, S. Li, L. Million, B. Dabaja, P. Gangar, M. Duvic, and Y. H. Kim. Low-dose total skin electron beam therapy as an effective modality to reduce disease burden in patients with mycosis fungoides: results of a pooled analysis from 3 phase-ii clinical trials. *J Am Acad Dermatol*, 72(2):286–92, 2015.
- [63] Douglas R. Adkins, John F. DiPersio, and Douglas R. Adkins. Total body irradiation before an allogeneic stem cell transplantation: Is there a magic dose? *Current Opinion in Hematology*, 15(6):555–560, 2008.
- [64] A-R Hartman, S F Williams, and J J Dillon. Survival, disease-free survival and adverse effects of conditioning for allogeneic bone marrow transplantation with busulfan/ cyclophosphamide vs total body irradiation: a meta-analysis. *Bone marrow transplantation*, 22(5):439–443, 1998.
- [65] G. Svahn-Tapper, P. Nilsson, C. Jönsson, and T. A. Alvegård. Calculation and measurements of absorbed dose in total body irradiation. *Acta Oncologica*, 29(5):627–633, 1990.

- [66] E. D. Thomas, C. D. Buckner, M. Banaji, R. A. Clift, A. Fefer, N. Flournoy, B. W. Goodell, R. O. Hickman, K. G. Lerner, P. E. Neiman, G. E. Sale, J. E. Sanders, J. Singer, M. Stevens, R. Storb, and P. L. Weiden. One hundred patients with acute leukemia treated by chemotherapy, total body irradiation, and allogeneic marrow transplantation. *Blood*, 49(4):511–33, 1977.
- [67] J. Y. C. Wong, A. R. Filippi, B. S. Dabaja, J. Yahalom, and L. Specht. Total body irradiation: Guidelines from the international lymphoma radiation oncology group (ilrog). *Int J Radiat Oncol Biol Phys*, 101(3):521–529, 2018.
- [68] S. A. Carruthers and M. M. Wallington. Total body irradiation and pneumonitis risk: a review of outcomes. *Br J Cancer*, 90(11):2080–4, 2004.
- [69] A Shinde, D Yang, P Frankel, A Liu, C Han, B Del Vecchio, T Schultheiss, J Cheng, R Li, D Kim, EH Radany, S Hui, G Somlo, J Rosenthal, A Stein, S Forman, and JYC Wong. Radiation-related toxicities using organ sparing total marrow irradiation transplant conditioning regimens. *Intl J Rad Onc Bio Phys*, 105(5):1025–1033, 2019.
- [70] G. Moliner, F. Izar, R. Ferrand, M. Bardies, S. Ken, and L. Simon. Virtual bolus for total body irradiation treated with helical tomotherapy. *Journal of Applied Clinical Medical Physics*, 16(6):164–176, 2015.
- [71] TE Schultheiss, Jeffrey Wong, A Liu, G Olivera, and G Somlo. Image-guided total marrow and total lymphatic irradiation using helical tomotherapy. *Intl J Rad Onc Bio Phys*, 67(4), 2007.
- [72] J. Y. Wong, A. Liu, T. Schultheiss, L. Popplewell, A. Stein, J. Rosenthal, M. Es-sensten, S. Forman, and G. Somlo. Targeted total marrow irradiation using three-dimensional image-guided tomographic intensity-modulated radiation therapy: an alternative to standard total body irradiation. *Biol Blood Marrow Transplant*, 12(3):306–15, 2006.
- [73] A. Sarfehnia, E. Poon, S. D. Davis, A. Fleming, D. Mitchell, and C. R. Freeman. A novel approach to total skin irradiation using helical tomotherapy. *Pract Radiat Oncol*, 4(5):330–5, 2014.
- [74] C. H. Hsieh, P. W. Shueng, S. C. Lin, H. J. Tien, A. C. Shiau, Y. H. Chou, M. H. Wu, J. Y. Wang, C. K. Chen, and Y. J. Chen. Helical irradiation of the total skin with dose painting to replace total skin electron beam therapy for therapy-refractory cutaneous cd4+ t-cell lymphoma. *Biomed Res Int*, 2013:717589, 2013.
- [75] A. Nalichowski, D. G. Eagle, and J. Burmeister. Dosimetric evaluation of total marrow irradiation using 2 different planning systems. *Med Dosim*, 41(3):230–5, 2016.

- [76] T. E. Schultheiss, J. Wong, A. Liu, G. Olivera, and G. Somlo. Image-guided total marrow and total lymphatic irradiation using helical tomotherapy. *Int J Radiat Oncol Biol Phys*, 67(4):1259–67, 2007.
- [77] G. Somlo, R. Spielberger, P. Frankel, C. Karanes, A. Krishnan, P. Parker, L. Popplewell, F. Sahebi, N. Kogut, D. Snyder, A. Liu, T. Schultheiss, S. Forman, and J. Y. Wong. Total marrow irradiation: a new ablative regimen as part of tandem autologous stem cell transplantation for patients with multiple myeloma. *Clin Cancer Res*, 17(1):174–82, 2011.
- [78] R Boyd, K Jeong, and Wolfgang A. Tomé. Determining efficient helical imrt modulation factor from the mlc leaf-open time distribution on precision treatment planning system. *Journal of Applied Clinical Medical Physics*, 20(5):64–74, 2019.
- [79] Y. Takahashi, M. Verneris, K. Dusenbery, C. Wilke, D.J. Weisdorf, and S.K. Hui. Peripheral dose heterogeneity due to the thread effect in total marrow irradiation with helical tomotherapy. *International Journal of Radiation Oncology, Biology, Physics*, 87(4):832–9, 2013.
- [80] N. V. N. Madhusudhana Sresty, Deleep Gudipudi, A. Krishnam Raju, T. Anil kumar, V. R. P. Lakshmi, G. Srikanth, and M. Narasimha. Total body irradiation of bone marrow transplant using helical tomotherapy with a focus on the quality of dose contribution at junction target volumes. *Strahlentherapie und Onkologie*, 197(8):722–729, 2021.
- [81] C Beltran, J Trussell, and TE Merchant. Dosimetric impact of intrafractional patient motion in pediatric brain tumor patients. *Medical Dosimetry*, 35(1):43–48, 2010.
- [82] M Geurts, A. Bayliss, B Thapa, and G Nelson. Total skin tomotherapy for treatment of mycosis fungoides. In *Accuray AERO Users' Meeting; The Frontiers of Image-Guidance: Margins, Motion & Adaptation*, 2014.
- [83] D. Zuro, S. Vagge, S. Broggi, S. Agostinelli, Y. Takahashi, J. Brooks, P. Leszcynska, A. Liu, C. Zucchetti, S. Saldi, C. Han, M. Cattaneo, S. Giebel, M. A. Mahe, J. F. Sanchez, P. Alaei, C. Anna, K. Dusenbery, A. Pierini, G. Storme, C. Aristei, J. Y. C. Wong, and S. Hui. Multi-institutional evaluation of mvct guided patient registration and dosimetric precision in total marrow irradiation: A global health initiative by the international consortium of total marrow irradiation. *Radiother Oncol*, 141:275–282, 2019.
- [84] A. Haraldsson, A. Hauer Karlsson, L. Ambolt, and P. Engström. Plan specific pitch on tomotherapy-plans effect on gamma pass rate for patient qa measured on delta4. *Radiotherapy and Oncology*, 119:S740–S740, 2016.

- [85] H. Dhiraj, S. Thomas, and S. McGowan. Ep-1537: Developing an in vivo dosimetry system for tomotherapy® using the ct detector array. *Radiotherapy and Oncology*, 119(Supplement 1):S712–S712, 2016.
- [86] MC Han, KH Chang, J Kim, SC Han, K Park, DW Kim, H Kim, and JS Kim. Tomoeqa: Dose verification for patient-specific quality assurance in helical tomotherapy using an exit detector. *Physica Medica*, 82:1–6, 2021.
- [87] T. Y. Lee, H. H. F. Choi, W. K. R. Wong, Y. W. Ho, K. Y. Cheung, and S. K. Yu. Ep-1754: Robustness of the tomotherapy exit detector for verifying mlc fluence post-irradiation. *Radiotherapy and Oncology*, 127(Supplement 1):S940–S941, 2018.
- [88] M. Parisotto, V. Marco, and S. Maggi. Po-1371: A feasibility study of using tomotherapy exit detector data for pretreatment verification. *Radiotherapy and Oncology*, 152(Supplement 1):S728–S729, 2020.
- [89] T Rajesh, S Dayananda Shamurailatpam, K Suryakant, S Mayur, K. Ganapathy, NAN Raj, C Srinivas, CS Sham, Patro Kartikeswar Ch, M Arjunan, M. P. Noufal, S Rangasamy, E Jose, and J Rakesh. Leaf open time sinogram (lots): a novel approach for patient specific quality assurance of total marrow irradiation. *Radiation Oncology*, 15(1):1–12, 2020.
- [90] K Sheng, R Jones, W Yang, S Saraiya, B Schneider, Q Chen, G Sobering, G Olivera, and P Read. 3d dose verification using tomotherapy ct detector array. *International Journal of Radiation Oncology, Biology, Physics*, 82(2):1013–1020, 2012.
- [91] F Crop, D Pasquier, A Baczkievic, J Doré, L Bequet, E Steux, A Gadroy, J Bouillon, C Florence, L Muszynski, M Lacour, and E Lartigau. Surface imaging, laser positioning or volumetric imaging for breast cancer with nodal involvement treated by helical tomotherapy. *Journal of Applied Clinical Medical Physics*, 17(5):200–211, 2016.
- [92] M Kügele, A Mannerberg, S Nørring Bekke, S Alkner, L Berg, F Mahmood, C Thornberg, A Edvardsson, S Bäck, C Behrens, and S Ceberg. Surface guided radiotherapy (sgrt) improves breast cancer patient setup accuracy. *Journal of Applied Clinical Medical Physics*, 20(9):61–68, 2019.
- [93] L Delombaerde, S Petillion, S Michiels, C Weltens, and T Depuydt. Development and accuracy evaluation of a single-camera intra-bore surface scanning system for radiotherapy in an o-ring linac. *Physics and Imaging in Radiation Oncology*, 11:21–26, 2019.
- [94] J. L. Fromer, D. O. Johnston, F. A. Salzman, J. G. Trump, and K. A. Wright. Management of lymphoma cutis with low megavolt electron beam therapy: nine year follow-up in 200 cases. *South Med J*, 54:769–76, 1961.

- [95] C. T. Lin, A. C. Shiau, H. J. Tien, H. P. Yeh, P. W. Shueng, and C. H. Hsieh. An attempted substitute study of total skin electron therapy technique by using helical photon tomotherapy with helical irradiation of the total skin treatment: a phantom result. *Biomed Res Int*, 2013:108794, 2013.
- [96] S. Sampath, T. E. Schultheiss, and J. Wong. Dose response and factors related to interstitial pneumonitis after bone marrow transplant. *Int J Radiat Oncol Biol Phys*, 63(3):876–84, 2005.
- [97] T. Fukuda, R. C. Hackman, K. A. Guthrie, B. M. Sandmaier, M. Boeckh, M. B. Maris, D. G. Maloney, H. J. Deeg, P. J. Martin, R. F. Storb, and D. K. Madtes. Risks and outcomes of idiopathic pneumonia syndrome after nonmyeloablative and conventional conditioning regimens for allogeneic hematopoietic stem cell transplantation. *Blood*, 102(8):2777–85, 2003.
- [98] D. Y. Kim, I. H. Kim, S. S. Yoon, H. J. Kang, H. Y. Shin, and H. C. Kang. Effect of dose rate on pulmonary toxicity in patients with hematolymphoid malignancies undergoing total body irradiation. *Radiat Oncol*, 13(1):180, 2018.
- [99] R. S. Weiner, M. M. Bortin, R. P. Gale, E. Gluckman, H. E. Kay, H. J. Kolb, A. J. Hartz, and A. A. Rimm. Interstitial pneumonitis after bone marrow transplantation. assessment of risk factors. *Ann Intern Med*, 104(2):168–75, 1986.
- [100] M Joiner, N Mogili, B Marples, and J Burmeister. Significant dose can be lost by extended delivery times in imrt with x rays but not high-let radiations. *Medical Physics*, 37(6Part2):2457–2465, 2010.
- [101] D Ward, D Carter, M Homer, L Marucci, and A Gampel. Mathematical modeling reveals differential effects of erythropoietin on proliferation and lineage commitment of human hematopoietic progenitors in early erythroid culture. *Haematologica*, 101(3):286–296, 2016.
- [102] P Getto, A Marciniak-Czochra, Y Nakata, and M Vivanco. Global dynamics of two-compartment models for cell production systems with regulatory mechanisms. *Mathematical Biosciences*, 245(2):258–268, 2013.
- [103] A Marciniak-Czochra and T Stiehl. *Mathematical Models of Hematopoietic Reconstitution After Stem Cell Transplantation*, volume 4, book section Mathematical Models of Hematopoietic Reconstitution After Stem Cell Transplantation. Springer-Verlag, Heidelberg, Germany, 2013.
- [104] T. Stiehl, A. D. Ho, and A. Marciniak-Czochra. The impact of cd34+ cell dose on engraftment after scts: personalized estimates based on mathematical modeling. *Bone Marrow Transplant*, 49(1):30–7, 2014.

- [105] M Kitaguchi, H Yamashita, R Takenaka, K Okuma, K Nawa, and K Nakagawa. Helical skin radiation therapy including total skin radiation therapy using tomotherapy for primary cutaneous lymphoma with bone marrow suppression as a related adverse event. *Practical Radiation Oncology*, 11(3):e308–e321, 2021.
- [106] T. E. Wheldon. The radiobiological basis of total body irradiation. *Br J Radiol*, 70(840):1204–7, 1997.
- [107] J. M. Bowen and H. R. Wardill. Advances in the understanding and management of mucositis during stem cell transplantation. *Curr Opin Support Palliat Care*, 11(4):341–346, 2017.
- [108] A. Haraldsson, W. Stina, J. Engellau, C. Ceberg, S. Bäck, S. Ceberg, S. Engelholm, S. Warsi, and P. E. Engström. Po-0916: Dose-rate dependence in haematological recovery following total marrow irradiation. *Radiotherapy and Oncology*, 152(Supplement 1):S489–S489, 2020.
- [109] N. J. Tarbell, D. A. Amato, J. D. Down, P. Mauch, and S. Hellman. Fractionation and dose rate effects in mice: a model for bone marrow transplantation in man. *Int J Radiat Oncol Biol Phys*, 13(7):1065–9, 1987.
- [110] J. Y. C. Wong, A. R. Filippi, M. Scorsetti, S. Hui, L. P. Muren, and P. Mancosu. Total marrow and total lymphoid irradiation in bone marrow transplantation for acute leukaemia. *Lancet Oncol*, 21(10):e477–e487, 2020.
- [111] S Sampath, TE. Schultheiss, and J Wong. Dose response and factors related to interstitial pneumonitis after bone marrow transplant. *International Journal of Radiation Oncology, Biology and Physics*, 63(3):S0360–3016, 2005.
- [112] T. J. Glass, S. K. Hui, B. R. Blazar, and T. C. Lund. Effect of radiation dose-rate on hematopoietic cell engraftment in adult zebrafish. *PLoS One*, 8(9):e73745, 2013.
- [113] S. Herberg, G. Kondrikova, K. A. Hussein, S. Periyasamy-Thandavan, M. H. Johnson, M. E. Elsalanty, X. Shi, M. W. Hamrick, C. M. Isales, and W. D. Hill. Total body irradiation is permissive for mesenchymal stem cell-mediated new bone formation following local transplantation. *Tissue Eng Part A*, 20(23-24):3212–27, 2014.
- [114] M. M. Horowitz, R. P. Gale, P. M. Sondel, J. M. Goldman, J. Kersey, H. J. Kolb, A. A. Rimm, O. Ringdén, C. Rozman, B. Speck, and et al. Graft-versus-leukemia reactions after bone marrow transplantation. *Blood*, 75(3):555–62, 1990.
- [115] H. B. Kal, M. Loes van Kempen-Harteveld, M. H. Heijenbrok-Kal, and H. Struikmans. Biologically effective dose in total-body irradiation and hematopoietic stem cell transplantation. *Strahlenther Onkol*, 182(11):672–9, 2006.

- [116] D. I. Marks, S. J. Forman, K. G. Blume, W. S. Pérez, D. J. Weisdorf, A. Keating, R. P. Gale, M. S. Cairo, E. A. Copelan, J. T. Horan, H. M. Lazarus, M. R. Litzow, P. L. McCarthy, K. R. Schultz, D. D. Smith, M. E. Trigg, M. J. Zhang, and M. M. Horowitz. A comparison of cyclophosphamide and total body irradiation with etoposide and total body irradiation as conditioning regimens for patients undergoing sibling allografting for acute lymphoblastic leukemia in first or second complete remission. *Biol Blood Marrow Transplant*, 12(4):438–53, 2006.
- [117] D. Cowen, P. Richaud, S. Landriau, P. Lagarde, F. X. Mahon, J. J. Baudet, F. Belloc, N. Gualde, and J. Reiffers. Radiobiological features of acute myeloblastic leukemia: comparison of self-renewal versus terminally differentiated populations. *Int J Radiat Oncol Biol Phys*, 30(5):1133–40, 1994.
- [118] A Stein, J Palmer, NC Tsai, MM Al Malki, I Aldoss, H Ali, A Aribi, L Farol, C Karanes, S Khaled, A Liu, M O'Donnell, P Parker, A Pawlowska, V Pullarkat, E Radany, J Rosenthal, F Sahebi, A Salhotra, JF Sanchez, T Schultheiss, R Spielberger, SH Thomas, D Snyder, R Nakamura, G Marcucci, SJ Forman, and J Wong. Phase i trial of total marrow and lymphoid irradiation transplantation conditioning in patients with relapsed/refractory acute leukemia. *Biology of blood and marrow transplantation: journal of the American Society for Blood and Marrow Transplantation*, 23(4):618–624, 2017.
- [119] J. Y. Wong, S. Forman, G. Somlo, J. Rosenthal, A. Liu, T. Schultheiss, E. Radany, J. Palmer, and A. Stein. Dose escalation of total marrow irradiation with concurrent chemotherapy in patients with advanced acute leukemia undergoing allogeneic hematopoietic cell transplantation. *Int J Radiat Oncol Biol Phys*, 85(1):148–56, 2013.
- [120] Z Bao, H Zhao, D Wang, J Gong, Y Zhong, Y Xiong, D Deng, C Xie, A Liu, X Wang, and H Liu. Feasibility of a novel dose fractionation strategy in tmi/tmli. *Radiation Oncology*, 13(1):248, 2018.
- [121] S. Hui, C. Brunstein, Y. Takahashi, T. DeFor, S. G. Holtan, V. Bachanova, C. Wilke, D. Zuro, C. Ustun, D. Weisdorf, K. Dusenbery, and M. R. Verneris. Dose escalation of total marrow irradiation in high-risk patients undergoing allogeneic hematopoietic stem cell transplantation. *Biol Blood Marrow Transplant*, 23(7):1110–1116, 2017.
- [122] J Wong, S Forman, G Somlo, J Rosenthal, An Liu, T Schultheiss, E Radany, J Palmer, and A Stein. Dose escalation of total marrow irradiation with concurrent chemotherapy in patients with advanced acute leukemia undergoing allogeneic hematopoietic cell transplantation. *International Journal of Radiation Oncology, Biology, Physics*, 85(3):148–156, 2013.

- [123] M. Duvic, M. Donato, B. Dabaja, H. Richmond, L. Singh, W. Wei, S. Acholonu, I. Khouri, R. Champlin, and C. Hosing. Total skin electron beam and non-myoablative allogeneic hematopoietic stem-cell transplantation in advanced mycosis fungoides and sezary syndrome. *J Clin Oncol*, 28(14):2365–72, 2010.
- [124] M Buglione, L Spiazzi, M Urpis, L Baushi, R Avitabile, N Pasinetti, P Borghetti, L Triggiani, S Pedretti, F Saiani, A Fiume, D Greco, S Ciccarelli, A Polonini, R Moretti, and SM Magrini. Light and shadows of a new technique: is photon total-skin irradiation using helical imrt feasible, less complex and as toxic as the electrons one? *Radiation Oncology*, 13(1):158, 2018.
- [125] V Batista, J Meyer, M Kügele, and H Al-Hallaq. Clinical paradigms and challenges in surface guided radiation therapy: Where do we go from here? *Radiotherapy and Oncology*, 153:34–42, 2020.
- [126] O. J. Gurney-Champion, D. McQuaid, A. Dunlop, K. H. Wong, L. C. Welsh, A. M. Riddell, D. M. Koh, U. Oelfke, M. O. Leach, C. M. Nutting, S. A. Bhide, K. J. Harrington, R. Panek, and K. L. Newbold. Mri-based assessment of 3d intrafractional motion of head and neck cancer for radiation therapy. *Int J Radiat Oncol Biol Phys*, 100(2):306–316, 2018.
- [127] P. P. Pang, J. Hendry, S. L. Cheah, Y. L. Soong, K. W. Fong, T. S. Wee, W. K. Tan, W. L. Nei, F. Wang, R. X. Wong, W. L. Ng, and J. Chen. An assessment of the magnitude of intra-fraction movement of head-and-neck imrt cases and its implication on the action-level of the imaging protocol. *Radiother Oncol*, 112(3):437–441, 2014.
- [128] T Lustberg, J van Soest, M Gooding, D Peressutti, P Aljabar, J van der Stoep, W van Elmpt, and A Dekker. Clinical evaluation of atlas and deep learning based automatic contouring for lung cancer. *Radiotherapy and Oncology*, 126(2):312–317, 2018.
- [129] W.J Zabel, J.L. Conway, A Gladwish, J Skliarenko, G Didiodato, L Goorts-Matthews, A Michalak, S Reistetter, J King, K Nakonechny, K Malkoske, MN. Tran, and N McVicar. Clinical evaluation of deep learning and atlas-based auto-contouring of bladder and rectum for prostate radiation therapy. *Practical Radiation Oncology*, 11(1):e80–e89, 2021.
- [130] A. Moignier, S. Huger, V. Marchesi, and L. Guinement. Delivery analysis, a useful tool for adaptive radiotherapy in tomotherapy? *Physica Medica*, 44:35, 2017.

Publications

Conference proceedings in Appendix A.1

Paper I





Technical note

Implementing safe and robust Total Marrow Irradiation using Helical Tomotherapy – A practical guide

André Haraldsson^{a,b,*}, Jacob Engellau^{a,b}, Stig Lenhoff^b, Silke Engelholm^b, Sven Bäck^b, Per E. Engström^b

^a Medical Radiation Physics, Lund University, Lund, Sweden

^b Department of Haematology, Oncology and Radiation Physics, Skåne University Hospital, Lund, Sweden



ARTICLE INFO

Keywords:
TMI
Total
Marrow
Irradiation
Radiotherapy
Tomotherapy
Helical

ABSTRACT

Total Marrow Irradiation (TMI) with Helical Tomotherapy is a radiotherapy treatment technique that targets bone marrow and sanctuary sites prior to stem cell or bone marrow transplantation (SCT/BMT). TMI is a complex procedure that involves several critical steps that all need to be carefully addressed for a successful implementation, such as dose homogeneity in field junctions, choice of target margins, integrity of treatment and back-up planning. In this work we present our solution for a robust and reproducible workflow throughout the treatment chain and data for twenty-three patients treated to date.

Material & Methods: Patients were immobilized in a whole body vacuum cushion and thermoplastic mask. CT-scanning and treatment were performed in two parts with field matching at the upper thigh. Target consisted of marrow containing bone and sanctuary sites. Lungs, kidneys, bowel, heart and liver were defined as organs at risk (OAR). A fast surface scanning system was used to position parts of the body not covered by the imaging system (MVCT) as well as to reduce treatment time.

Results: All patients completed their treatment and could proceed with SCT/BMT. Doses to OARs were significantly reduced and target dose homogeneity was improved compared to TBI. Robustness tests performed on field matching and patient positioning support that the field junction technique is adequate. Replacing MVCT with optical surface scanning reduced the treatment time by 25 min per fraction.

Conclusion: The methodology presented here has shown to provide a safe, robust and reproducible treatment for Total Marrow Irradiation using Tomotherapy.

1. Introduction

Total body irradiation (TBI) is used in conditioning regimes to suppress the immune system and eradicate tumor cells prior to hematopoietic stem cell transplantation (SCT). The treatment's viability is shown by the lower relapse rate when patients are treated with radiotherapy and chemotherapy versus chemotherapy alone [1,2].

The standard treatment for TBI is anterior-posterior irradiation using a conventional linear accelerator at extended source-to-skin distance (SSD), with lead blocks shielding the lungs. This technique is simple, robust, and can be implemented on virtually any linear accelerator provided the treatment room is sufficiently large. However, the treatment often results in large dose heterogeneities in the patient, and the technique offers no sparing of organs at risk (OAR) except for lungs. The treatment is toxic, especially in combination with chemotherapy [3] and may cause significant side effects to a number of organs such as

lungs, kidneys, bowel, and liver. The high toxicity has been shown to rule out attempted dose escalation, and lower relapse rate with higher dose has not affected the overall survival [4]. Helical Tomotherapy (HT) is a treatment modality that combines continuous gantry rotation and couch translation during irradiation. This allows treating targets up to about 135 cm length without any field junctions. These properties make HT a powerful option for irradiating long complex targets such as bone marrow [5,6], although TMI treatments need to be split in two fields due to treatment length exceeding the 135 cm limit. Total Marrow Irradiation using Helical Tomotherapy to target bone marrow has been described previously [5,7–14]. However, the aim of this work is to present a straightforward guideline for implementing safe and robust Total Marrow Irradiation in a single Tomotherapy unit clinic. We believe that there is great gain in TMI treatment for these patients but challenges in implementing such a complex technique need to be addressed and illustrated. Here we describe a working procedure for

* Corresponding author at: Skånes Universitetssjukhus, Klinikgatan 5, 22185 Lund, Sweden.
E-mail address: andre.haraldsson@med.lu.se (A. Haraldsson).

<https://doi.org/10.1016/j.ejmp.2019.03.032>

Received 21 November 2018; Received in revised form 22 March 2019; Accepted 30 March 2019
1120-1797/ © 2019 Published by Elsevier Ltd on behalf of Associazione Italiana di Fisica Medica.

immobilization, beam junction optimization, surface scanning for patient positioning and backup planning for TMI. Potential pitfalls, difficulties and solutions are discussed for the entire treatment chain.

2. Material & Methods

A multidisciplinary group consisting of all personnel involved in the TMI treatment was formed to develop and implement the treatment process. The TMI treatment chain included: determination of the conditioning regimen for radiotherapy, patient immobilization, computed tomography (CT), target and OAR delineation, treatment planning, quality control (QC), setup and imaging, treatment and backup planning.

2.1. Patient characteristics

Twenty-three patients presented with a wide range of body mass indices, ranging from 15 to 40, of which 7 (41%) were females. The median age of the patients was 22 years, range 12–58 and 4 out of 17 (24%) were paediatric patients aged 12, 12, 14 and 18 years. All patients were heavily pre-treated, and all but one were referred to the department of radiotherapy from the department of haematology. One paediatric patient was referred from another hospital, and treated with a reversed order of conditioning – TMI prior to chemotherapy. Standard radiotherapy prescription was 12 Gy given in 6 fractions twice daily over 3 days, with minimum 6 h between fractions. The characteristics, diagnosis and fractionation regimens of the patients are presented in Table 1. All patients were informed of the TMI treatment and the conventional TBI treatment, and all consented to undergo TMI treatment. The study has been approved by the local ethics committee.

2.2. Immobilization

Prior to CT acquisition, patients were firmly and reproducibly immobilized in a large vacuum cushion (VacFix, Par Scientific A/S, Odense Denmark) encompassing the entire body (Fig. 1). A 5 point open-face thermoplastic mask (Orfit Industries, Wijnegem, Belgium) together with an individually moulded neck support (MOLDCARE, Qfix,

PA, US) was used to immobilize the head and shoulders. Cotton pads served as spacers between mask and body to enable room for port-cath and central venous catheter. Hands and arms were placed as tight as possible alongside the body since minimising the distance between the arms improves the target dose homogeneity [15] and also maximises the body volume within the field of view of the MVCT.

Knees were slightly flexed to minimise the curvature of the lumbar vertebrae which we found facilitated the setup reproducibility. Feet were immobilized with firm imprints of the heels.

2.3. Computer tomography

All patients were CT-scanned in two parts of opposite direction due to the limited treatment length of the Tomotherapy unit (135 cm). First, from vertex to thigh in head first supine position (HFS) followed by the second scan from toes to upper thigh in feet-first supine position (FFS) using the same immobilization but rotated 180 degrees and with net immobilization removed. The two scans, acquired using 5 mm slice thickness, overlapped by approximately 20 cm to allow sufficient image data for accurate registration of the two CT-sets later in the dose summation phase (Fig. 2). Multiple transversal lines were drawn on all extremities together with corresponding positions on the vacuum cushion (Fig. 1). Two internal reference points were defined with tattoos and fiducial markers; for the upper body at the level of mammillae and for the lower body (legs) at the level of the field junction on the upper thighs. The fiducial junction markers on the thigh were encompassed by both CT-sets. To avoid image acquisition in deep inspiration or expiration phase, the patient was instructed to breathe calmly to ensure a CT scan representative of the treatment position.

2.4. Structure delineation

Following CT, both scans were exported to the treatment planning system (TPS) Eclipse (Varian Medical Systems) where OARs and target structures were delineated. All relevant OARs were delineated for dose monitoring purposes but only heart, bowel, liver, lungs and kidneys were used in the optimisation process.

Clinical target volume (CTV) was defined as bone and auto-

Table 1

Patients treated with Total Marrow Irradiation 2014–2018. Basic patient information is presented with diagnosis and treatment given as well as targeted organs. Patient #6 received an additional boost to 20 Gy/5F to the right humerus, and thoracic column due to FDG-PET positive myeloma involvement and patient #10 received a boost to enlarged lymph nodes. Deviations from standard prescription (12 Gy) by request from referring haematologist.

Patient	Sex/Age (years)	BMI	Diagnosis	Fractionation	Target volumes
1	Female (49)	40	Sp11 MPD + T-ALL	12 Gy/6F b.i.d	BM, CNS, Spleen
2	Male (45)	29	CML + ALL recurrence	12 Gy/6F b.i.d	BM, CNS, Spleen, Scrotum
3	Female (14)	29	Pre-B ALL recurrence	12 Gy/6F b.i.d	BM, CNS, Spleen
4	Male (22)	24	Ph + pre-B ALL	12 Gy/6F b.i.d	BM, CNS, Spleen, Scrotum
5	Female (12)	15	Pre-B ALL recurrence	12 Gy/6F b.i.d	BM, CNS, Spleen
6	Male (18)	25	Myeloma	12 Gy/6F b.i.d	BM
7	Male (22)	24	Pre-B ALL	12 Gy/6F b.i.d	BM, CNS, Spleen, Scrotum
8	Male (40)	24	Ph + Pre-B ALL	8 Gy/4F b.i.d	BM, CNS, Spleen, Scrotum
9	Female (23)	26	MPAL	12 Gy/6F b.i.d	BM
10	Female (58)	38	Follicular lymphoma recurrence	6 Gy/2F 1F/d	BM
11	Male (27)	29	T-ALL CNS recurrence	12 Gy/6F b.i.d	BM, CNS, Spleen, Scrotum
12	Male (19)	26	Pre-B ALL recurrence	12 Gy/6F b.i.d	BM, CNS, Spleen, Scrotum
13	Male (20)	22	BPCDN	12 Gy/6F b.i.d	BM
14	Female (45)	32	Pre-B ALL	12 Gy/6F b.i.d	BM, CNS, Spleen
15	Male (21)	23	Pre-B ALL recurrence	12 Gy/6F b.i.d	BM, CNS, Spleen, Scrotum
16	Male (12)	19	Pre-B ALL recurrence	11 Gy/4F 1F/d	BM, CNS, Spleen, Scrotum
17	Male (30)	28	T-ALL	12 Gy/6F b.i.d	BM, CNS, Spleen, Scrotum
18	Male (30)	25	Pre-B ALL "Ph-like ALL"	12 Gy/6F b.i.d	BM, CNS, Spleen, Scrotum
19	Male (10)	14	Pre-B ALL Recurrence	12 Gy/6F b.i.d	BM, CNS, Spleen, Scrotum
20	Female (46)	32	Follicular lymphoma recurrence	12 Gy/6F b.i.d	BM, CNS, Spleen
21	Male (29)	28	Pre-B ALL recurrence	12 Gy/6F b.i.d	BM, CNS, Spleen, Scrotum
22	Male (35)	24	Pre-B ALL	12 Gy/6F b.i.d	BM, CNS, Spleen, Scrotum
23	Female (42)	26	Myeloma	12 Gy/6F b.i.d	BM

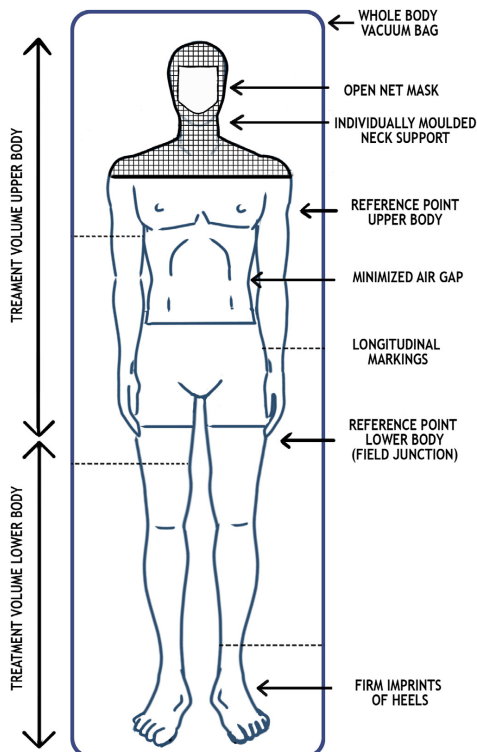


Fig. 1. Illustration of the patient setup including extension of treatment fields, immobilization equipment and reference points. Setup markings on patient are shown as dotted lines.

contoured by the TPS but manually corrected; ribs were joined to a single volume but cartilage was excluded ventrally. In addition, brain, spleen, lymph nodes and testes were included or omitted as target depending on the patient's diagnosis, as seen in Table 1. Structures considered to lack red bone marrow such as sesamoid bones, hyoid bone, larynx, patella, toes and the distal part of the fingers were excluded from CTV. Margins from CTV to PTV were applied based on established values used in our clinic for similar treatment sites, such as craniospinal irradiation (CSI) or total lymph node irradiation (TLI). For the torso an additional 3-mm margin was applied compared to 7 mm used for CSI and TLI, in all 10 mm. For the head, immobilized with an open net mask, 2 mm was added to the 5 mm margin normally used for targets of the head and neck, in all 7 mm. For patients having a left-to-right arm distance exceeding 40 cm, a 13–15 mm PTV margin was generally used due to the 40 cm field of view (FOV) limitation of the MVCT.

To avoid optimization in air of superficial parts of the target (e.g. skull, clavicle and shins), optimization bolus was added extending 4 mm beyond the PTV with a density override of 0.6 g/cc. The technique and thickness of bolus used was similar to the one described by Moliner et al. [15], with the exception of the bolus density, where Moliner et al. used a density of 0.4 g/cc.

2.5. Treatment planning

After delineation, both CT scans along with corresponding structure sets were exported to the Tomotherapy TPS. Planning parameters were set according to clinical practice, initial testing and literature [16–19], as follows; a pitch of 0.397, field width of 5 cm, a modulation factor of 2.5–2.8 for the upper body. This pitch value was selected to minimise the thread effect for the especially lateral targets, such as the arms, and presents a good compromise between dose homogeneity, beam-on time and MLC segment complexity [18]. The same pitch and field width were used also for the lower body but the modulation factor was reduced to 1.6 to minimise treatment time. Planning optimization criteria were set to achieve 100% of the prescribed dose to cover 60% of the PTV and a minimum of 98% of prescribed dose to cover 95% of the PTV. Optimization was then continuously progressed until lowest possible doses to OARs were achieved with uncompromised PTV coverage.

Because of the lateral extension of the arms, the target coverage was generally lower than that of the torso and head. This can be mainly attributed to the threading effect [18], and due to the maximum field width of 40 cm at isocenter was less than the patient width. Multiple objectives were put on each OAR to minimise the dose. For each OAR, an optimization volume was created as a copy but separated 5 mm from the PTV. For lungs, a 10-mm separation was used. This generally facilitates the optimization and reduces the risk of hotspots at the PTV-OAR border.

The fields of the upper and lower body plans were matched at the upper thigh. This position presents the least complicated target geometry when merging two Tomotherapy fields since the target here only consists of the two femoral shafts with no nearby organs at risk. To create a robust plan with homogeneous dose across the field junction, shallow dose gradients were created in the optimisation as shown in Fig. 2. The target dose of the upper body was ramped down from 100% to 0% over the last 6 cm using six target segments of 1.0 cm assigned descending dose values of approximately 2 Gy per segment. The cranial dose of the lower body was ramped down correspondingly resulting in a homogeneous dose across the junction. This sizable dose ramping volume allows for a minor longitudinal mismatch of the two fields without compromising target coverage. After completing optimization, both dose matrices were exported to the Eclipse TPS for dose summation. The CT sets for the upper and the lower body were automatically registered based on anatomy, and manually corrected to align the fiducial thigh markers. In Eclipse (version 13.6), the correct image orientation of the registration is handled internally but is always visually confirmed afterwards.

To validate the choice of CTV-PTV margins and to verify that all patients received the prescribed dose, we applied the concept of Dose Coverage Histogram (DCH) [21]. Basically, the Dose Coverage Histogram tells the probability that the dose to the CTV is covered to a certain level based on the variation in DVHs calculated from a number of treatments. MVCT data were collected for all delivered fractions and the CTV structure position was corrected by rigid adjustment (translationally) slice by slice to match the target in treated position. The treatment plan was then recalculated based on the geometry at the time of treatment and compared to the original treatment plan. From these data, dose coverage histograms were calculated and evaluated. We evaluated the DCH for the 15 first patients.

To evaluate the dose homogeneity around the field junction from setup deviations, a recalculation was performed with an independent dose calculator. The upper and the lower body image set was moved 5 mm longitudinally in both directions, and 10 mm laterally and vertically in both directions. 5 mm longitudinal was used since the registration and setup during treatment was based on the longitudinal position of the junction markers. The recalculated datasets were combined in Python and evaluated based on the CTV \pm 2.0 cm from the junction markers on the thigh. The robustness of the CTV dose homogeneity in the field junction was evaluated for 8 patients.

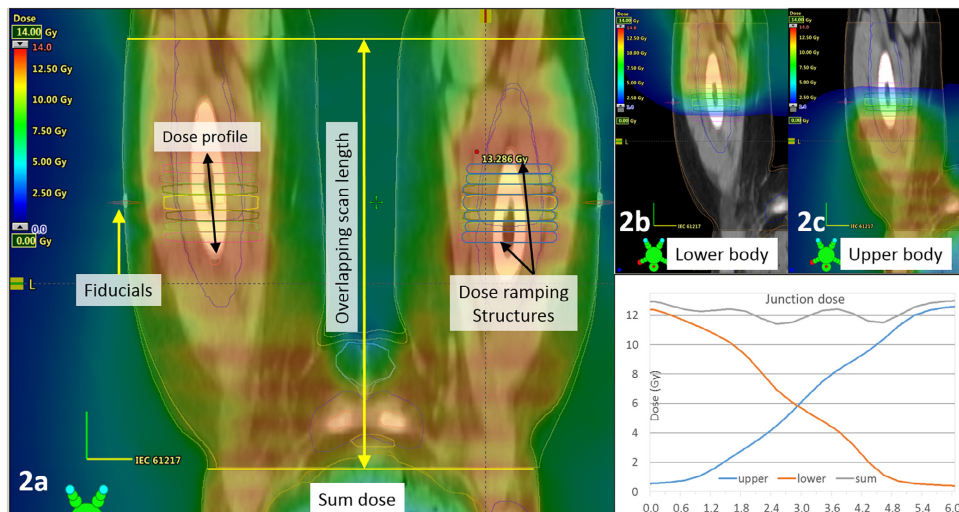


Fig. 2. Coronal plane of thigh area including junction section. Dose distribution from lower body plan and upper body plan (2b and 2c) add up to (2a). Lower right plot shows a 6-cm dose profile across the junction with individual plan contributions.

2.6. Delivery quality control (DQC)

A dose verification was performed on all patients before treatment start. For treatment DQC, the Delta4 phantom was used (ScandiDos, Uppsala, Sweden); a cylindrical PMMA phantom with a cross-plane diode array of 1069 diodes. Agreement between delivered and planned dose was evaluated with gamma analysis [20] in accordance with our clinical practice: 3% dose difference, 2 mm distance to agreement with a minimum pass rate of 90% with global dose normalization and a 15% threshold. Due to the extensive length of the target, multiple measurements were necessary to cover the entire volume.

2.7. Imaging, registration & treatment

Patient positioning and imaging was performed with the aid of two independent systems: Sentinel optical surface scanning system (C-RAD, Uppsala, Sweden) (henceforth designated the surface guided radiotherapy (SGRT) system), and MVCT using the built-in detector array. Sentinel is a fast laser-based optical surface scanning system that acquires 3D images of the patient surface and calculates the position using rigid registration based on a reference scan or imported external structure from the TPS.

Before MVCT, radio-opaque fiducial markers were placed on the internal reference tattoos of the upper thigh, marking the position of the field junction. When treating the upper body, patients were positioned using the reference markings at mid-thorax level (Fig. 1). In case of left-to-right arm distance exceeding 40 cm, the upper body was SGRT scanned prior to MVCT. After assuring proper positioning of the arms, an MVCT was acquired from vertex to mid-thigh. Image registration was performed automatically, reviewed, and if necessary adjusted manually. The longitudinal shift was also applied but not exceeding 5 mm from the junction markers in order to keep a homogeneous junction dose.

Prior to treatment of the lower body, the entire immobilization was rotated 180 degrees and the neck rest and mask were replaced with a pillow for patient comfort. Here, no longitudinal deviation in junction

marker position was allowed at registration in order to maintain a homogeneous junction dose and only lateral or vertical corrections were applied if necessary.

In order to save patient time on the treatment couch, MVCT registration was replaced with SGRT for the lower body. Image registration data of MVCT and SGRT scans were taken sequentially for the first three fractions and analysed and correlated. If the two image sets correlated within 3 mm, only SGRT was used for the lower body for the remaining fractions.

2.8. Backup treatment preparation

Being a single Tomotherapy unit centre, to prevent treatment course interruption in case of machine breakdown, a conventional TBI treatment plan was prepared for each patient as described by Svahn-Tapper et al. [21]. In vivo TLD or diode measurements performed at the first fractions were used for dose verification and if necessary also a dose correction. A conventional linac was kept in stand-by to complete the TMI treatment with the TBI backup treatment if required. In case of interruption during treatment, the partial TMI treatment length was calculated based on elapsed treatment time and couch travel parameters, and the treatment field of the backup TBI plan was matched at the skin where the Tomotherapy treatment ended. This procedure does not aim at perfect matching of the field junction but rather to avoid a larger underdosage. Instead, an overdosage of a small section is anticipated and each case is reviewed by the radiation oncologist.

3. Results

Since October 2014, twenty-three patients have been treated with TMI (Table 1). All patients completed their treatment as planned and could proceed with subsequent SCT without delay. Two patients received partial TBI backup treatment due to temporary machine malfunction. None of the patients required anaesthesia, but three patients received mild sedatives during some of the TMI fractions due to anxiety. Dose to targets are reported as near minimum and near maximum dose

Table 2

Mean dose (D_{mean}) to organs at risk, near maximum dose ($D_{2\%}$) and near minimum ($D_{98\%}$) dose to target with lower body and upper body plans summarized but excluding any boost treatment. Doses are normalized to the prescribed dose and patients are numbered consecutively. The transition volume (PTV_{Trans}), extends 2 cm cranio-caudally across the junction.

	Mean (%)	SD (%)	Range (%)	
PTV _{Thorax} D _{98%}	94.5	2.1	87.1	98.4
PTV _{Thorax} D _{2%}	106.6	1.2	104.9	110.6
PTV _{Thorax} D _{mean%}	100.6	1.1	96.2	101.9
PTV _{Legs} D _{98%}	95.6	3.5	89.6	101.1
PTV _{Legs} D _{2%}	109.0	3.8	101.5	118.3
PTV _{Legs} D _{mean}	102.6	2.3	95.8	107.5
PTV _{Trans} D _{98%}	94.8	4.1	88.7	104.0
PTV _{Trans} D _{2%}	109.6	5.2	101.9	122.0
Lungs D _{mean}	77.3	3.3	70.1	87.5
Liver D _{mean}	69.0	5.2	59.7	79.2
Heart D _{mean}	61.1	5.7	53.0	75.1
Kidneys D _{mean}	62.3	5.2	54.7	77.7
Bowelbag D _{mean}	61.3	4.2	52.8	71.0

whereas OARs are reported as average doses (Table 2). All doses to OARs are below those previously received by patients treated with standard TBI. Dose calculated in the Eclipse TPS simulating a TBI treatment geometry yields an average dose of 99% of the prescribed target dose to kidneys, heart, bowel bag and liver for a patient of average BMI. The average dose to kidneys, heart and bowel was reduced by approximately 40% with the TMI treatment compared to the conventional TBI treatment. Typically, one day was allocated for sessions of immobilization and CT, one day to TBI immobilization and planning for backup purpose, one day to delineation, and 3–4 days to planning, DQC and treatment preparation.

3.1. Planning

The values of planning parameters and optimization objectives differed only little between patients. For the upper body, the median values of modulation factor and beam-on time were 1.94 ± 0.13 and 21.0 ± 2.0 min respectively and corresponding values for the lower body were 1.3 and 9 min. Except for the first patient, all patients receiving 2.0 Gy/fraction were planned with a field width of 5 cm and pitch value of 0.397. Hence a class solution was created and used for planning almost all of the patients, cutting planning time considerably. Fig. 2 shows a coronal plane of the junction volume at and the dose distribution from each plan summed up to the total dose.

For all patients calculated with DCH, the probability of achieving dose coverage of at least 98% of prescribed dose to at least 93% of the target volume was on average $P[D_{98\%} \geq 93\%] = 0.9$ (0.8–1.0) for delivered fractions, and 1.0 for all planned fractions.

All treatment plans passed the QC measurements using the Delta4 detector, with an average gamma pass rate of 97% (91–100%).

3.2. Image registration and treatment

Optical surface scanning using the Sentinel system was initially tested on both upper and lower body to replace MVCT and save patient time on the treatment couch. A time analysis of the radiation treatment procedure was performed where 11 different steps were timed and noted in order to identify procedures that could be streamlined. The treatment time (patient entrance to exit) was on average 1 h 56 min (1:44–2:07 h) for treatment fractions with MVCT on both lower and upper body, and on average 1 h 31 min (1:25–1:36 h) for treatment fractions with MVCT on upper body and surface scanning positioning on lower body. The difference in setup time was significant, as tested with Mann-Whitney two-sided U test ($p < 0.005$) indicating that the SGRT system (Median = 12 min) is faster for setup of lower body than

MVCT (Median = 31 min).

For the lower body, the 3-mm correlation criteria were met for most but not all patients. For one patient that showed exceptional setup reproducibility after the first three fractions, SGRT was also performed on the upper body and reduced the total treatment time (entrance to exit) to 60 min. For the rest of the patients, the flexibility of joints and bony structures resulted in too large daily variations and IGRT was restricted to the lower body only. However, SGRT continued to be used for re-registering the position of the arms due to the insufficient FOV of the Tomotherapy MVCT.

The offset plans had a mean $D_{0.5\%} = 1.85$ Gy (SD = 0.11 Gy) and a mean $D_{5\%} = 2.24$ Gy (SD = 0.15 Gy) with the original plans had a $D_{0.5\%} = 1.89$ Gy (SD = 0.04 Gy) and a mean $D_{5\%} = 2.21$ Gy (SD = 0.06 Gy).

4. Discussion

Radiotherapy plays an important part of the conditioning prior to bone marrow transplantation. The traditional technique, TBI with shielded lungs, exhibit large dose heterogeneity and high doses to OARs. The technique implemented in this work, TMI with HT, significantly reduces the doses to OARs, but is more demanding on optimization of treatment, immobilization, quality assurance, treatment planning and beam delivery. To our knowledge, this is the first published method to incorporate backup planning and SGRT in TMI treatment. The fact that two patients were transferred to a conventional linac for partial TBI treatment completion confirms the need for a backup solution in case of e.g. machine failure or other unexpected circumstances.

The immobilization technique used was based on extensive experience with HT from similar treatments of long targets, such as cranio-spinal irradiation and total lymph node irradiation. Our strategy for a safe treatment was to define PTVs with margins sufficiently large to avoid repositioning with a lengthy rescanning and registration, while still managing significant OAR sparing. Compared to most other studies, we have initially opted for more generous PTV margins to minimise the risk of missing targets and hence report slightly higher doses to sensitive organs than other publications [22]. Movement of the ribs from free breathing poses no problem since a normal 3–4 mm anterior-posterior amplitude is covered by the 10-mm PTV. The applied margins have shown to be appropriate based on reviewed images and dose coverage histograms, but there may be room for reduction in certain areas of the body. A larger patient cohort may identify where the setup variation is at its largest and smallest. Risk organs of smaller children are especially difficult to spare because of the large PTV volume relative to the body but can benefit significantly from a mere 2-mm PTV shrinkage. Nevertheless, even among the paediatric patients, considerable sparing of OARs were obtained with the present margins. In this study we focussed on reducing dose to a smaller number of organs. Retrospective data of from TBI treatments show that the late side effects mainly concern kidneys, lungs and liver but also bowel bag and heart [23]. By forcing to reduce dose to numerous sensitive organs, an increased dose heterogeneity is introduced and hence an increased complexity of the treatment. This may convey risks and needs to be carefully thought through.

Another advantage with the TMI treatment is that optimisation in the Tomotherapy TPS gives the radiation oncologist full control over customizing target extensions and dose differentiation. For example, Patient #6 received an additional boost to 20 Gy/5F to the right humerus and thoracic columna due to FDG-PET positive myeloma involvement, and patient #10 received a boost to enlarged lymph nodes.

In contrast to a few other published studies, we have opted for the helical technique throughout the treatment as opposed to the mixed technique that adjoins the helical irradiation field of the upper body with anterior-posterior fields on the lower body using a conventional accelerator [24]. Reasons for this are a better control of the dose to the

junction area, a superior dose distribution and avoiding transit between treatment units. We have consistently planned with the *fixed jaw* option by tradition, but dynamic jaw works equally well.

This work describes an effortless procedure to plan, match and add the doses from the upper and lower body plans without DICOM file manipulation as described by Zeverino et al. [14]. By introducing an optimised shallow gradient of the abutting fields at the junction, the robustness is greatly improved. A very similar approach has been described by Mancosu et al in their TMI approach using VMAT [25].

The time required for delineation can possibly be reduced by auto-contouring, such as atlas-based segmentation. Planning time was considerably reduced by using a class solution for TMI optimization and an acceptable plan is generally achieved within a day. A combination of gained experience and the use of SGRT has cut treatment time substantially and is today comparable to TBI treatment time slots. SGRT has shown great potential to reduce time on the treatment table for the patient but needs to be further investigated and developed into e.g. a multi-camera system. Such a system could also be used to monitor patient motion in real time by compensating the couch motion and quantify the intra-fraction motion in a way that is not yet available for Tomotherapy treatments. This would improve treatment safety especially for patients with very long treatment times such as TMI. However, the Sentinel system may still be used to confirm that the patient position is still unchanged, by acquiring a second surface scan immediately after the treatment to compare with the pre-treatment scan.

In addition, from our robustness analysis of the junction volume we can conclude that the field matching technique is safe within normal setup deviations.

Compared to TBI, TMI with HT is able to deliver a more uniform dose to bone marrow and significantly reduce dose to OAR and allow for sophisticated individual dose delivery including simultaneously treating boost volumes. After 23 treated patients, no increased toxicity, recurrence or severity of GVHD have been reported as compared to the conventional TBI technique.

5. Conclusion

In this paper, we have described a procedure of implementing TMI in a clinical routine using a multidisciplinary team with members of each involved staff group. By forming a dedicated TMI team already from the beginning, procedures were consistently followed and continuously improved. Critical steps in the process have been identified and refined using various robustness techniques. TMI protocol has resulted in very reproducible treatments regardless of anatomy or conditioning of the patients. Feedback and new ideas are still discussed at regular TMI group meetings and has been a vital part of the implementation procedure.

Funding details

Department of corresponding author have an ongoing research agreement with Accuray Inc. which includes funding.

Ethics

Approved by local ethics committee, written consent from patients and all patient information have been fully anonymised.

References

- Adkins DR, DiPersio JF, Adkins DR. Total body irradiation before an allogeneic stem cell transplantation: Is there a magic dose? *Curr Opin Hematol* 2008;15:555–60. <https://doi.org/10.1097/MOH.0b013e3283188f5>.
- Hartman A-R, Williams SF, Dillon JJ. Survival, disease-free survival and adverse effects of conditioning for allogeneic bone marrow transplantation with busulfan/cyclophosphamide vs total body irradiation: a meta-analysis. *Bone Marrow Transplant* 1998;22:439–43. <https://doi.org/10.1038/gj.bmt.1701334>.
- Giral S, LeMaistre CF, Vriesendorp HM, Andersson BS, Dimopoulos M, Gajewski J, et al. Etoposide, cyclophosphamide, total body irradiation, and allogeneic bone marrow transplantation for hematologic malignancies. *J Clin Oncol* 1994;12:1923–30. <https://doi.org/10.1200/JCO.1994.12.9.1923>.
- Cliff RA, Buckner CD, Appelbaum FR, Bryant E, Bearman SI, Petersen FB, et al. Allogeneic marrow transplantation in patients with chronic myeloid leukemia in the chronic phase: a randomized trial of two irradiation regimens. *Blood* 1991;8:1660–5.
- Peñagaricano JA, Chao M, Rhee FV, Moros EG, Corry PM, Ratanatharathorn V. Clinical feasibility of TBI with helical tomotherapy. *Bone Marrow Transplant* 2011;46:929–35. <https://doi.org/10.1038/bmt.2010.237>.
- Nalichowski A, Eagle DG, Burmeister J. Dosimetric evaluation of total marrow irradiation using 2 different planning systems. *Med Dosim* 2016;41:230–5. <https://doi.org/10.1016/j.meddos.2016.06.001>.
- Schultheiss TE, Wong J, Liu A, Olivera G, Somlo G. Image-guided total marrow and total lymphatic irradiation using helical tomotherapy. *Int J Radiat Oncol Biol Phys* 2007;67:1259–67. <https://doi.org/10.1016/j.ijrobp.2006.10.047>.
- Corvò R, Zeverino M, Vagge S, Agostinelli S, Barra S, Taccini G, et al. Helical tomotherapy targeting total bone marrow after total body irradiation for patients with relapsed acute leukemia undergoing an allogeneic stem cell transplant. *Radiother Oncol* 2011;98:382–6. <https://doi.org/10.1016/j.radonc.2011.01.016>.
- Somlo G, Spielberger R, Frankel P, Karanes C, Krishnan A, Parker P, et al. Total marrow irradiation: a new ablative regimen as part of tandem autologous stem cell transplantation for patients with multiple myeloma. *Clin Cancer Res* 2011;17:174–82. <https://doi.org/10.1158/1078-0432.CCR-10-1912>.
- Gruen A, Ebell W, Wlodarczyk W, Neumann O, Kuchl JS, Stromberger C, et al. Total body irradiation (TBI) using Helical Tomotherapy in children and young adults undergoing stem cell transplantation. *Radiat Oncol* 2013;8:92. <https://doi.org/10.1186/1748-717X-8-92>.
- Wong JYC, Forman S, Somlo G, Rosenthal J, Liu A, Schultheiss T, et al. Dose escalation of total marrow irradiation with concurrent chemotherapy in patients with advanced acute leukemia undergoing allogeneic hematopoietic cell transplantation. *Int J Radiat Oncol Biol Phys* 2013;85:148–56. <https://doi.org/10.1016/j.ijrobp.2012.03.033>.
- Hui SK, Vermeris MR, Higgins P, Gerbi B, Weigel B, Baker SK, et al. Helical tomotherapy targeting total bone marrow first clinical experience at the University of Minnesota. *Acta Oncol* 2007;46:250–325. <https://doi.org/10.1080/02841860601042449>.
- Zhuang AH, An L, Schultheiss TE, Wong JYC. Dosimetric study and verification of total body irradiation using helical tomotherapy and its comparison to extended SSD technique. *Med Dosim* 2010;35:243–9. <https://doi.org/10.1016/j.meddos.2009.07.001>.
- Zeverino M, Agostinelli S, Taccini G, Cavagnetto F, Garelli S, Gusinu M, et al. Advances in the implementation of helical tomotherapy-based total marrow irradiation with a novel field junction technique. *Med Dosim* 2012;37:314–20. <https://doi.org/10.1016/j.meddos.2011.12.001>.
- Moliner G, Izar F, Ferrand R, Bardies M, Ken S, Simon L. Virtual bolus for total body irradiation treated with helical tomotherapy. *J Appl Clin Med Phys* 2015;16:164–76. <https://doi.org/10.1120/jacmp.v16i6.5580>.
- Kissick MW, Fenwick J, James JA, Jeraj R, Kapatoes JM, Keller H, et al. The helical tomotherapy thread effect. *Med Phys* 2005;32:1414–23. <https://doi.org/10.1118/1.1896453>.
- Chen M, Chen Y, Chen Q, Lu W. Theoretical analysis of the thread effect in helical Tomotherapy. *Med Phys* 2011;38:5945–60. <https://doi.org/10.1118/1.3644842>.
- Takahashi Y, Vermeris M, Dusenbery K, Wilke C, Weisdorf DJ, Hui SK. Peripheral dose heterogeneity due to the thread effect in total marrow irradiation with helical tomotherapy. *Int J Radiat Oncol Biol Phys* 2013;87:832–9. <https://doi.org/10.1016/j.ijrobp.2013.07.017>.
- Haraldsson A, Hauer Karlsson A, Ambolt L, Engström P. Plan specific pitch on Tomotherapy-plans effect on gamma pass rate for patient QA measured on Delta4. *Radiother Oncol* 2016;119:S740. [https://doi.org/10.1016/S0167-8140\(16\)32843-2](https://doi.org/10.1016/S0167-8140(16)32843-2).
- Low DA, Dempsey JF. Evaluation of the gamma dose distribution comparison method. *Med Phys* 2003;30:2455–64. <https://doi.org/10.1118/1.1598711>.
- Svahn-Tapper G, Nilsson P, Jönsson C, Alvegård TA. Calculation and measurements of absorbed dose in total body irradiation. *Acta Oncol* 1990;29:627–33. <https://doi.org/10.3109/02841869009090064>.
- Paix A, Antoni D, Waissi W, Ledoux MP, Bilger K, Fornecker L, et al. Total body irradiation in allogeneic bone marrow transplantation conditioning regimens: a review. *Crit Rev Oncol Hematol* 2018;123:138–48. <https://doi.org/10.1016/j.critrevonc.2018.01.011>.
- Leiper AD. Late effects of total body irradiation. *Arch Dis Child* 1995;72:382–5.
- Wong JYC, Liu A, Schultheiss T, Popplewell L, Stein A, Rosenthal J, et al. Targeted total marrow irradiation using three-dimensional image-guided tomographic intensity-modulated radiation therapy: an alternative to standard total body irradiation. *Biol Blood Marrow Transplant* 2006;12:306–15. <https://doi.org/10.1016/j.bbmt.2005.10.026>.
- Mancosu P, Navarra P, Castagna L, Reggiori G, Stravato A, Gaudino A, et al. Plan robustness in field junction region from arcs with different patient orientation in total marrow irradiation with VMAT. *Phys Med* 2015;31:677–82. <https://doi.org/10.1016/j.ejmp.2015.05.012>.

Paper II



A Helical tomotherapy as a robust low-dose treatment alternative for total skin irradiation

André Haraldsson^{1,2} | Jens Engleson¹ | Sven Å. J. Bäck^{1,2} | Silke Engelholm¹ | Per E. Engström¹

¹Department of Hematology, Oncology and Radiation Physics, Skåne University Hospital, Lund, Sweden

²Medical Radiation Physics, Department of clinical sciences, Lund University, Lund, Sweden

Author to whom correspondence should be addressed. André Haraldsson
E-mail: andre.haraldsson@med.lu.se;
Telephone: +46 46175605

Funding information
Accuray Inc.

Abstract

Mycosis fungoides is a disease with manifestation of the skin that has traditionally been treated with electron therapy. In this paper, we present a method of treating the entire skin with megavoltage photons using helical tomotherapy (HT), verified through a phantom study and clinical dosimetric data from our first two treated patients. A whole body phantom was fitted with a wetsuit as bolus, and scanned with computer tomography. We accounted for variations in daily setup using virtual bolus in the treatment plan optimization. Positioning robustness was tested by moving the phantom, and recalculating the dose at different positions. Patient treatments were verified with *in vivo* film dosimetry and dose reconstruction from daily imaging. Reconstruction of the actual delivered dose to the patients showed similar target dose as the robustness test of the phantom shifted 10 mm in all directions, indicating an appropriate approximation of the anticipated setup variation. *In vivo* film measurements agreed well with the calculated dose confirming the choice of both virtual and physical bolus parameters. Despite the complexity of the treatment, HT was shown to be a robust and feasible technique for total skin irradiation. We believe that this technique can provide a viable option for Tomotherapy centers without electron beam capability.

PACS
87.55kh

KEY WORDS
fungoides, helical, mycosis, skin, tomotherapy, total skin irradiation

1 | INTRODUCTION

Mycosis fungoides is a rare form of non-Hodgkin T-cell lymphoma mainly affecting the cutaneous tissue. The incidence is around three per 1000 000 person-years in Sweden. Early clinical manifestation is characterized by limited plaques, and later by tumors, widespread ulceration, and systemic involvement which can cause severe itching. A number of treatments are available, but none induces long-term

remission, and treatment is therefore often regarded as palliative despite long survival. Mycosis fungoides has been treated with radiotherapy since the 1960s,¹ and Total Skin Electron Beam Therapy (TSEBT) is considered the standard treatment today.²⁻⁴ Traditionally, a prescribed dose of 30–36 Gy over 6–10 weeks has been recommended,⁴ but recently, doses as low as 10–12 Gy have been used for step-wise short-term palliation.⁵ Lower-dose regimes have two main advantages: the treatment time is shorter, and the toxicity

This is an open access article under the terms of the Creative Commons Attribution License, which permits use, distribution and reproduction in any medium, provided the original work is properly cited.

© 2019 The Authors. *Journal of Applied Clinical Medical Physics* published by Wiley Periodicals, Inc. on behalf of American Association of Physicists in Medicine.

lower, which allows re-irradiation. To cover as large an area of the skin as possible, TSEBT is administered with the patient standing on a rotating platform or at several fixed positions at an extended source to skin distance (SSD) of 3–8 m using a beam degrader. TSEBT offers good short-term remission and few reported cases of severe toxicity.⁴ However, it is not possible to irradiate all the cutaneous tissue with this technique, and several patch fields are needed, raising questions regarding over- and underdosage at the field junctions. In addition, lead shielding of genitals, eyes and lips is necessary, making the technique cumbersome.

An alternative mode of treatment is total skin irradiation (TSI) with helical tomotherapy (HT),⁶ a technique combining couch translation and continuous gantry rotation. With this technique,^{7,8} targets as long as 135 cm can be irradiated in one field.⁹ Treatment of longer targets requires the field to be split but still allowing the whole skin to be treated on one occasion. Furthermore, skin folds can be covered by defining them as target in the optimization, and organs such as the eyes, genitals and lips can be avoided. For TSI with HT, the patient can lie down in supine position during the entire treatment as opposed to standing. This technique can be of value for centers without capability of electron treatment of the entire skin, but also for partial irradiation of the skin. A few studies have previously reported on TSI with HT,^{7,10,11} In this work, we evaluate the robustness of TSI with HT and implementation of virtual and physical bolus in the form of a wet suit and verify phantom data with clinical data.

The feasibility, deliverability, and assessment of robustness for the first two patients treated at our clinic is described.

2 | MATERIALS AND METHODS

2.A | Overview

Several issues regarding patient positioning, treatment planning, and delivery needed to be addressed before commencing clinical TSI. In order to achieve a geometrically robust treatment plan, a virtual bolus was designed and applied in the optimization. To test the robustness of the treatment plan, a whole body phantom was shifted and recalculated in the planning system for several positions and verified with dose measurements. Since the dose delivery of TSI is extremely complex, given that only tangential beams are used, the dose calculation accuracy of the treatment planning system (TPS) was verified for both surface dose and scattered central dose. During treatment, the patients were fitted with a wet suit of Neoprene, which is a non-tissue equivalent material of unknown electron density and hence the bolus effect of Neoprene needed to be carefully evaluated. *In vivo* measurements were performed to verify the dose to the skin, on both patients and phantom.

2.B | Patient characteristics

The first patient was a 72-yr-old male diagnosed with MF 2003. He had previously received radiotherapy with kilovoltage x-ray on several

occasions and had also been treated with PUVA + Methotrexate, Neotigason, and Targretin. At the time of TSI he had patches and plaques covering more than 10% of the body surface.

Patient 2 was a 43-yr-old female diagnosed with MF in 2007. She had been treated with TSEBT in Cairo in 2008, 32 Gy in 24F and she had also been given 35 treatments on different lesions with kV x-ray. She had received systemic therapies with Interferon, Tagretin, Neotigason, and Methotrexate. At the time of treatment, she had patches and plaques covering more than 10% of the body surface. The TSI treatment was followed by a haploidentical allogenic bone marrow transplant with her 18-yr-old daughter as donor 3 weeks after the last fraction.

2.C | Phantoms and detectors

A number of phantoms and detectors were used in this study.

- An anthropomorphic whole body phantom, PH-2B CT (PBU-60) (Kyoto Kagaku, Kyoto, Japan), with and without a neoprene suit. The density of simulated soft tissue of the phantom is 1.061 g/cm³, with a relative electron density of 0.975. The weight is 50 kg and the length 165 cm. The phantom includes relevant organs such as a lung cavity and a synthetic skeleton.
- A TomoTherapy phantom (Accuray Inc., Madison, WI, USA), which is a cylindrical Solid Water (RMI Gammex) phantom with varying density plugs, inserts for an A1SL ion chamber, and a removable midsection for film dosimetry.
- Solid Water slabs, size of 550 × 150 mm with thicknesses of 5–50 mm.
- A Delta4 1042 cross-plane PMMA diode array detector with a density of 1.19 g/cm³ and relative electron density of 1.16 (Scandidos, Uppsala, Sweden).
- Two separate Exradin A1SL ion chamber (Standard Imaging Inc., Middleton, WI, USA).
- Gafchromic EBT3 film (ISP, Wayne, NJ, USA) together with evaluation software FilmQA Pro (Ashland, Bridgewater, NJ, USA) and an Epson 4990 flatbed scanner (Seiko Epson Corporation, Nagano, Japan).

2.D | Immobilization and computed tomography (CT)

2.D.1 | Phantom

Prior to CT, the PBU-60 phantom was immobilized with a large vacuum cushion (VacFix, Par Scientific A/S, Odense, Denmark), an individually molded neck rest, and a 3-point open-face thermoplastic mask (Orfit Industries, Wijnegem, Belgium). Arms and hands were placed close to the trunk, the knees were slightly flexed, and the feet immobilized by the vacuum cushion, as shown in Fig. 1. Fiducial markers and tape were placed on the phantom marking the position of the lasers and the field junction position on the thighs. Since the phantom was longer than 135 cm, it was scanned in two parts, using a Siemens CT Somatom Definition Plus Scanner (Erlanger, Germany), with the wet suit in place. The first scan covered vertex to the thigh

in head-first supine (HFS) position, and the second from the toes to the upper thigh in feet-first supine (FFS) position. Between scans, the vacuum cushion was rotated 180° and the head and neck immobilization removed. The two scans were performed with a slice thickness of 5 mm and overlapped by approximately 15 cm.

2.D.2 | Patients

The patients were immobilized and scanned following the same procedure as the phantom, but with a 5 point open-face thermoplastic mask (Orfit Industries, Wijnegem, Belgium) and added wet suit socks, hood, and gloves. Patients were CT-scanned wearing the full wet suit in order to assess and account for anatomical effects from the tight fitting suit both in treatment planning and in image registration during treatment. The body mass index (BMI) of patient #1 was 24, and 28 for patient #2.

2.E | Planning and optimization

2.E.1 | Phantom

The results of both scans were exported to the TPS Eclipse (Varian Medical Systems, Palo Alto, CA, USA) and oncology information system Aria (Varian Medical Systems, Palo Alto, CA, USA) where the target and all relevant organs at risk (OARs) were delineated. The clinical target volume (CTV) was defined as the entire area of the skin to a depth of 5 mm, excluding the genitals, lips, and eyes. The planning target volume (PTV) was defined as a 5 mm isotropic expansion of the CTV.

The prescribed dose was defined as 12 Gy in 6 fractions for the phantom. Optimization was performed in the TomoTherapy treatment planning software (Accuray Inc., Madison, WI, USA) using fine resolution ($1.95 \times 1.95 \text{ mm}^2$) for both optimization of the treatment plan and for final dose calculation. Planning parameters were set to a pitch of 0.200,¹² a field width of 5 cm, a modulation factor of 2.3, and a minimum of 500 iterations. To aid in

optimization, several internal blocking structures were defined. These structures were cropped from the PTV inwards by 5, 15, and 30 mm, where the 30-mm structure were set to completely block the fluence. This procedure prevented all except tangential beams from entering the patient/phantom, thus reducing the dose to deep-lying organs. The aim of planning optimization was to achieve the prescribed dose to cover 60% of the PTV, and a minimum of 95% of the prescribed dose would cover 95% of the PTV. The shape of the blocking structures was modified until target coverage was deemed acceptable.

The field junction was designed to be robust for uncertainties in patient positioning. A dose gradient was achieved on both CT sets by contouring a junction structure centered at the junction markers in the longitudinal direction. We started with a 4 cm long junction structure and then adjusted the length until coverage was acceptable. The junction structure was set as a target structure, without setting the structure *in use* and with an overlap priority higher than any other target structure. This achieves a similar effect as cropping the PTV. In combination with optimization with fixed jaws, this procedure creates a dose fall-off at the field junction. The dose distribution from both treatment plans were imported to Eclipse for dose summation. In addition, we used the delivery quality analysis (DQA) module to reposition and recalculate the upper body of the PBU-60 phantom by 5 mm and by 10 mm in all directions, where the resulting dose matrices were exported to Eclipse and added together with the lower body. The repositioned dose distribution was evaluated to assess the robustness of the junction under positioning deviations.

2.E.2 | Patient

The prescribed dose was defined as 12 Gy in six fractions for the first patient whereas the second patient was prescribed 20 Gy in ten fractions. Planning and optimization were performed using similar planning parameters as in the phantom study, with several internal

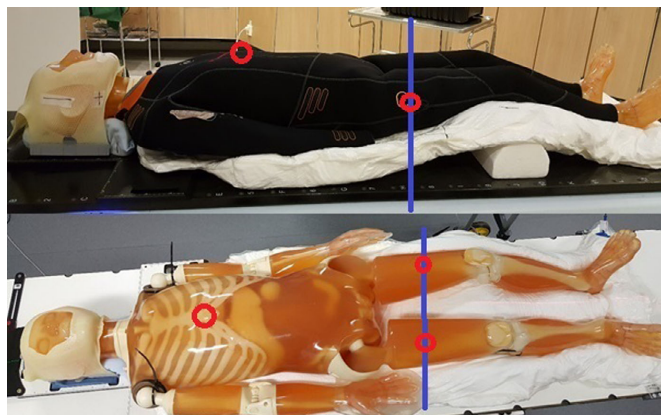


FIG. 1. The anthropomorphic whole body PBU-60 phantom, immobilized by a large vacuum cushion, with and without the thermoplastic mask and support under the knees. Red circles mark the position of the internal reference points for the two plans and the blue line marks the position of the field junction.

blocking structures to prevent dose to internal organs such as bone marrow.

2.F | Virtual bolus

A virtual bolus was used to prevent over-optimization of the fluence in air, due to expansion of the PTV outside the body. The wet suit was replaced by virtual bolus in the optimization since the fit of the suit varied from day to day. Targets very close to the tissue–air border causes the TPS to compensate the fluence to achieve full dose in the build-up region and in the air surrounding the body. If the patient is not perfectly aligned during treatment, the patient may receive a dose well above that prescribed during treatment (Fig. 2). This can be managed by using a virtual bolus.

2.F.1 | Phantom

With the whole body phantom, optimization tests were performed in the TPS using a varying bolus density of 0, 0.4, and 1.0 g/cm³. The thickness of the virtual bolus was 8 mm, that is, the PTV with an additional 3 mm margin, as suggested by Moliner.¹³

2.F.2 | Patients

Although the patients were CT-scanned wearing the full wet suit, a virtual bolus of water of specified density was still added in the TPS for two reasons; to account for daily variations caused by the fit of the wet suit and secondly, to replace the unconventional bolus material of neoprene with a material of well-known dosimetric properties. The bolus was applied uniformly over the entire skin.

2.G | Physical bolus

2.G.1 | Phantom

A 7 mm thick foamed neoprene (polychloroprene), wetsuit (AquaLung Dive, US) was used as a physical bolus for the PBU-60 phantom. A wetsuit was chosen as bolus since it can be made to cover almost the entire body, has a uniform thickness and no metal components. The wetsuit covered the entire phantom except hands, feet and head.

2.G.2 | Patients

For the patients, a hood, gloves, and socks of neoprene were also added. In addition, patient #2 had a 5 mm water equivalent bolus (Superflab bolus, Radiation Products Design Inc., Albertville, MN, USA) covering eye lids and forehead, due to lesions in the face. The hood was open in the face but covering chin, ears, and above hair line.

2.H | Robustness tests

2.H.1 | Phantom

To verify the geometric robustness of the technique using a virtual bolus of 0.4 g/cm³ of 8 mm thickness together with a 7 mm neoprene bolus, the final treatment plans were exported to the built-in module for DQA. This module can be used to recalculate treatment plans for different geometries and phantoms. In this study, the treatment plan was recalculated for the upper body omitting the virtual bolus. The PBU-60 phantom was then repositioned by ±10 mm in the longitudinal, vertical, and lateral directions. The resulting dose matrices were exported to the Eclipse TPS for summation and comparison.

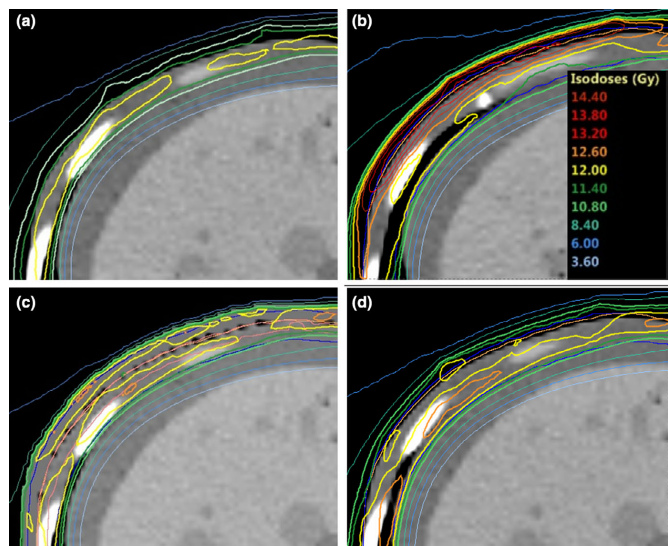


FIG 2. Difference in skin dose to patient 1 when the position is shifted by 5 mm lateral from the planned position for virtual bolus with a density of 0 g/cm³ (b) and a virtual bolus with a density of 1 g/cm³ (d) as compared to original position (a, c) when the treatment is planned without a virtual or physical bolus.

2.H.2 | Patients

To assess the robustness of the patients' treatment, data acquired from the daily megavoltage computed tomographic (MVCT) was used to recalculate the delivered dose and compare it to the original treatment plan. For the first six fractions, we recontoured the CTV on the daily MVCT images and recalculated the treatment plans. The calculations were performed in the TomoTherapy Planned Adaptive module, and the registration data from the treatment was used to match the images. The obtained dose volume histograms were compared to the original plan and to the robustness calculations of the whole body phantom as described in the previous section. In addition to calculations, we measured the skin dose *in vivo* with film at the first fraction. Because the position of the junction of the first patient at the hip differed from the PBU-60 phantom, the dose across the field junction was verified by shifting translating the upper body 5 mm in six directions ($\pm x$, $\pm y$, $\pm z$) and the resulting dose matrices was summed in Eclipse for verification.

2.I | Film measurements

2.I.1 | Skin dose

Phantom

To verify the delivered surface dose, 24 Gafchromic EBT3 film strips of 2×3 cm were placed on the surface of the phantom beneath the wet suit, and distributed over the entire body. The PBU-60 phantom was positioned and irradiated first in the HFS position and then in the FFS position, with field edge matching at the mid-thigh position. One strip from each sheet was irradiated with 2 Gy at a depth of 1.5 cm in Solid Water and used as a dose reference.

Patients

To assess the patient dose to the skin at treatment, we performed *in vivo* dosimetry with EBT3 film at the first fraction. At least 20 film strips of 1×1.5 cm² were taped on several positions on the patients' skin. A reference irradiation was performed at 2 Gy in solid water at 1.5 cm depth with a minimum of 20 cm backscatter.

2.I.2 | Bolus measurement

The bolus effect of the neoprene wet suit fitted on the PBU phantom was quantified by paired film measurements, where film where placed beneath the wetsuit for the first measurements and replaced for the second measurement without wetsuit. In addition, a strip of film was placed on a 20 cm thick Solid Water slab and irradiated with and without a $200 \times 200 \times 7$ mm³ square of neoprene to measure the buildup effect of neoprene. We compared the two measured groups using Wilcoxon signed-rank test.

2.I.3 | Film evaluation

Prior to each film measurement, a strip of film from the same sheet as that used for measuring was irradiated with 2 Gy at depth of 1.5 cm in

Solid Water with at least 20 cm backscatter and the TomoTherapy set in verification mode, that is fixed gantry with no couch travel. The films were scanned with an Epson 4990 flatbed scanner at least 24 h after exposure, and evaluated using the FilmQA Pro software using the reference film strip for dose normalization. The films strips were covered with a glass sheet, and scanned with a 16-bit pixel value, and 5×5 mm region of interests (ROIs) for averaging. The same evaluation procedure was used for both phantom and patient measurements. Film and dose calibration were verified using film strips at depths of 1.5, 5, and 10 cm in solid water slabs, irradiated twice at different occasions. The values obtained were compared to the dose measured with an A1SL ion chamber at corresponding points of measurements. Surface dose measurement were compared to the calculated dose in the TPS, obtained with the plan recalculated without the virtual bolus.

2.J | Ion chamber measurements

The optimized plan, restricted to only tangential irradiation was delivered to the cylindrical Tomotherapy phantom, to verify the accuracy of the dose calculation algorithm of the TomoTherapy TPS, at depths far from the main interaction sites. The plan was optimized with the phantom surface as target, to 4 Gy per fraction, and with margins and a virtual bolus specification identical to those used for the whole body phantom. The depth dose was measured using two A1SL ion chambers at several positions in the phantom and compared to the dose calculated by the TPS.

2.K | Diode array measurements

Dose verification was also performed using the Delta4 diode array detector placed at several locations to cover the entire irradiation volume of the treatment plan. The measured dose was compared to the planned dose using gamma evaluation.¹⁴ Quality control (QC) acceptance criterion was set to 90% pass rate using 2 mm distance to agreement, 3% dose difference, and global dose normalization.

The dose delivery across the junction was verified by irradiating both plans using the Delta4 detector in the same measurement session. For both plans, we positioned the Delta4 at the lateral and sagittal green laser position and longitudinally in the plan junction markers, due to the red to green laser separation limit of 15 cm for. The distance from the longitudinal green laser position to the Delta4 was measured in the DQA module and applied at setup. After irradiation of the upper plan, the detector was rotated and aligned to the lasers for the lower plan and subsequently irradiated in the same measurement session. The planned dose for the upper and lower body was manually summed using Python.

3 | RESULTS

3.A | Phantom

Doses to OARs are presented in Table 1. The optimization time for 500 iterations ranged between 4 and 6 h with a GPU-assisted dose

calculation engine. The beam on-times for the final plan were 31 and 19 min, for the upper and lower body, respectively. In the optimization, some adjustment of the blocking structure was required to compensate for the flat back of the phantom (see Fig. 3). This adjustment resulted in higher dose to the lungs of the phantom, due to the thin thorax wall of the PBU-60 phantom (6 mm). For the patients, this was corrected for by immobilizing the back in a rounded position.

Verification of the dose to the surface of the whole body phantom using EBT3 film agreed well with the dose to the PBU-60 phantom calculated without the virtual bolus. The results indicate that the dose calculated in the TPS provides a good approximation of the delivered skin dose. When using the virtual bolus and neoprene for build-up, the average dose difference between TPS and film measurements was -0.6% (SD = 3%; Fig. 4). The paired measurements, with and without wet suit, on the PBU-60 phantom showed a significantly higher surface dose with the 7 mm neoprene bolus than irradiation without bolus (Wilcoxon signed-rank test, $P < 0.05$; Figure 5). Measurements at 0 cm depth with and without a 7 mm sheet of neoprene placed on a Solid Water slab resulted in a 57% higher dose with the bolus, confirming the advantage of using neoprene as bolus material. Central dose measurements using two A1SL ion chambers in the cylindrical Tomotherapy phantom showed good agreement with the values given by the TPS; being within 2% of the TPS values at all 6 measured points. This indicated that the measurements are correctly represented by the superimposed convolution algorithm in the TPS, even though the measured points are far away

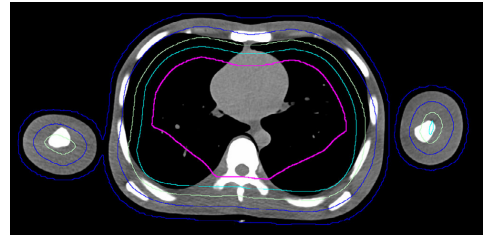


Fig. 3. Transverse slice of the PBU-60 phantom with planning target volume (blue) and several blocking structures (green, turquoise, pink) adjusted for increased target coverage in the back region, close to the vertebral column.

from the interaction site (2–15 cm) of the primary target.¹⁵ Measurements with the Delta4 diode array detector were performed at three different positions to cover different areas of the treatment plan, including the junction position of the plans, yielding gamma pass rates of 90%, 93%, and 97%, with global dose normalization. Consequently, the delivered dose was generally in good agreement with the planned dose at all measured positions, and within the pass rate criteria used at our clinic (90%). The dose across the junction region was evaluated with a structure created as a copy of the PTV, extending 2 cm cranially and 2 cm caudally of the junction markers. Dose to the structure was $D_{98\%}$ of 11.2 Gy, D_{mean} of 12.8 Gy, and $D_{2\%}$ of 14.2 Gy.

TABLE 1 Dose to the PBU-60 phantom (Gy) with a prescribed dose of 12 Gy in 6 fractions, patient 1 with a prescribed dose of 12 Gy in 6 fractions, and patient 2, with a prescribed dose of 20 Gy in 10 fractions.

Structure	Phantom			Patient 1			Patient 2		
	$D_{2\%}$	$D_{98\%}$	D_{mean}	$D_{2\%}$	$D_{98\%}$	D_{mean}	$D_{2\%}$	$D_{98\%}$	D_{mean}
Bladder	1.9	1.1	1.4	1.1	0.8	0.9	13.4	2.1	7.5
Body	12.4	0.4	6.4	12.7	0.8	6.0	1.5	21.0	10.9
Bone	12.2	0.6	6.1	12.1	0.8	4.2	20.2	1.4	7.7
Bowelbag	7.9	0.7	1.6	5.3	0.7	1.3	1.4	3.5	1.9
Brain	11.1	0.6	3.1	9.7	0.7	2.6	15.0	1.4	4.5
CTV 5 mm	12.9	10.5	11.9	13.0	10.9	12.1	22.0	16.5	20.0
Eye (left)	9.9	0.8	4.4	7.7	1.4	4.6	20.3	7.9	17.4
Eye (right)	10.0	0.8	3.9	7.6	1.4	4.6	20.6	7.9	17.6
Heart	1.5	0.7	0.9	1.8	0.9	1.1	2.6	1.7	2.0
Kidney (left)	1.5	0.7	1.0	1.8	0.9	1.3	2.6	1.5	1.9
Kidney (right)	1.7	0.7	1.0	1.6	0.9	1.2	2.3	1.4	1.8
Lens (left)	7.2	5.1	6.7	4.8	3.6	4.0	19.8	20.2	20.0
Lens (right)	7.1	4.6	5.7	4.8	3.8	4.1	20.0	20.5	20.3
Liver	3.5	0.6	1.1	7.3	0.9	1.6	2.3	1.5	2.0
Lung (left)	9.6	0.9	3.3	5.7	1.1	1.9	10.9	2.1	3.3
Lung (right)	10.9	0.9	4.1	6.8	1.0	1.9	10.9	2.0	3.1
Oral cavity	9.3	0.9	4.6	1.1	0.8	3.4	18.5	1.8	5.5
PTV	13.0	9.6	11.9	12.9	10.1	11.9	22.0	16.4	20.0

CTV: clinical target volume; PTV: planning target volume.

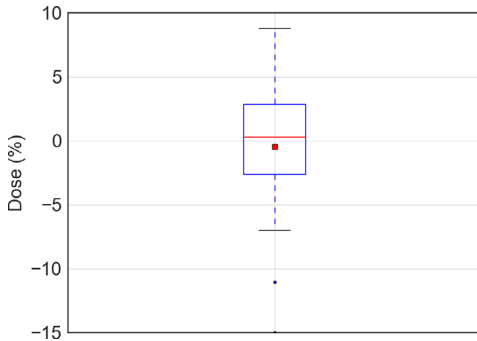


FIG. 4. The dose measured with electron beam therapy 3 film on the PBU phantom relative to that predicted by the treatment planning system recalculated without the virtual bolus, shown as a box-and-whisker plot, where the red line shows the mean of 23 measurements, median (red line), 1 SD (box) and 95% confidence interval (outer line) as well as outliers (black point).

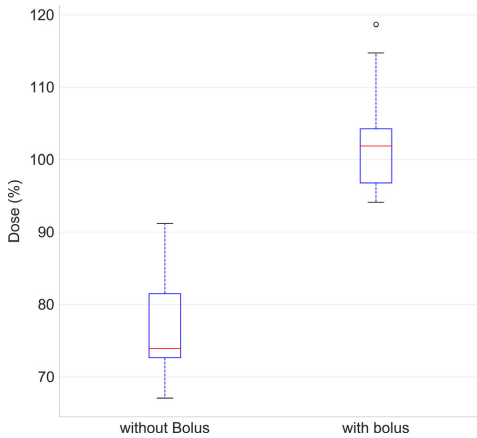


FIG. 5. Measurements with and without wet suit using electron beam therapy 3 film on the PBU-60 phantom presented as a box-and-whisker plot. The median (red line), as well as first and third quartile (box) and 1.5 times past the interquartile range (outer line) is plotted with outliers (black points). Dose is presented as percentage of prescribed dose.

The setup robustness test, performed by shifting the PBU-60 phantom in six directions yielded an average $D_{98\%}$ of 10.4 Gy (SD = 0.3 Gy) and $D_{2\%}$ of 13.4 Gy (SD = 0.1 Gy), indicating that this setup, combining a virtual bolus of 8 mm with a density of 0.4 g/cm³ and a physical neoprene bolus provides robust treatment for positioning errors of up to 10 mm. Recalculating the plan with different densities of the virtual bolus resulted in differences in the average dose to the CTV of -0.2 %, 0.2%, and 2.7%, for densities of 0 g/

cm³, 0.4 g/cm³, and 1 g/cm³, respectively, justifying the use of a virtual bolus with a density lower than that of water as proposed by Moliner et al.¹³

The extension of the junction structure between the lower and upper body of the PBU-60 was adjusted until an acceptable dose distribution was achieved, which was 4.5 cm for the phantom. The resulting test of the robustness, with repositioning and recalculation of the upper body and subsequent summation in Eclipse with the lower body, yielded a $D_{95\%}$ range of 11.5 to 11.7 Gy, and $D_{5\%}$ range of 14.2 to 14.7 Gy for 5 mm translational offset. For 10 mm translations, the $D_{95\%}$ dose ranged from 8.9 to 12.1 Gy and $D_{5\%}$ ranged from 12.2 to 14.8 Gy. The lowest doses found were in all cases from longitudinal setup errors. Line profiles from measurements with Delta4 as compared to planned dose recalculated on the Delta4 and summed over the junction region are reported in Fig. 6, and line profiles of the junction for different total length of the junction structure in Fig. 7.

3.B | Patient

Based on the experience from the immobilization of the PBU-60 phantom, the patients were immobilized with the back in a laterally curved position to better facilitate tangential irradiation in the optimization.

For both patients, the six-first fractions were recalculated based on daily MVCT images and compared to the robustness calculations performed with the PBU-60 phantom (Fig. 8). In addition, *in vivo* film dosimetry corresponded well with dose calculated in TPS, with a mean difference from TPS of 5.3% (SD = 11.9%) and 1.5% (SD = 9.0%) for patient 1 and 2 respectively (Fig. 9). Robustness test of the junction dose performed on the first patient yielded an average $D_{98\%}$ of 10.8 Gy (SD = 0.2 Gy) and $D_{2\%}$ of 13.4 Gy (SD = 0.2 Gy) for 5 mm translations.

Both patients could put the wetsuit on within a few minutes, with no notable effort. The fit for patient 2 was not optimal which was compensated for by taping air gaps to achieve a snug fit. Figure 10 shows examples of planning CT and MVCT image registration at the time of treatment. The CTV coverage was regarded adequate despite daily variations in fit of wet suit and skin folds. The total beam on time for the patients were 92 and 54 min for patient 1 and 2 respectively, with the length of the patient the deciding factor, 190 vs 165 cm. Both patients completed their treatment as planned and tolerated the treatment well with the second patient given only a mild sedative.

4 | DISCUSSION

4.A | Bolus

The surface dose measured with EBT3 film agreed well with that provided by the TPS for both the PBU-60 and the TomoTherapy phantom. The difference in the surface dose found for paired measurements with and without the neoprene bolus was significant, justifying the use of a virtual bolus as well as a physical bolus for total

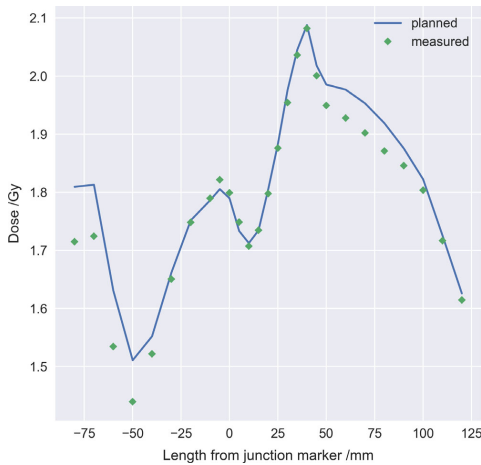


FIG. 6. Longitudinal line dose profile across the plan junction (0 mm) for both plans recalculated on the Delta4 phantom (blue line) and summed manually as compared to the measured dose (green diamond) with the Delta4 rotated for measurement of the lower body plan.

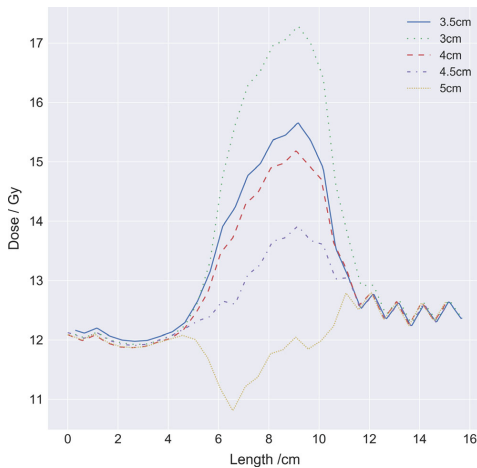


FIG. 7. Longitudinal line dose profiles for different total length of junction structures, between 3 and 5 cm in increments of 0.5 cm. The upper and lower body plan was summed in Eclipse and the line profile was acquired at 3 mm depth centered lateral over the junction marker.

skin delivery, despite the fact that neoprene is not a standard material, and the lack of water equivalence in the material. The results quantify the difference with using neoprene as bolus and stands in contrast to other studies that did not find it necessary to use bolus

for skin irradiation.^{8,16} The dosimetric advantage to a non-bolus treatment is clear, any attempt at optimizing or deliver photons to the skin performs better with bolus added.

4.B | Robustness

The robustness test showed that calculated and delivered dose corresponded well for displacements up to 10 mm, despite a CTV-to-PTV margin of only 5 mm. Underdosage to the skin of up to 20%, and an increase in average dose to the target, have been reported previously,⁹ depending on the parameters of the virtual bolus. When a thick high-density virtual bolus is used, the lack of corresponding physical bolus at treatment delivery causes overdosage to the skin and to a depth up to a few centimeters. When no bolus is used, physical or virtual, underdosage of the skin is likely due to build-up, and large dose deviations can be expected with normal patient displacements since optimization to the lower density (air) causes a high fluence. The measured and calculated skin dose agreed within a few percent in this study, even with displacements of up to 10 mm, by careful selection of the virtual bolus density and thickness (0.4 g/cm³, 8 mm) and planning parameters. The largest setup uncertainties in the phantom measurements were found around the arms, due to the difficulty of correct alignment caused by the limited field of view of the TomoTherapy MVCT (40 cm), that is, parts of the patient more than 40 cm from the isoaxis as seen in a transversal plane are not included in the MVCT. This issue may be resolved by using, for example, an external surface scanning system. Predicted doses to OARs in this study are similar to, or slightly higher than, those reported previously.^{7,8} These differences can be attributed to differences in CTV-to-PTV margins or differences in phantom anatomy.

The methodology for matching the junction dose of the treatment plans worked well for the treated patients and the phantom, but the dose distribution was more heterogeneous than in other parts of the target. The effect of using an overlapping structure works similar to cropping the PTV, but the benefit of a junction structure was the ability of adjusting the overlap region and still get the dose coverage correct in the PTV used for optimization. Improvement such as creating an extended optimization region with several optimization structures to better control the dose fall-off, would probably improve the dose homogeneity and robustness across the field junction. Line dose profiles acquired longitudinally for different junction lengths showed that a difference in junction length may result in an unproportional response in overlap dose, probably attributed to a combination of the amount of blocking and the gantry angle position at the current slice. Line dose profiles for measured dose compared to planned dose agreed well, showing the highest deviation at maximum and minimum dose owing to the difference in resolution, were the detectors in the Delta4 have 5 mm dispersion and the plan was calculated with a grid of 2.3 mm.

The first two patients were very different regarding BMI and fit of wet suit. Experience showed that a snug fit is vital to keep the workflow easy and daily variations to a minimum. For patient #2, loose skin and fatty tissue caused different skin folding from day to

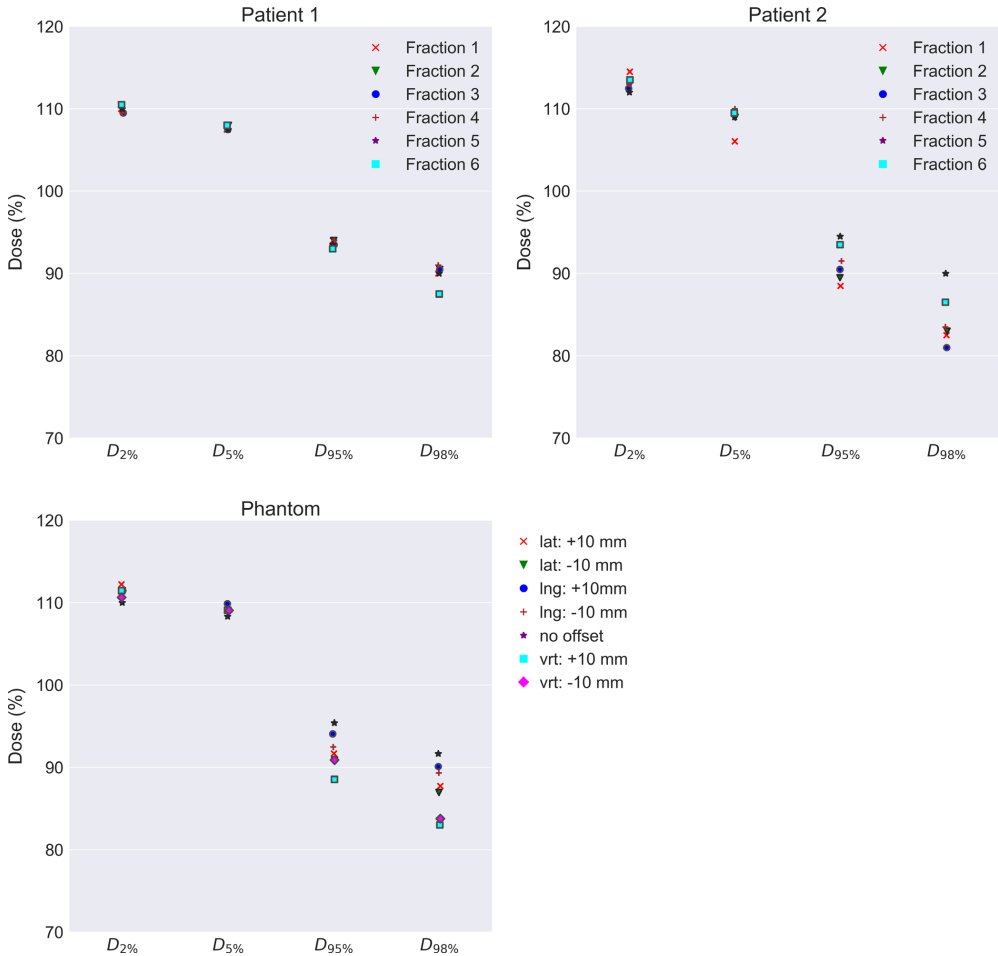


FIG. 8. Fraction dose delivered recalculated on megavoltage computed tomographic daily imaging for the first 6 fraction for patient 1 and 2, compared to robustness test data of the setup position using the PBU-60 phantom. For the phantom, the clinical target volume (CTV) coverage for the upper body is plotted for 10 mm offset in each direction against coverage with no offset. For the patients, CTV coverage for the upper body is plotted for the first 6 fractions.

day. However, no repositioning was needed, indicating that the skin folds was considered within tolerance. These issues affected the delivered dose as seen by the daily fraction calculations in and should be addressed by focusing on proper fitting of the wet suit. Another learning experience was to keep the arms close to the body. Although arms positioned farther from the thorax facilitate optimization of the arm circumference, it counteracts the optimization of dose homogeneity to the arms. As shown by *in vivo* film measurements, the measured dose to the skin was closer to the predicted (1.5%–5.3%) than reported in other studies with different physical

and virtual bolus.^{7,8} Previous studies on skin doses in the tomotherapy TPS has shown an overestimation of the calculated dose by approximately 9%.^{17,18} The number of patients in the study makes this a first experience, and more patients need to be added to draw any general conclusions. A clinical study is in the planning phase.

4.C | Comparison to standard treatment

TSEBT is today regarded as the standard treatment of mucositis fungoides and in comparison, TSI using HT is a lengthy and complex

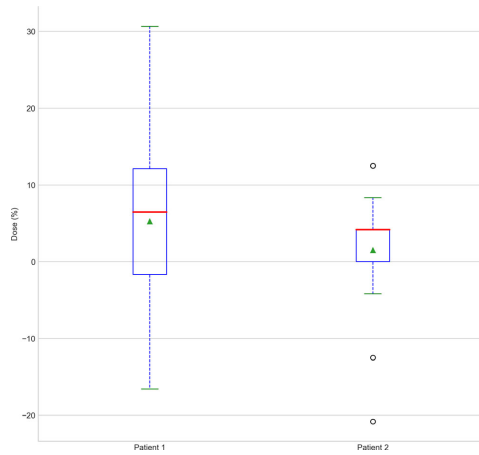


Fig. 9. Measured dose with electron beam therapy 3 film for patient 1 and 2 at the first fraction. Dose is plotted as the difference to prescribed fraction dose. Data are shown as a box-and-whisker plot, where the red line shows the mean of 23 measurements, median (red line), mean (green triangle), 1 SD (box), and 95% confidence interval (outer line) as well as outliers (black point).

treatment. The average beam on time was 73 min for our two patients and the in-room time between 3 and 3.5 h. In comparison, TSEBT is given twice daily, and with separate x-ray treatments given to the hands, the soles of the feet and scalp. Piotrowski et al.¹⁹ argued that the rotational TSEBT requires less time, but did not include the time for added extra x-ray fields necessary to cover scalp and other areas not covered in the electron irradiation in their estimation. Our experience from other complex treatments is that a new clinical routine takes a number of patients to set, and treatment time can very likely be reduced with surface guided positioning. For comparison, at our clinic, total marrow irradiation with HT took

almost 3 h for the first patient and the fastest fraction treated after 23 patients is closer to 1 h, partly as a result of surface guided positioning and an efficient clinical routine.

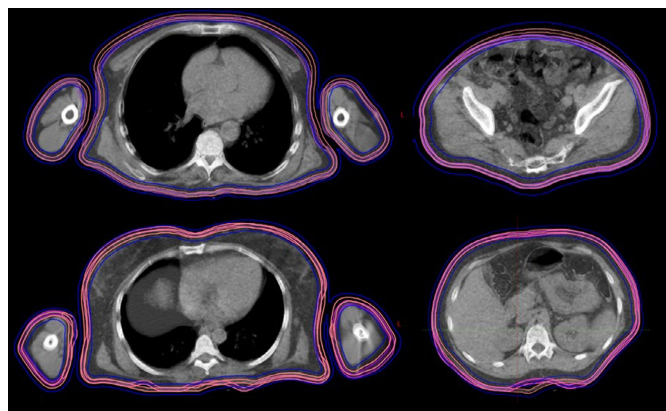
Doses to organs at risk are generally below clinically used dose constraints, but a comparison with TSEBT is not possible as, to the best of the authors' knowledge, doses to organs at risk have not been published for TSEBT. Slightly higher doses are expected to deep-lying organs in TSI with HT compared to TSEBT, which is a trade-off. In contrast, high robustness and a homogeneous target coverage can be achieved on a single treatment occasion using Tomotherapy.

Similar to results reported by Buglione et al.¹⁶ we believe TSI with TT to be a complement to electron treatment and in certain cases where treatment with Tomotherapy could be beneficial. In addition, since TSI with HT is an image guided technique, problems that may arise during treatment can be evaluated by dose recalculation or re-optimization of the treatment plan. Previously treated areas and organs at risks can be avoided, and simultaneous integrated boost to for example, plaque areas can be implemented. The results from this study can be of use when treating patients with partial irradiation of large areas, especially of convex shape such as the scalp²⁰ or melanoma.²¹ Furthermore, this technique may be an alternative to centers where electron therapy is not available.

4.D | Film dosimetry

The EBT3 film is an established and appropriate dosimetry system for surface dose measurement.^{22–24} It has a low angle dependence and stable response over a wide dose and energy range, especially when used with the FilmQApro scanning system, where all color channels can be evaluated. The largest uncertainty stems from positioning accuracy, that is, the problem to correctly assess the points of measurement of the films in the TPS for correct dose comparison.

Fig. 10. Daily megavoltage computed tomographic (MVCT) from the first fraction compared to planning computed tomography (CT) for patient 1 and 2. The CT and daily MVCT are overlaid with 50% transparency. Transversal slices for abdomen and thorax are displayed with original clinical target volume (CTV) (pink) with CTV for daily MVCT (magenta) and planning target volume (blue) from planning CT.



4.E | Conclusions

The presented technique was shown to be feasible and robust to deliver for both phantoms and for two individual patients. We believe that TSI with tomotherapy may be an alternative for centers without electron beam capability, if a more homogenous dose is desirable, or for partial skin irradiation where electron therapy for any reason is not feasible.

CONFLICT OF INTEREST

Department of corresponding author have an ongoing research agreement with Accuray Inc. which includes funding.


REFERENCES

- Fromer JL, Johnston DO, Salzman FA, et al. Management of lymphoma cutis with low megavolt electron beam therapy: nine year follow-up in 200 cases. *South Med J*. 1961;54:769–76.
- Maingon P, Truc G, Dalac S, et al. Radiotherapy of advanced mycosis fungoides: indications and results of total skin electron beam and photon beam irradiation. *Radiother Oncol*. 2000;54:73–8.
- Micaily B, Campbell O, Moser C, et al. Total skin electron beam and total nodal irradiation of cutaneous T-cell lymphoma. *Int J Radiat Oncol Biol Phys*. 1991;20:809–13.
- Jones GW, Kacinski BM, Wilson LD, et al. Total skin electron radiation in the management of mycosis fungoides: consensus of the European Organization for Research and Treatment of Cancer (EORTC) Cutaneous Lymphoma Project Group. *J Am Acad Dermatol*. 2002;47:364–370.
- Hoppe RT, Harrison C, Tavallaei M, et al. Low-dose total skin electron beam therapy as an effective modality to reduce disease burden in patients with mycosis fungoides: results of a pooled analysis from 3 phase-II clinical trials. *J Am Acad Dermatol*. 2015;72:286–292.
- Mackie TR, Holmes T, Swerdloff S, et al. Tomotherapy: a new concept for the delivery of dynamic conformal radiotherapy. *Med Phys*. 1993;20:1709–1719.
- Lin CT, Shiau AC, Tien HJ, et al. An attempted substitute study of total skin electron therapy technique by using helical photon tomotherapy with helical irradiation of the total skin treatment: a phantom result. *Biomed Res Int*. 2013;2013:108794.
- Sarfehniah A, Poon E, Davis SD, et al. A novel approach to total skin irradiation using helical TomoTherapy. *Pract Radiat Oncol*. 2014;4:330–335.
- Accuray I. TOMOTHERAPY® H™ SERIES: TomoH™, TomoHD™ and TomoHDA™ Systems Technical Specifications. In: Accuray I, editor. Madison, WI, US; 2017.
- Hui SK, Kapatoes J, Fowler J, et al. Feasibility study of helical tomotherapy for total body or total marrow irradiation. *Med Phys*. 2005;32:3214–3224.
- Hsieh CH, Shueng PW, Lin SC, et al. Helical irradiation of the total skin with dose painting to replace total skin electron beam therapy for therapy-refractory cutaneous CD4 + T-cell lymphoma. *Biomed Res Int*. 2013;2013:717589.
- Chen M, Chen Y, Chen Q, et al. Theoretical analysis of the thread effect in helical TomoTherapy. *Med Phys*. 2011;38:5945–5960.
- Moliner G, Izar F, Ferrand R, et al. Virtual bolus for total body irradiation treated with helical tomotherapy. *J Appl Clin Med Phys*. 2015;16:164–176.
- Low DA, Dempsey JF. Evaluation of the gamma dose distribution comparison method. *Med Phys*. 2003;30:2455–2464.
- Lissner S, Schubert K, Wiezorek T, et al. Investigations of peripheral dose for helical tomotherapy. *Z Med Phys*. 2013;23:324–331.
- Buglione M, Spiazzi L, Urpis M, et al. Light and shadows of a new technique: is photon total-skin irradiation using helical IMRT feasible, less complex and as toxic as the electrons one? *Radiat Oncol*. 2018;13:158.
- Avanzo M, Drigo A, Ren Kaiser S, et al. Dose to the skin in helical tomotherapy: results of in vivo measurements with radiochromic films. *Phys Med*. 2013;29:304–311.
- Ramsey CR, Seibert RM, Robison B, et al. Helical tomotherapy superficial dose measurements. *Med Phys*. 2007;34:3286–3293.
- Piotrowski T. Total skin electron irradiation—the technique where the electron beams are still irreplaceable. *Rep Pract Oncol Radiother*. 2014;19:69–71.
- Song JH, Jung JY, Park HW, et al. Dosimetric comparison of three different treatment modalities for total scalp irradiation: the conventional lateral photon-electron technique, helical tomotherapy, and volumetric-modulated arc therapy. *J Radiat Res*. 2015;56:717–726.
- Kramkimel N, Dendale R, Bolle S, et al. Management of advanced non-melanoma skin cancers using helical tomotherapy. *J Eur Acad Dermatol Venereol*. 2014;28:641–650.
- Devic S, Seuntjens J, Abdel-Rahman W, et al. Accurate skin dose measurements using radiochromic film in clinical applications. *Med Phys*. 2006;33:1116–1124.
- Mathot M, Sobczak S, Hoornaert MT. Gafchromic film dosimetry: four years experience using FilmQA Pro software and Epson flatbed scanners. *Phys Med*. 2014;30:871–877.
- Bilge H, Cakir A, Okutan M, et al. Surface dose measurements with GafChromic EBT film for 6 and 18MV photon beams. *Phys Med*. 2009;25:101–104.

Paper III



Surface-guided tomotherapy improves positioning and reduces treatment time: A retrospective analysis of 16 835 treatment fractions

André Haraldsson^{1,2}  | Sofie Ceberg² | Crister Ceberg² | Sven Bäck^{1,2} | Silke Engelholm¹ | Per E. Engström¹

¹Department Hematology, Oncology and Radiation Physics, Skåne University Hospital, Lund, Sweden

²Medical Radiation Physics, Department of Clinical Sciences, Lund University, Lund, Sweden

Author to whom correspondence should be addressed. André Haraldsson
E-mail: andre.haraldsson@med.lu.se;
Telephone: +46 46175605.

Abstract

Purpose: In this study, we have quantified the setup deviation and time gain when using fast surface scanning for daily setup/positioning with weekly megavoltage computed tomography (MVCT) and compared it to daily MVCT.

Methods: A total of 16 835 treatment fractions were analyzed, treated, and positioned using our TomoTherapy HD (Accuray Inc., Madison, USA) installed with a Sentinel optical surface scanning system (C-RAD Positioning AB, Uppsala, Sweden). Patients were positioned using in-room lasers, surface scanning and MVCT for the first three fractions. For the remaining fractions, in-room laser was used for setup followed by daily surface scanning with MVCT once weekly. The three-dimensional (3D) setup correction for surface scanning was evaluated from the registration between MVCT and the planning CT. The setup correction vector for the in-room lasers was assessed from the surface scanning and the MVCT to planning CT registration. The imaging time was evaluated as the time from imaging start to beam-on.

Results: We analyzed 894 TomoTherapy treatment plans from 2012 to 2018. Of all the treatment fractions performed with surface scanning, 90 % of the residual errors were within 2.3 mm for CNS (N = 284), 2.9 mm for H&N (N = 254), 8.7 mm for thorax (N = 144) and 10.9 for abdomen (N = 134) patients. The difference in residual error between surface scanning and positioning with in-room lasers was significant ($P < 0.005$) for all sites. The imaging time was assessed as total imaging time per treatment plan, modality, and treatment site and found that surface scanning significantly reduced patient on-couch time compared to MVCT for all treatment sites ($P < 0.005$).

Conclusions: The results indicate that daily surface scanning with weekly MVCT can be used with the current target margins for H&N, CNS, and thorax, with reduced imaging time.

KEY WORDS

helical, radiotherapy, SGRT, surface scanning, tomotherapy

This is an open access article under the terms of the Creative Commons Attribution License, which permits use, distribution and reproduction in any medium, provided the original work is properly cited.

© 2020 The Authors. *Journal of Applied Clinical Medical Physics* published by Wiley Periodicals, Inc. on behalf of American Association of Physicists in Medicine

J Appl Clin Med Phys 2020; 21:8:139–148

wileyonlinelibrary.com/journal/jacmp | 139

1 | INTRODUCTION

Accurate, reproducible, and fast setup of the patient is of great importance for a successful radiotherapy treatment, and in particular in helical tomotherapy due to the treatment complexity and number of degrees of freedom. The treatment margins are defined or calculated based on the uncertainties associated with the treatment,^{1,2} and hence, affect the size of the treated volume. Helical tomotherapy³ is an established treatment technique where the patient is treated on a slice by slice basis using a rotating linac, megavoltage (MV) photons and a continuous couch translation. The TomoTherapy can treat targets of up to 135 cm in length in one field.⁴

Megavolt beam imaging is used for image guidance of the patient setup.⁵ The treatment beam is combined with an on-board single row computed tomography (CT) detector array and the captured projection images are used to reconstruct a volumetric MVCT image of the patient.⁶ Daily imaging using MVCT contributes to absorbed dose outside the treatment volume.⁶ Also, MVCT is time consuming which decrease the patient throughput, and contributes to an increased risk of intra-fraction patient movement.⁷ To reduce the amount of MVCT images while keeping an accurate patient setup several imaging strategies have been adopted, such as weekly MVCT imaging with daily patient setup using in-room lasers.⁸ A recent strategy is to use surface guided radiotherapy (SGRT), where the patient's skin surface is scanned by an optical surface scanning (OS) system for patient setup.⁹ The OS system compare the patient's surface at treatment setup to a reference surface and accurately calculates the patient position.⁹ The advantage of using surface scanning is that the information from the surface can improve the patient setup compared to in-room lasers.^{10–12} Also, a surface scan takes seconds, in comparison to minutes for MVCT. Thus, surface scanning has the potential to increase the accuracy, without substantially adding time for setup compared to setup with in-room lasers. The surface can be correlated to the MVCT images with a similar method as the in-room lasers. In this study, the Sentinel surface scanning system (C-Rad, Uppsala, Sweden)⁹ was used to position the patients at a TomoTherapy HD (Accuray, Madison, US) linac between 2012 to 2018. Crop et al has previously reported improved patient setup for breast cancer patients using SGRT at tomotherapy¹²; however, in this study an extensive number of targets in head and neck (H&N), intra- and extracranial (CNS), thorax and abdomen were included. The aim of this study was to retrospectively investigate the potential improvements of surface guided setup compared to in-room lasers, both verified by weekly MVCT. Also, the potential time gain using SGRT compared to daily and weekly MVCT was to our knowledge investigated for the first time.

2 | MATERIALS AND METHODS

2.A | Positioning

2.A.1 | Surface scanning

The Sentinel OS system is a laser-based OS system that acquires a three-dimensional (3D) surface image of the patient over several

seconds. The daily surface scanned is registered to a reference surface and the patient's position is calculated using rigid registration.⁹ The scanner is mounted in the ceiling, at the end of the treatment couch. To avoid shadowing of the surface due to the closed bore of the TomoTherapy, the patient setup was carried out at the virtual isocenter, 700 mm longitudinal outside the bore. The Sentinel OS system has been found to be reproducible to < 1 mm and < 1° of rotation.¹³ The Sentinel system and the TomoTherapy lack communication, and thus for safety any couch shifts that were carried out based on the OS system was followed by a second surface scan to verify that the shifts were carried out correctly.

2.A.2 | Megavoltage computed tomography

The standard imaging modality on the TomoTherapy is MVCT acquired using a built-in detector array with the treatment beam at 3.5 MV energy. The collimator is positioned in the longitudinal direction and was set to 4 mm width for imaging. Images were acquired slice-by-slice and using a pitch set to fine, normal, or coarse. The reconstruction interval was 2 or 4 mm optionally. Transversal slice spatial image resolution for MVCT imaging was ≤ 1.6 mm per pixel at 512×512 pixels. The scan length for MVCT imaging was chosen to include the PTV in the longitudinal direction. The MVCT image was reconstructed and compared to the reference CT using automatic registration with manual adjustment. The patient was repositioned if the automatic registration resulted in a rotation of more than 2°. If the patient was repositioned, a second scan was acquired. The registration was further performed with only translational axis, the correction was applied, and the couch was moved from the control room. Prior to 2012, the couch was controlled solely from inside the treatment room, which increased the setup and imaging time.

2.A.3 | Positioning procedure

Prior to CT, patients were immobilized with either a thermoplastic mask (Orfit Industries, Wijnegem, Belgium), a vacuum bag (VacFix, Par Scientific A/S, Odense Denmark), or a light mattress. Head and neck patients were immobilized using a 5-points mask, CNS patients using a three-point mask, and thorax and abdomen patients using either a light mattress or vacuum bag. The patients were positioned in three steps; (a) with in-room lasers with external markers as reference, (b) with surface scanning matched to a reference surface, and (c) using MVCT with the planning CT as reference. This procedure was performed at the first three fractions. On the third fraction, after MVCT couch correction, a surface scan was acquired to use as reference surface during the following fractions. For ensuing treatment fractions the patients were positioned daily with first in-room lasers followed by surface scanning, and weekly MVCT for verification of positioning and internal anatomy. The weekly MVCT imaging was performed after in-room laser and surface scanning setup correction. Thus, each patient was positioned by laser, followed by surface scanning and MVCT for three fractions. A surface scan reference based on MVCT and couch correction performed on the

third fraction was then used as primary position procedure except for MVCT scans performed once weekly, Fig. 1. The procedure has been derived from the work of Månsson,¹⁴ which concluded that weekly imaging with laser setup and three initial imaging verification procedures were sufficient with the used imaging protocol. The threshold for deviation between MVCT and surface scanning was 2 mm in any direction. A deviation larger than 2 mm prompted MVCT the following treatment fraction, as did any large anatomical changes. The protocol at the time of the study was a NAL protocol⁸ with action limits of 2 mm for H&N and CNS, for thorax and abdomen patients the action limit was 3 mm. CTV to PTV margins differ between sites and diagnosis, but was generally 5–7 mm for CNS and H&N and 7–10 mm for thorax and abdomen patients.

2.A.4 | Positioning data statistics

The MVCT was registered with the planning CT as reference. The resulting translational couch movement from the original position to the registered position was defined as the *setup correction vector*, Fig. 2. The positional data was quantified by randomly selecting one MVCT image setup correction vector per plan. Random selection was used to avoid overestimation of the confidence interval, since the treatment fractions is correlated to the patient, we cannot simply

sum all treated fractions for all patients without any correction. In addition, the number of fractions varied between patients. This correction vector was used to assess the residual setup deviation of the surface scanning performed prior to the MVCT. One setup correction vector from the surface scanning was selected at random to assess the residual setup deviation between in-room lasers and surface scanning. The correction vector from the surface scanning was added to the MVCT correction vector to measure the total residual error between the in-room laser setup and the registered based on the MVCT image. The setup data from the first three fractions were omitted from the analysis since the reference surface was acquired during the third fraction. In addition, correction for systematic deviations was simulated by calculating a correction factor based on the first three fractions adapted from de Boer et al. and Bortfeld et al.,^{8,15}

$$c_p = -\frac{N}{N+1} \sum_{i=1}^N \frac{\vec{c}_i}{N} \tag{1}$$

where c_p was the setup correction for patient p that was corrected for the N first fractions with the setup correction vector \vec{c}_i . The correction factor was applied to the remaining fractions thus simulating a systematic correction. The Mann-Whitney U test was used for hypotheses testing.

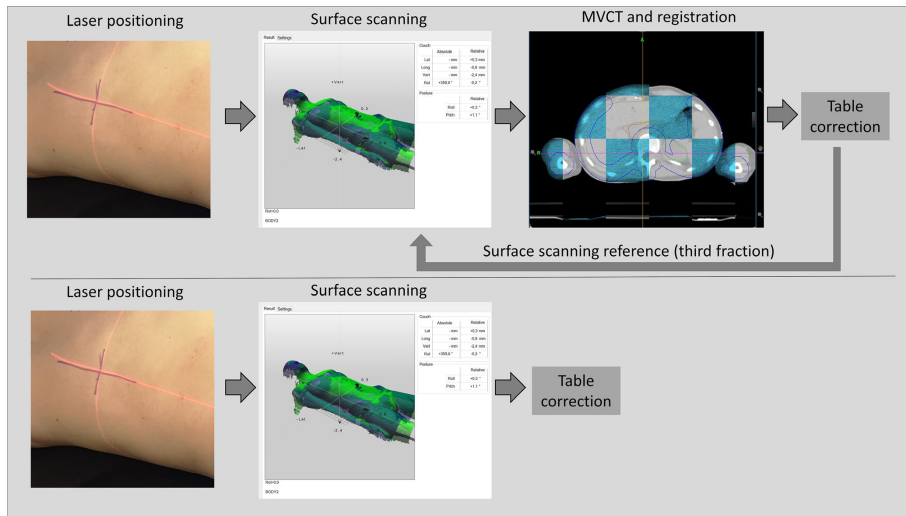


Fig. 1. [Daily workflow for surface scanning positioning procedure]. The first three fractions laser based setup was followed by surface scanning and then megavoltage computed tomography (MVCT) imaging. After table correction on the third fraction a new surface scanning reference was acquired provided that the surface scan based correction and the MVCT based correction correlated (top). The following fraction MVCT imaging was omitted and the table correction was based on surface scanning (bottom). The surface scanning was checked with weekly MVCT imaging

2.B | Imaging time

The time from imaging start to beam-on was defined as the *imaging time*, Fig. 2. The imaging time for surface scanning was calculated from the first surface scan to beam-on and thus included any following surface scans, MVCT procedures, registration, and couch translations. Similarly, the imaging time for MVCT was defined from the first MVCT scan to beam-on, including any following scans and registration or realignment of the patient. The imaging time for one fraction was randomly selected per treatment plan and imaging modality. The difference in total imaging time per fraction was tested against the null hypotheses using the Mann-Whitney U test, since normality could not be assumed. The imaging time was then multiplied by the number of treatment fractions to yield the total time difference per treatment plan.

2.C | Data selection

The data were collected between January and April 2018. Data were gathered retrospectively as all patients treated with TomoTherapy from the time period 2012–2018 and included treatments to the head and neck, CNS, thorax, and abdomen or pelvic area. Patients that received treatment to the abdomen and pelvis were included in the same treatment site group called abdomen. Only patients with more than three treatment fractions were included and patients positioned using in-room lasers, surface scanning, and MVCT performed on more than three fractions. Data was extracted from the Sentinel database and from the TomoTherapy archive using an in-house developed C# program. The resulting

data were analyzed using Python (Version 3.6, Python software foundation, 2019).

3 | RESULTS

A total of 696 patients with 894 plans were analyzed – in total 16 835 treatment fractions. Of the 894 plans, 78 plans were undefined treatment sites or treatment sites other than H&N, CNS, thorax, or abdomen and thus omitted from the analysis.

3.A | Positioning

For patients immobilized with 3- or 5-point mask (CNS and H&N), only 1.7% of the fractions positioned with surface scanning had a residual error larger than 5 mm, compared to laser-based setup where 27.5% of the fractions had a residual error larger than 5 mm. When in-room lasers are corrected for systematic error based on the first three fractions, 11.8% of the fractions had a residual error larger than 5 mm. The difference in length of the residual error between in-room lasers and optical surface scanning was significant ($P < 0.005$) for all sites. We compared the residual error to assess the positioning accuracy of in-room lasers and optical surface scanning (Figs. 3 and 4), as well as residual error per axis, Table 1. The smallest residual errors are seen for cranial and head and neck patients, with larger setup residual errors for the thorax and abdomen treatment sites, Figs. 3 and 4. On average, the difference between the residual error per axis was 1.7, 2.9, and 2.5 mm for the lateral, longitudinal and the vertical axis respectively. For in-room lasers, the largest error was mostly found in the vertical direction

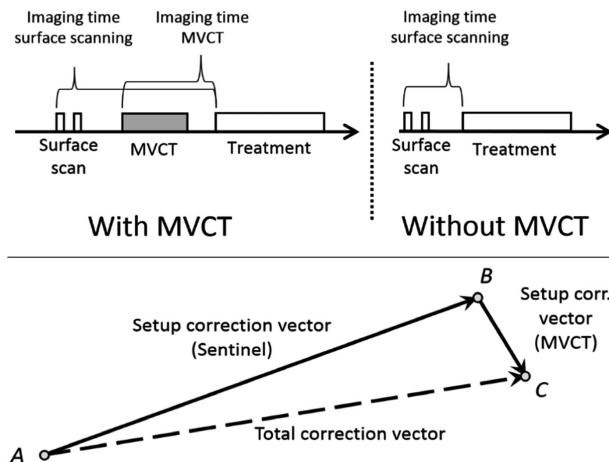


FIG. 2. [Setup correction vector and imaging time]. For surface scanning the time includes any following surface scans, couch movement, repositioning of the patient and megavoltage computed tomography (MVCT) imaging up till beam on. MVCT was performed for first three fractions and weekly if no relevant anatomical deviation was found and if the difference between MVCT and surface scanning was < 2 mm in any direction. The definition of the total setup correction vector (bottom) is here visualized as a sum of the individual correction vectors

followed by the longitudinal direction. For surface scanning, the largest error was mostly in the longitudinal direction followed by the lateral direction. The residual error was further separated into a systematic and a random error.¹⁶ Table 2. The random and systematic error was substantially larger for in-room lasers than optical surface scanning, for all sites. The number of MVCT scans that prompted a rescan due to the difference between surface scanning and MVCT was over the action limit was for H&N.

3.B | Imaging time

The difference in imaging time was assessed as total imaging time per treatment plan, modality, and treatment site, Fig. 5, where total imaging time per treatment plan refers to the accumulated time for each image modality as in all the weekly MVCT and surface scans for the length of the treatment for that plan. For the image modality MVCT that refers to the accumulated MVCT imaging time for the entire treatment as if the MVCT was taken daily. Patients that received treatment prior to the upgrade of the couch movement from the control room was excluded from the time analysis. The difference in total imaging time between surface scanning and MVCT per fraction was significant for all sites ($P < 0.005$). The mean time saved per fraction for a head and neck patient receiving 34 fractions was 4.8 min ($\sigma = 0.8$ min) and for a CNS patient with 30 fractions the mean saved time per patient was 3.7 min ($\sigma = 0.5$ min) when positioning with surface scanning. Similar mean saved time was achieved, 4.0 min ($\sigma = 0.9$ min) and 3.4 min ($\sigma = 0.7$ min) for patients receiving treatment to the thorax and abdomen with 34 and 30 fractions respectively.

4 | DISCUSSION

In this study, we analyzed a total of 16 835 treatment fractions over a 7-yr period. The large dataset enables analysis of subgroups and contributes to robust statistics. However, the following uncertainties have been identified in the study; the treatment machine was changed from Hi-Art to HD in 2012 and several upgrades has been made during this period. In addition, the possibility to move the couch from the control room was installed in 2013, which may add uncertainties to the data. Prior to analysis, data with implausible values were removed.

With in-room laser based setup, the largest magnitude of setup deviation was in the vertical direction, which is consistent with other studies.^{17–19} This deviation was found to be systematic for all treatment sites, and in the positive direction meaning that the couch is generally too low when compared with MVCT imaging. The effect stems from the positioning being performed in the virtual isocenter, 700 mm outside the bore. When the table top is moved into treatment position inside the bore, the couch sags, usually 1–3 mm. This effect has been reported in other studies.^{17,18} The error in the vertical direction was almost entirely compensated with the surface scanning since the surface reference was acquired after MVCT imaging

and setup correction and hence corrected for the sag, as the MVCT imaging is done inside the bore/in treatment position. This type of systematic deviation can be compensated with in-room laser setup, if the setup deviation is larger than the tolerance.

The image pitch was set to fine for patients immobilized with thermoplastic mask, and normal or fine for other patients in the study. The reconstruction interval normally used in each case was 2 or 4 mm. The resolution has been shown to affect to possible registration accuracy as compared to an independent system,²⁰ but the deviations were in general in the submillimeter range and at least half that of the voxel resolution for the investigated phantom.

The largest setup deviation with surface scanning was found in the longitudinal direction. At our clinic, the Sentinel was mounted in the ceiling at the foot end of the couch. This allows space during service to remove the covers of the TomoTherapy. The downside is the shallow angle to the patient. This problem could be managed by mounting the camera on a rail closer to the bore, allowing the camera to be moved during service of the TomoTherapy. This mounting can increase the uncertainty in camera mounting position and increases the QA workload. To better solve the uncertainty in longitudinal positioning with surface scanning, we are currently placing Styrofoam cubes on the patient to better aim the surface scanning for abdomen and thoracic patients. In this study, the effect of rotational deviations has not been tested. If the Sentinel or the registration of MVCT to CT indicated any rotation outside tolerance, the patient was readjusted in their immobilization.

There was a notable difference between patients immobilized with mask and other fixations. This can be attributed to the immobilization but also to the distance from surface to target, which is generally greater for thoracic and abdomen patients. In addition, thoracic patients and abdomen patients may exhibit larger intra- and inter-fractional movement of target relative to surface. Scanning of the CNS and H&N patients is mainly based on the mask, but the scanning for positioning seems to work well in most cases, as seen in the results. Problems such as weight loss and rotation inside the mask is hard to spot under the mask fixation, this is why using open masks can be an alternative when using surface scanning for setup. To account for any large anatomical changes, the treatment personnel was trained to monitor the response on the surface scanner in areas commonly associated with weight loss, such as the abdomen, large changes prompted MVCT rescans and acquiring of a new reference surface. An added benefit of the surface scanning compared to MVCT is the potential larger field of view, positioning of arms and shoulders can be better imaged with surface scanning. This is especially important with total marrow and total skin irradiations which have large target areas, extending wider than the field of view. Regarding abdomen and thoracic patients, we believe that surface scanning can be suitable for certain subgroups where the surface and target does not exhibit any large intra- or inter fractional movement in relation to each other. Further analysis within the subgroup would be needed to clarify which subgroups is suitable for surface scanning.

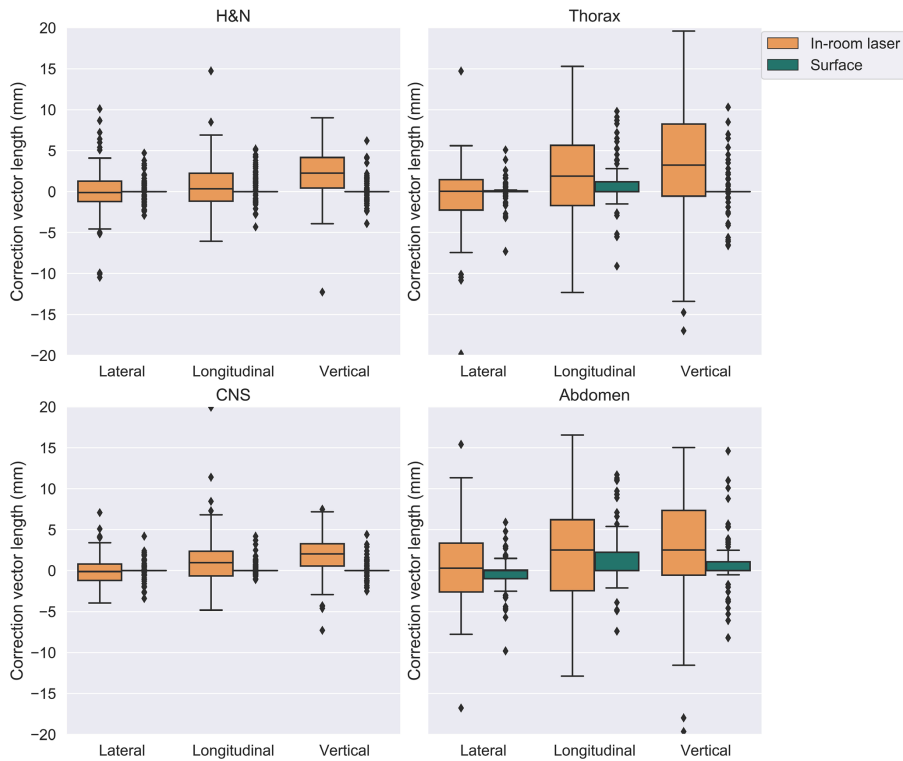


FIG. 3. [Setup correction per axis and image modality] The residual error for surface scanning and the residual error for in-room lasers, plotted per axis and treatment site. The residual error was assessed from the setup correction with megavoltage computed tomography to CT. Shown as a box-and-whisker plot, where the mid-line represents the median (line), the interquartile range (box) and 1.5 times past the quartile range (outer line) and outliers (black point)

We found that with surface scanning only 1.7% of the setup deviations was larger than 5 mm for H&N and CNS, which was the target margin for patients immobilized with a thermoplastic mask. To the authors knowledge, this is the only setup protocol to achieve this accuracy apart from daily imaging with MVCT. Other studies have investigated the residual errors for different treatment sites with daily in-room lasers,^{18,21–24} using no action limit protocols (NAL)⁸ and determined the residual deviation after daily in-room and NAL to be 2.6–14.2% for head and neck patients, depending on the number of fractions for evaluation and action limit. This would imply that a protocol with weekly MVCT imaging using daily surface scanning is as good or better than setup with in-room lasers and NAL protocol. Our positioning data was found similar to published data with an older laser scanning system.¹⁹ To improve the positioning with surface scanning, a NAL protocol

could be implemented based on the first three fractions, or by evaluating similar to methods on conventional linac.⁸ Despite the high accuracy, there will be a few fractions that will be outside the treatment margins. Similar to population based margin recipes were the margins is deducted were 90% of the population receives 95% of the prescribed dose a imaging protocol which does not include daily imaging should prompt a discussion on each clinic if the treatment margins are sufficient and what are the effects depending on the fractionation.

We found the difference in imaging time between daily surface scanning and daily MVCT significant ($P < 0.005$). The average time saved was reasonable considering the imaging and registration time for the different patient groups. A possible source of uncertainty was that beam-on as saved in the archive is the press of the beam-on button which can differ from the actual beam on.

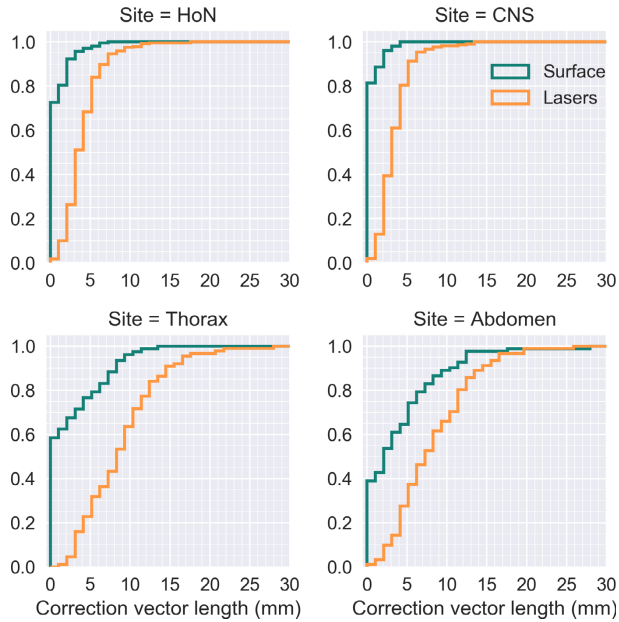


Fig. 4. [Length of setup deviation per image modality] residual error for in-room lasers and surface scanning as assessed by the sum of the megavoltage computed tomography (MVCT) and Sentinel correction vector (orange) and the MVCT setup correction vector (green) respectively. Here plotted as the cumulative sum of the setup correction deviation

TABLE 1 [Residual setup error] Residual setup error for in-room lasers and surface scanning as assessed by the megavoltage computed tomography correction, per treatment site. The 50% and 90% percentile are tabulated over the different axis together with the length of the error vector. Two millimeters at the 90% percentile is interpreted as 10% of all values are over 2 mm. The setup vectors were randomly selected, one per patient. lat = lateral couch direction, long = longitudinal couch direction, vrt = vertical couch direction. Error length is the length of the image correction vector against the reference image, that is, the residual positioning deviation after surface scanning and in-room laser positioning respectively

Site	Percentile (%)	Surface scanning				In-room lasers			
		x (mm)	y (mm)	z (mm)	Length (mm)	x (mm)	y (mm)	z (mm)	Length (mm)
HoN	50	0.0	0.0	0.0	0.0	1.1	1.6	2.7	4.0
CNS	50	0.0	0.0	0.0	0.0	1.2	2.0	2.5	3.6
Thorax	50	0.0	0.0	0.0	0.0	2.5	3.6	6.2	8.4
Abdomen	50	0.7	1.0	0.5	2.6	3.3	4.2	6.0	8.8
HoN	90	1.5	2.1	1.4	2.9	4.9	4.5	4.5	8.1
CNS	90	0.9	0.6	1.2	2.3	2.3	4.2	4.0	6.3
Thorax	90	2.0	5.7	5.9	8.7	5.3	7.2	14.9	15.7
Abdomen	90	3.3	7.4	5.4	10.9	5.0	9.8	12.5	17.5

It has been shown that a shorter treatment time can decrease the positioning uncertainty,¹² since patients treated for radiotherapy exhibit a baseline drift during treatment that is time dependent,^{7,25-29} and this shift has a dosimetric impact³⁰ on critical structures. We compared daily MVCT imaging to the use of three initial MVCT imaging followed by weekly MVCT imaging, with surface scanning as

setup tool on fractions without MVCT. This potential reduces the number of scans from 34 to 9 for a normal head and neck patient, not only reducing the time for acquiring the image but also the registration time. The time required for adjustments based on the surface scanning is in part negated by the assistance it provides to position the patient on the couch. For the time saving to have effect on

TABLE 2 [Deviations from megavoltage computed tomography imaging for surface scanning and in-room lasers] Systematic and random residual error based on the setup for in-room lasers and surface scanning respectively, tabulated with simulated correction for systematic error based on the first three fractions for in-room laser positioning (Laser NAL). Calculated from all treated setup vectors (N = 16 835). All values are presented in mm

Site	Axis	Systematic			Random	
		Laser	Laser NAL	Surface	Laser	Surface
H&N	Lateral	1.3	0.7	0.4	2.0	0.7
	Longitudinal	1.6	1.6	0.8	2.4	1.2
	Vertical	2.6	1.3	0.4	2.6	2.1
CNS	Lateral	1.0	0.6	0.2	0.8	0.5
	Longitudinal	1.4	1.0	0.3	1.7	0.6
	Vertical	2.1	1.2	0.3	2.7	0.6
Thorax	Lateral	2.2	1.4	1.2	2.8	1.4
	Longitudinal	3.6	3.2	3.2	5.9	4.0
	Vertical	5.2	2.5	1.9	5.0	2.5
Abdomen	Lateral	2.3	1.9	1.6	2.6	1.1
	Longitudinal	3.5	2.9	3.1	5.6	3.3
	Vertical	5.0	3.5	2.9	5.7	2.5

throughput, any time saved must be adjusted in the time slot in the booking system and to fill those slots. The actual throughput effect of surface scanning has in that regard not been tested. There has been few publications discussing patient throughput on Tomotherapy, but our results are consistent with literature where an increased throughput of 40% has been observed where surface scanning has been used instead of MVCT imaging for H&N,³¹ and when surface scanning was used for total marrow irradiation a time saving of 25 min was seen on average.³²

The decrease in the number of MVCT scans could also potentially save normal tissue from imaging dose. The population effects need to be further analyzed, but the dose from one MVCT image is typical in the range of 2–3 cGy³³ which would imply a dose saving of approximately 60 cGy for a treatment with 34 fractions, if weekly MVCT and SGRT is compared to daily MVCT.

The result can be used to save time at the linac compared to daily MVCT or shrink the target margins compared to daily setup with in-room lasers. This has the potential to save dose to normal tissue and to increase throughput at the treatment machine. The actual implications of the setup deviations on the PTV margin should be further investigated. In addition, how the time reduction for patient on couch affects the intra-fraction motion and how NAL and surface scanning in TomoTherapy can be combined are areas of interest for further research.

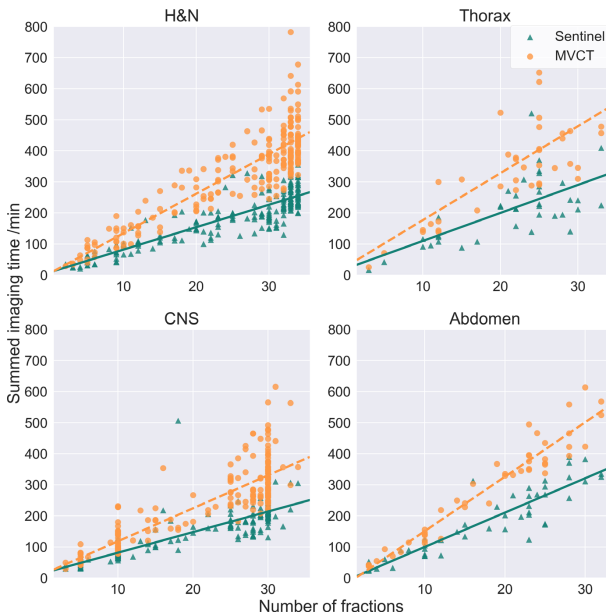


FIG. 5. [Total imaging time per modality] Accumulated imaging time against number of fractions per treatment plan, for imaging with Sentinel and with megavoltage computed tomography (MVCT) respectively. For surface scanning with sentinel, the time from first imaging to beam-on for each fraction was summed per treatment plan which includes all MVCT scans taken weekly. For MVCT, the time from first imaging to beam-on for each fraction with MVCT imaging, was divided with the number of MVCT imaging procedures per plan and multiplied with the number of fractions to simulate daily imaging with MVCT for comparison

5 | CONCLUSIONS

Optical surface scanning based setup on TomoTherapy has significant lower setup error as compared to in-room lasers based setup for all site, H&N, CNS, thorax and abdomen. Surface scanning was found to result in low setup error compared to the target margins for all sites but abdomen. In addition, surface scanning with weekly MVCT was found to significantly reduce the average patient on-couch time compared to daily MVCT. The results indicate that daily surface scanning with weekly MVCT can be used with the current target margins for H&N and CNS. The largest gain for surface scanning was found with H&N which had large difference in deviation from MVCT as compared to lasers, and the group also had a large time gain when the number of MVCT scans were reduced. The setup deviation was large for thoracic and abdomen patients, but further analysis is needed for those subgroups to assert if they are suitable for surface scanning.

ACKNOWLEDGMENTS

The authors would like to thank the MSc. Jonathan Snäll for technical assistance and MSc. Malin Kugele for thoughtful input. The main authors department receives funding from Accuray Inc.

CONFLICT OF INTEREST

The authors have no relevant conflict of interest.

REFERENCES

1. GuckenbergerM, Meyer J, Vordermark D, Baier K, Wilbert J, Flentje M. Magnitude and clinical relevance of translational and rotational patient setup errors: a cone-beam CT study. *Int J Radiat Oncol Biol Phys.* 2006;65:934–942.
2. LandbergT, Chavaudra J, Dobbs J, et al Report 50. *J Int Comm Radiat Units Meas.* 1993;os26:NP.
3. MackieTR, Holmes T, Swerdloff S et al Tomotherapy: a new concept for the delivery of dynamic conformal radiotherapy. *Med Phys.* 1993;20:1709–1719.
4. Accuray I. TOMOTHERAPY® H™ SERIES: TomoH™, TomoHD™ and TomoHDA™ Systems Technical Specifications. In: Accuray I, ed. Madison, WI, US; 2017.
5. MackieTR, Kapatoes J, Ruchala K, et al Image guidance for precise conformal radiotherapy. *Int J Radiat Oncol Biol Phys.* 2003;56:89–105.
6. DingGX, Alaei P, Curran B, et al Image guidance doses delivered during radiotherapy: quantification, management, and reduction: report of the AAPM Therapy Physics Committee Task Group 180. *Med Phys.* 2018;45:e84–e99.
7. JensenCA, Acosta Roa AM, Lund JA, Frengen J. Intrafractional baseline drift during free breathing breast cancer radiation therapy. *Acta Oncol.* 2017;56:867–873.
8. deBoer HC, Heijmen BJ. A protocol for the reduction of systematic patient setup errors with minimal portal imaging workload. *Int J Radiat Oncol Biol Phys.* 2001;50:1350–1365.
9. BrahmaA, Nyman P, Skatt B. 4D laser camera for accurate patient positioning, collision avoidance, image fusion and adaptive approaches during diagnostic and therapeutic procedures. *Med Phys.* 2008;35:1670–1681.


10. StanleyDN, McConnell KA, Kirby N, Gutierrez AN, Papanikolaou N, Rasmussen K. Comparison of initial patient setup accuracy between surface imaging and three point localization: a retrospective analysis. *J Appl Clin Med Phys/Am Coll Med Phys.* 2017;18:58–61.
11. KugeleM, Mannerberg A, Norring Bekke S, et al Surface guided radiotherapy (SGRT) improves breast cancer patient setup accuracy. *J Appl Clin Med Phys/Am Coll Med Phys.* 2019;20:61–68.
12. CropF, Pasquier D, Baczkiewicz A, et al Surface imaging, laser positioning or volumetric imaging for breast cancer with nodal involvement treated by helical TomoTherapy. *J Appl Clin Med Phys/Am Coll Med Phys.* 2016;17:200–211.
13. PallottaS, Marrazzo L, Ceroti M, Silli P, Buccioli M. A phantom evaluation of SentinelI), a commercial laser/camera surface imaging system for patient setup verification in radiotherapy. *Med Phys.* 2012;39:706–712.
14. MånssonS. *Patient Positioning Correction Strategies in Radiotherapy: A Portal Imaging Study.* Lund: Lund University; 2004. <https://www.lunduniversity.lu.se/current-students/academic-matters-support/lup-student-papers>
15. BortfeldT, Mv H, Jiang SB. When should systematic patient positioning errors in radiotherapy be corrected? *Phys Med Biol.* 2002;47: N297–N302.
16. YanD, Wong J, Vicini F, et al Adaptive modification of treatment planning to minimize the deleterious effects of treatment setup errors. *Int J Radiat Oncol Biol Phys.* 1997;38:197–206.
17. SchubertLK, Westerly DC, Tome WA, et al A comprehensive assessment by tumor site of patient setup using daily MVCT imaging from more than 3,800 helical tomotherapy treatments. *Int J Radiat Oncol Biol Phys.* 2009;73:1260–1269.
18. SahaA, Mallick I, Das P, Shrimali RK, Achari R, Chatterjee S. Evaluating the need for daily image guidance in head and neck cancers treated with helical tomotherapy: a retrospective analysis of a large number of daily imaging-based corrections. *Clin Oncol (R Coll Radiol).* 2016;28:178–184.
19. MoserT, Habl G, Uhl M, et al Clinical evaluation of a laser surface scanning system in 120 patients for improving daily setup accuracy in fractionated radiation therapy. *Int J Radiat Oncol Biol Phys.* 2013;85:846–853.
20. BoswellS, Tome W, Jeraj R, Jaradat H, Mackie TR. Automatic registration of megavoltage to kilovoltage CT images in helical tomotherapy: an evaluation of the setup verification process for the special case of a rigid head phantom. *Med Phys.* 2006;33:4395–4404.
21. HoughtonF, Benson RJ, Tudor GS, et al An assessment of action levels in imaging strategies in head and neck cancer using TomoTherapy. Are our margins adequate in the absence of image guidance? *Clin Oncol (R Coll Radiol).* 2009;21:720–727.
22. VaanderingA, Lee JA, Renard L, Gregoire V. Evaluation of MVCT protocols for brain and head and neck tumor patients treated with helical tomotherapy. *Radiother Oncol.* 2009;93:50–56.
23. ZumstegZ, DeMarco J, Lee SP, et al Image guidance during head-and-neck cancer radiation therapy: analysis of alignment trends with in-room cone-beam computed tomography scans. *Int J Radiat Oncol Biol Phys.* 2012;83:712–719.
24. YuY, Michaud AL, Sreeraman R, Liu T, Purdy JA, Chen AM. Comparison of daily versus nondaily image-guided radiotherapy protocols for patients treated with intensity-modulated radiotherapy for head and neck cancer. *Head Neck.* 2014;36:992–997.
25. KimS, Akpati HC, Kielbasa JE, et al Evaluation of intrafraction patient movement for CNS and head & neck IMRT. *Med Phys.* 2004;31:500–506.
26. Gurney-ChampionOJ, McQuaid D, Dunlop A, et al MRI-based Assessment of 3D Intrafractional Motion of Head and Neck Cancer for Radiation Therapy. *Int J Radiat Oncol Biol Phys.* 2018;100:306–316.

27. Pang PP, Hendry J, Cheah SL, et al An assessment of the magnitude of intra-fraction movement of head-and-neck IMRT cases and its implication on the action-level of the imaging protocol. *Radiother Oncol.* 2014;112:437–441.
28. Suzuki M, Nishimura Y, Nakamatsu K, et al Analysis of interfractional set-up errors and intrafractional organ motions during IMRT for head and neck tumors to define an appropriate planning target volume (PTV)- and planning organs at risk volume (PRV)-margins. *Radiother Oncol.* 2006;78:283–290.
29. Drabik DM, MacKenzie MA, Fallone GB. Quantifying appropriate PTV setup margins: analysis of patient setup fidelity and intrafraction motion using post-treatment megavoltage computed tomography scans. *Int J Radiat Oncol Biol Phys.* 2007;68:1222–1228.
30. Beltran C, Trussell J, Merchant TE. Dosimetric impact of intrafractional patient motion in pediatric brain tumor patients. *Med Dosim.* 2010;35:43–48.
31. Petersson K, Enmark M, Ceberg C, Knöös T. 1250 poster Increased patient throughput for treatment with helical tomotherapy. *Radiother Oncol.* 2011;99:S465–S466.
32. Haraldsson A, Engellau J, Lenhoff S, Engelholm S, Bäck S, Engström PE. Implementing safe and robust total marrow irradiation using helical tomotherapy - a practical guide. *Phys Med Eur J Med Phys.* 2019;60:162–167.
33. Shah AP, Langen KM, Ruchala KJ, Cox A, Kupelian PA, Meeks SL. Patient dose from megavoltage computed tomography imaging. *Int J Radiat Oncol Biol Phys.* 2008;70:1579–1587.

Paper IV



Organ sparing total marrow irradiation compared to total body irradiation prior to allogeneic stem cell transplantation

André Haraldsson^{1,2}  | Stina Wichert³ | Per E. Engström¹ | Stig Lenhoff³ |
Dominik Turkiewicz⁴ | Sarah Warsi^{3,5} | Silke Engelholm³ | Sven Bäck^{1,2} |
Jacob Engellau^{1,3}

¹Radiation Physics, Department of Hematology, Oncology and Radiation Physics, Skåne University Hospital, Lund, Sweden

²Department of medical radiation physics, Clinical Sciences, Lund university, Lund, Sweden

³Department of Hematology, Oncology and Radiation Physics, Skåne University Hospital, Lund, Sweden

⁴Department of Pediatric Oncology and Hematology, Skåne University Hospital, Lund, Sweden

⁵Division of Molecular Medicine and Gene Therapy, Lund Stem Cell Center, Lund University, Lund, Sweden

Correspondence

André Haraldsson, Radiation Physics, Department of Hematology, Oncology and Radiation Physics, Skåne University Hospital, Lund, Sweden.
Email: andre.haraldsson@med.lu.se

Abstract

Objectives: Total body irradiation (TBI) is commonly used prior to hematopoietic stem cell transplantation (HSCT) in myeloablative conditioning regimens. However, TBI may be replaced by total marrow irradiation (TMI) at centres with access to Helical Tomotherapy, a modality that has the advantage of delivering intensity-modulated radiotherapy to long targets such as the entire bone marrow compartment. Toxicity after organ sparing TMI prior to HSCT has not previously been reported compared to TBI or with regard to engraftment data.

Methods: We conducted a prospective observational study on 37 patients that received organ sparing TMI prior to HSCT and compared this cohort to retrospective data on 33 patients that received TBI prior to HSCT.

Results: The 1-year graft-versus-host disease-free, relapse-free survival (GRFS) was 67.5% for all patients treated with TMI and 80.5% for patients with matched unrelated donor and treated with TMI, which was a significant difference from historical data on TBI patients with a hazard ratio of 0.45 ($P = .03$) and 0.24 ($P < .01$). Engraftment with a platelet count over 20 [$K/\mu L$] and 50 [$K/\mu L$] was significantly shorter for the TMI group, and neutrophil recovery was satisfactory in both treatment cohorts. There was generally a low occurrence of other treatment-related toxicities.

Conclusions: Despite small cohorts, some significant differences were found; TMI as part of the myeloablative conditioning yields a high 1-year GRFS, fast and robust engraftment, and low occurrence of acute toxicity.

KEYWORDS

ALL, HSCST, TBI, TMI, Tomotherapy

1 | INTRODUCTION

Total body irradiation (TBI) is used in myeloablative conditioning regimes prior to hematopoietic stem cell transplantation (HSCT), primarily to younger patients with high-risk haematological malignancies.^{1,2}

The rationale of TBI is shown by lower relapse rate and improved overall survival (OS) when radiotherapy combined with chemotherapy is compared to chemotherapy alone.¹⁻³ However, the standard radiotherapy treatment with whole-body anterior-posterior irradiation is toxic, especially in combination with chemotherapy,⁴ and may cause significant side effects to several organs such as lungs, kidneys, bowel and liver. Increased toxicity has previously halted attempted dose escalation, a lower relapse rate with higher radiotherapy dose has not affected the overall survival.⁵ A consensus on TBI technique and fractionation^{6,7} has been lacking, which hampers comparisons between centres.

Helical Tomotherapy (HT; Accuray, CA, USA) is a radiotherapy treatment modality capable of delivering intensity-modulated treatments to complex and long targets like the bone marrow, generally referred to as total marrow irradiation (TMI). HT allows precise treatment and imaging of targets up to about 135 cm length without any field junctions, and with the built-in imaging, it delivers precise radiotherapy.^{8,9} This provides for the opportunity to deliver bone marrow targeted radiotherapy while sparing other organs, which may affect recovery, toxicity and outcome.

Toxicity after organ sparing TMI prior to HSCT has previously been reported,^{10,11} and dose escalation trials have been conducted^{12,13} as well as reduced intensity studies,¹⁴ but has thus far not been compared to standard TBI treatment with patients from the same clinic nor reported with regard to graft-versus-host disease-free, relapse-free survival (GRFS) or engraftment. In this paper, we compare prospectively observed patients that received TMI with retrospective data on a similar patient cohort receiving the same fractionated TBI during the 5-year period that preceded the introduction of the new TMI irradiation technology, with other treatment standards unchanged.

2 | MATERIALS AND METHODS

2.1 | Patient characteristic

In this study, all patients at our JACIE accredited transplant centre in Lund (Sweden) receiving TMI-based myeloablative conditioning prior to HSCT were consecutively included since the introduction of the treatment modality in October 2014. For comparison, we used retrospective data on all patients that have received TBI as part of a myeloablative conditioning regimen during the previous 5-year period, between July 2009 until August 2014. Patients receiving a haploidentical alpha/beta T-cell-depleted transplant were excluded. The stem cell source was for all adult patients' peripheral blood stem cells (PBSC) and for children's bone marrow (BM). For all patients,

Summary of significance

- This is the first reported comparison between two specific radiotherapy techniques with regard to haematological recovery and toxicity, where the newer technique irradiates less to the tissue surrounding the bone marrow as compared to the older radiotherapy technique.
- From our data, we conclude that the newer targeted radiotherapy is not worse than the older total body irradiation, and more patients survive without complications associated with side effects from either radiation or the transplantation.
- Patients irradiated prior to hematopoietic stem cell transplantation should be considered for the newer, more targeted radiotherapy, and could potentially reduce adverse events associated with the treatment.

cyclosporine and methotrexate were used as standard GvHD prophylaxis. In addition, in both cohorts, patients with a matched unrelated donor (MUD) all received Thymoglobuline, an anti-thymocyte globulin (ATG) in the conditioning, 4 mg/kg if the HLA match was $\geq 8/8$ and 6 mg/kg if the HLA match was 7/8. The date of the last follow-up is the 20th of August 2020. The study was approved by the Regional Ethical Review Board in Lund, Sweden (2013/149 and 2017/132). Signed informed consent according to local guidelines, the guidelines of the European Blood and Marrow Transplantation Group (EBMT), and the Declaration of Helsinki was obtained in all patients prior to treatment to register patients demographics, diagnosis, transplant characteristics, outcome and length of follow-up. The data were then retrieved from our institution's local transplant registry and supplemented in case of missing data by reviewing the patient's clinical charts.

2.2 | Radiotherapy treatment

Our method for TMI has previously been described in detail,¹⁵ but is summarised in this section. The patients were irradiated with 2 Gy/fraction twice daily, to a total dose of 12 Gy unless stated otherwise. The treatment was performed with a TomoTherapy HD that delivers radiation at a maximum of 860 cGy/min at 1.5 cm depth in a helical fashion. All patients were immobilised, scanned and treated in two positions due to the maximum treatment length of 140 cm on the TomoTherapy, and the upper body treated head-first followed by the lower body treated feet-first at every fraction. For all patients, the clinical target volume included the skeletal structures and the spleen. For patients with acute lymphoblastic leukaemia (ALL) the CNS and for male children, testicles were included. A 5-10 mm margin, depending on immobilisation of body site, was added as a planning margin to account for movement and geometrical uncertainties

called planning target volume (PTV). Dose to organs at risk was minimised without compromising dose to this PTV.

Patients receiving TBI were treated immobilised in a side position at 4.5 m distance from the radiation source¹⁶ with lead blocks to shield the lungs. The absorbed dose rate at the dose maximum depth of 1.5 cm was approximately 30 cGy/min.

2.3 | Evaluation of toxicity and outcome

Follow-up included overall survival (OS), 1-year GvHD-free/relapse-free survival (GRFS),¹⁷ 1-year transplant-related mortality (TRM), engraftment data, acute toxicities, scoring of acute and chronic graft-versus-host disease (GvHD) and relapse rate (RR). Where GRFS was defined as the fraction of patients that survived with no adverse event described in depth in the original article. For late effect complications, the median time of follow-up for the TMI cohort is slightly over one year, but we report on pulmonary and renal function tests before and at 3, 6 and 12 months, respectively, after HSCT.¹⁸ Engraftment was defined according to EBMT criteria: the first of three consecutive days with neutrophil count $\geq 0.5 \times 10^9/L$ and $\geq 1.0 \times 10^9/L$, and platelet count $\geq 20 \times 10^9/L$ and $\geq 50 \times 10^9/L$ (without transfusion), respectively. Acute GvHD was mainly scored according to the modified Glucksberg criteria.¹⁹ The TMI cohort was additionally scored according to the MAGIC criteria.²⁰ For the assessment of chronic GvHD, we have used standard NIH criteria.^{21,22} Glomerular filtration rate has previously been used to estimate the radiation and chemotherapy-related renal toxicity in TBI²³ and was calculated from the pre- and post-treatment S-creatinine. Idiopathic pneumonia syndrome (IPS) was defined as lung symptoms, dyspnoea and hypoxia, with radiological evidence of widespread alveolar injury, in which infectious aetiologies, as well as cardiac and renal dysfunction, has been excluded.²⁴ Function pulmonary test constituted of FEV1 (Forced Expiratory Volume in one second). The probability for complications was calculated using normal tissue complication probability (NTCP),^{25,26} a widely used logistic model for estimating the probability of radiation-induced toxicity in radiotherapy. Radiation toxicity scoring was done according to the common Radiation Therapy Oncology Group (RTOG) criteria.²⁷

2.4 | Statistical analysis

Hypothesis testing was performed using Mann-Whitney U test for continuous variables, and chi-squared or Fisher's exact test for categorical variables. Covariates and significance for toxicities and recovery where time to event existed was tested using Cox's proportional model. Kaplan-Meier was used to assess the non-parametric survival on group level for overall survival, and the log-rank test was used to compare the survival distribution between the two patient groups. The probability of relapse was calculated using non-relapse death and TRM as competing risk and TRM using relapse and

non-relapse death as a competing risk. GRFS events were defined as the first occurrence from severe (grade >II) acute GvHD, severe chronic GvHD, relapse or death from any cause. Patients that did not reach the specific time point was censored. For GvHD, competing risk included treating deaths, relapse and graft failure. For time to engraftment, patient with relapse or death was censored. The sub-distribution hazard model²⁸ was used for the analysis of outcomes with competing events.

All tests were two-sided and considered significant at $P < .05$, using 95% confidence intervals. All statistical analyses were performed with Python 3.6²⁹ or R.³⁰

The following variables were included in the analysis: recipient age, disease, disease status at HSCT, donor type, in vivo T-cell depletion, GvHD prophylaxis, Karnofsky performance score (KPS) for adult patients, donor-recipient sex match and year of transplant. All clinical variables were tested first for the affirmation of the proportional hazard assumption.

3 | RESULTS

3.1 | Patient characteristics

A total of 37 TMI patients and 33 TBI patients were analysed. Patient characteristics were very similar with respect to age, gender, diagnosis distribution, stem cell source and CD34 cell doses for the cohorts, Tables 1 and 2. Median follow-up (range) was 13 (2-70) and 72 (2-134) months for the TMI and TBI groups, respectively. There were more patients in the TMI cohort that had a disease of second complete remission (CR2) or worse. Dose distribution to the target was similar for the cohorts, two patients in the TMI group received reduced 10 Gy in 5 fractions, and one received 8 Gy on four fractions. Two patients from the TBI group received 10 Gy in 5 fractions. For the TMI patients, the dose was kept to a minimum in the kidneys, heart, bowel bag and liver, Figure 1. Generally, lower to (surrounding) normal tissue. Also, with TMI a larger portion of the bone marrow received closer to a prescribed dose, that is better homogeneity.

3.2 | Survival

The 1-year GRFS (no GRFS-related event at 1 year) for the two treatment types was 67.5% for TMI and 39.4% for TBI patients (HR = 0.45, 95% CI: 0.21-0.93, $P = .027$), Figure 2A. When only considering patients with MUD, the GRFS at 1 year was 80.5% for TMI and 42.3% for TBI patients, respectively (HR = 0.24, 95% CI: 0.09-0.67, $P = .003$), Figure 2B. More patients in the group that received TMI as radiotherapy survived without any adverse events such as graft-versus-host disease compared to historical data on TBI patients. A total of 27 patients treated with TMI had a follow-up time longer than 1 year, and 33 patients treated with TBI. Several variables were tested univariate and GRFS was additionally modelled with multivariate logistic regression, Table 3, where radiotherapy

TABLE 1 [Patient characteristics]: Thymoglobuline, an anti-thymocyte globulin (ATG), was used for all patients with matched unrelated donor (MUD). Diagnosis included was: B-Acute Lymphoblastic Leukaemia (B-ALL), T-Acute Lymphoblastic Leukaemia (T-ALL), Mixed Phenotype Acute Leukaemia (MPAL), Acute Myeloid Leukaemia (AML), Blastic Plasmacytoid Dendritic Cell Neoplasm (BPDCN), Chronic Myeloid Leukaemia (CML), MyeloProliferative Neoplasms (MPN), Multiple Myeloma (MM), Non-Hodgkin's Lymphoma (NHL), Myelodysplastic Syndrome (MDS). Stem cell sources included bone marrow (BM) or peripheral blood stem cells (PBSC). Human leukocyte antigens (HLA) for a matched unrelated donor (MUD) was compared as perfect match (8/8) versus less than 8/8. Similar, the number of patients in first complete remission (CR1) was compared to second complete remission (CR2) and partial remission (PR) or worse. Finally, the Hematopoietic Cell Transplantation-Comorbidity Index (HCT-CI) was available for all adult patients in both cohorts, 31 of the TMI patients and 29 of the TBI patients. *Cyclophosphamide 60 mg/kg day -6 and day -5, Etoposide 60 mg/kg day-5 (maximum dose of 3600 mg)

Patient characteristics	TMI (N = 37)	TBI (N = 33)
Median age (range) /years	29 (5-57)	28 (10-53)
HCT-CI		
Score 0	19 (51%)	19 (58%)
Score 1	3 (8%)	4 (12%)
Score 2	7 (19%)	6 (18%)
Score 3	1 (3%)	0 (0%)
Missing	7 (19%)	4 (12%)
Gender		
Female	15	12
Male	22	21
Diagnosis		
B-ALL	18	12
T-ALL	3	5
MPAL	2	0
AML (incl. BPDCN)	2	7
CML	3	1
MPN	1	1
MM	3	0
NHL	5	4
MDS	0	3
Stem cell source		
BM	7	4
PBSC	30	29
CD34 cell dose, median [$\times 10^6$ /kg]	6.0 ($\sigma = 1.2$)	6.0 ($\sigma = 1.1$)
Transplantation type		
MUD	29	26
MRD	8	7
Donor age, median (range)	27 (16-55)	32 (15-55)
MUD HLA match 7/8	4	7
Stage at tx		
CR1	16	20
>CR1 (or MDS)	21	13
Chemotherapy*		
Cyclophosphamide	21	29
Etoposide	16	4

technique was a significant contributing factor. There was no significant difference in OS between the radiotherapy treatment types at 12 months ($P = .509$), TRM $P = .239$ or relapse $P = .309$. However, the cohorts are small, and the follow-up too short to assess long-term effects, and they are included merely for reference.

3.3 | Engraftment

The engraftment time for patients with peripheral blood stem cells (PBSCs) as stem cell source was generally satisfactory for both TMI and TBI. The median (range) was 14 days (11-124) for TMI and 16 days

TABLE 2 [Disease characteristics]: Disease characteristics with radiotherapy type (RT), diagnosis, subclassification, disease stage at Tx, HCT-CI score for adults, age at Tx and Disease Risk Index (DRI) according to CIMBTR

RT	Diagnosis	Subclassification	Disease stage at Tx	HCT-CI score	DRI (Disease Risk Index CIMBTR)	Age at Tx
TMI	MPN	8p11-syndrome (t(8;13)) with T lymphoblastic lymphoma	PR1 (FISH positive for FGFR-1-rearrangement)	2	Intermediate	49
	CML	Ph+, p210, with lymphoid blast crisis	CP2, no CHR (complete hematologic response) ^b	1	Low	45
	ALL	Pre-B-ALL	CR2	NA	NA	14
	ALL	Ph+, p210	CR1	0	Intermediate	35
	ALL	Pre-B-ALL, t(12;21)	CR2 (CNS relapse)	NA	NA	12
	Myeloma	IgG st IIIA, ISS stage II	PR2 ^a	0	Intermediate	18
	ALL	Pre-B-ALL, non responder day 29.	CR1	1	Intermediate	22
	ALL	Pre-B-ALL, Ph+, p190	CR1	3	Intermediate	50
	MPAL	MPAL (dominant pre-B-ALL clone)	CR1	0	NA	23
	ALL	T-ALL, del(9p)	CR2	0	High	27
	ALL	Pre-B-ALL	CR2	0	High	19
	AML	Blastic plasmacytoid dendritic cell neoplasm	CR1	0	Intermediate	20
	ALL	Pre-B-ALL	CR1	2	Intermediate	45
	ALL	B-ALL	CR2	0	High	21
	ALL	T-ALL/LBL, bulky disease	CR1	0	Intermediate	30
	ALL	B-ALL Ph-like SFPQ-ABL1 fusion gene	CR1	0	Intermediate	30
	ALL	Pre-B-ALL, Ph+p190	CR3	NA	NA	10
	NHL	FL, FLIPPI 3A	VGPR3	0	Intermediate	47
	ALL	B-ALL	CR2 (CNS and BM relapse)	0	High	29
	ALL	Pre-B-ALL, complex karyotype, Li-Fraumeni mosaicism	CR1	0	Intermediate	35
	Myeloma	IgA, ISS 3, t(4;14)	CR2 ^a	2	Intermediate	42
	ALL	Pre-B-ALL	CR2 (CNS and BM relapse)	NA	NA	8
	NHL	hepatosplenic T cells lymphoma (gamma/delta)	CR1	0	Intermediate	44
	CML	Ph+, p210, with lymphoid blast crisis	CP2, Ph+ 96% ^b	2	Low	30
	CML	Ph+, p210, with lymphoid blast crisis	CP2 with MMR (major molecular response) ^b	2	Low	20
	ALL	Pre-B-ALL	CR2	NA	NA	13
	Myeloma	RRMM with del(17p), PR3 on 6th line of therapy with VTD-PACE	PR3 ^a	2	High	43
	NHL	hepatosplenic T cells lymphoma (gamma/delta)	CR1	NA	NA	9
	NHL	DLBCL	PR3	2	Intermediate	52
	AML	MLL-rearrangement, complex karyotype, extensive extramedullary disease	CR1	0	High	23
	ALL	B-ALL	CR1	1	Intermediate	57
	NHL	Waldenstrom macroglobulinemia	CR3	0	Low	55
	ALL	T-ALL, bulky disease	CR1	0	Intermediate	20

(Continues)

TABLE 2 (Continued)

RT	Diagnosis	Subclassification	Disease stage at Tx	HCT-CI score	DRI (Disease Risk Index CIBMTR)	Age at Tx
	ALL	Ph+, p190	CR1	0	Intermediate	33
	MPAL		CR1	0	NA	20
	ALL	Pre-B-ALL	CR2	0	High	33
	ALL	Pre-B-ALL, ABL2-translocation	CR2 (CNS and BM relapse)	NA	NA	5
TBI	ALL	Pre-B-ALL, t(1;22)	CR1	NA	NA	15
	MDS	RAEB-2 (10% blasts), normal karyotype	cytological remission	0	Intermediate	19
	ALL	pre-B-ALL, Ph+, p190	CR1	0	Intermediate	32
	AML	trisomy 13, FLT3 neg, NPM1 neg.	CR1	0	Intermediate	50
	AML	M4. Inversion 16	CR2	0	Low	45
	AML	Ph+, p210	CR1	0	Intermediate	53
	ALL	T-ALL, t(7;11)	CR1	NA	NA	10
	AML	normal karyotype, FLT3-ITD+, NPM1+	CR1	0	Intermediate	37
	AML	normal karyotype, FLT3-ITD+, NPM+	CR1	2	Intermediate	50
	ALL	T-ALL	CR1	0	Intermediate	24
	MPN	sAML post-PV, trisomy 13, FLT3-ITD+, NPM1+	CR1	0	Intermediate	39
	MDS	RAEB-2 (14% blasts), t(3;3)	PR (reduction of blasts to 6%-7%)	1	Intermediate	26
	AML	FLT3-ITD+, NPM1 neg	CR1	0	Intermediate	31
	ALL	Pre-B, t(8;14), not Burkitt	CR2	1	High	38
	ALL	Pre-B, trisomy 21	CR1	NA	NA	10
	ALL	Pre-B, t(4;11), MLL+	CR1	0	Intermediate	29
	NHL	T lymphoblastic lymphoma (LBL)	CR2	0	Intermediate	28
	AML	FLT3 neg, NPM1+	CR2	1	Intermediate	47
	MDS	RAEB-2/AML (20% blasts), complex monosomal karyotype, including -5 och -7	cytological remission	2	High	51
	ALL	T-ALL + minor clone with pre-B-ALL and CNS involvement	CR1	NA	NA	10
	NHL	Lymphoplasmacytic lymphoma, stage IV	PR1	0	Low	44
	ALL	Pre-B-ALL	CR1	2	Intermediate	27
	CML	Ph+, p210, with lymphoid blast crisis	CP2 with MMR (major molecular response) ^b	1	Low	22
	ALL	Pre-B-ALL	CR2	0	High	24
	NHL	T lymphoblastic lymphoma (LBL)	CR2	2	Intermediate	46
	ALL	T-ALL, t(1;1), del(9), extramedullary bulky disease	CR1	0	Intermediate	24
	ALL	Pre-B-ALL	CR2	2	High	28
	ALL	MLL-rearrangement, t(4;11), XXY	CR1	0	Intermediate	24
	ALL	Pre-B-ALL	CR1	0	Intermediate	42
	ALL	Pre-B-ALL, t(4;11)	CR1	2	Intermediate	28

(Continues)

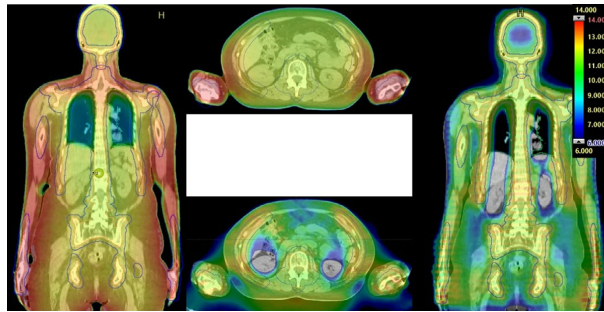
TABLE 2 (Continued)

RT	Diagnosis	Subclassification	Disease stage at Tx	HCT-CI score	DRI (Disease Risk Index CIBMTR)	Age at Tx
	ALL	T-ALL, t(8;22) with fusion bcr/FGFR1	CR1	0	Intermediate	42
	ALL	Pre-B-ALL	CR1	0	Intermediate	26
	NHL	Sezarys syndrome with lymphadenopathy and bone marrow involvement	PR 1	0	Intermediate	25

^aAccording to IMWG response criteria for multiple myeloma [56].

^bCML response according to ELN (European Leukaemia Net) criteria [57].

FIGURE 1 [Example dose distribution for the two radiotherapy types] Reconstructed dose distribution for total body irradiation (left/middle upper) and planned dose distribution for total marrow irradiation (right/middle lower) for the same patient and prescribed dose. The dose for TBI was reconstructed using delivered monitor units and reconstructed blocks from saved data. Absorbed dose is presented in Gy



(11-52) for TBI for a thrombocyte count of 20 [K/ μ L] ($P < .01$), and median (range) of 16 days (12-144) and 19 days (12-136), respectively, for a count over 50[K/ μ L] ($P < .01$). Similar for neutrophil recovery with absolute neutrophil count (ANC) over 0.5 [K/ μ L] and PBSC as stem cell source, the median (range) was 18 (12-26) days and 18 (12-31) for TMI and TBI, respectively. Similar, for an ANC over 1.0 [K/ μ L], the median (ranges) was 20 (13-29) days and 19 (12-39) for TMI and TBI, respectively. Similar for bone marrow (BM) as stem cell source, the time to engraftment for the TMI and TBI patients was 26 days (14-33) versus 29 days (20-176), 30 days(17-76) versus 72.5 days (23-226), 18 days (12-29) versus 25.5 days (19-29) and 21 days (13-33) versus 26 days (19-34) for a thrombocyte count of 20 [K/ μ L], thrombocyte count of 50 [K/ μ L], ANC over 0.5 [K/ μ L] and ANC over 1.0 [K/ μ L].

Engraftment with a platelet count over 20 [K/ μ L] and 50 [K/ μ L] was significantly shorter for the TMI group for patients with PBSCs as a stem cell source ($P = .01$, $P = .03$) Figure 3, but not for patients with BM as stem cell source ($P = .25$, $P = .25$). With a subdistribution hazard model, the difference between radiotherapy treatment types was significant for time to platelet count over 20 [K/ μ L], Table 4. Further, time to engraftment was modelled as a dependent variable with a neutrophil count over 1.0 [K/ μ L] and a thrombocyte count over 20 [K/ μ L], Table 4, where the difference was significantly impacted by radiotherapy type and stem cell source for time to platelet recovery, but no such correlation was seen for time to neutrophil count.

Three months after transplantation, all but two patients in the TMI cohort and three patients in the TBI cohort showed complete T-lymphocytic and myeloid chimerism in peripheral blood. Two patients in the TMI cohort had mixed T-lymphocytic chimerism with 10%-15% and 6%, respectively, of their recipient cells. Both patients are alive and disease-free 53 and 16 months after transplantation. Three patients in the TBI cohort with mixed chimerism had progressive disease four, five and eight months, respectively, post-transplant.

3.4 | Graft-versus-host disease

The incidence of acute GvHD scored >II according to the modified Glucksberg criteria was 4 for the TMI cohort ($N = 37$) and 6 for the TBI cohort ($N = 33$), Table 3. Using standard NIH criteria for chronic GvHD, there were 3 moderate-to-severe incidents for the TMI cohort ($N = 36$) and 8 for the TBI cohort ($N = 32$), Table 3. Only considering patients with MUD, the incidence was 0/28 and 5/25 for TMI and TBI. Further, with multiple regression analysis, moderate-to-severe chronic GvHD was modelled as dependent where transplantation was significant as independent variables, Table 3. Similar, acute GVHD with grade >II was analysed with multiple regression, Table 3. Similar results were obtained with Cox's regression, where donor age ($P < .01$) and CMV serostatus ($P < .01$) were significant factors influencing acute GVHD but radiotherapy type ($P = .29$)

FIGURE 2 [Kaplan-Maier plot for graft-versus-host disease-free survival]. GRFS over time presented for all patients (top) and for patients transplanted from MUD (bottom). Hazard ratio (HR) was calculated using Cox's proportional model, with radiotherapy treatment type as independent variable and significance testing with the log-rank test

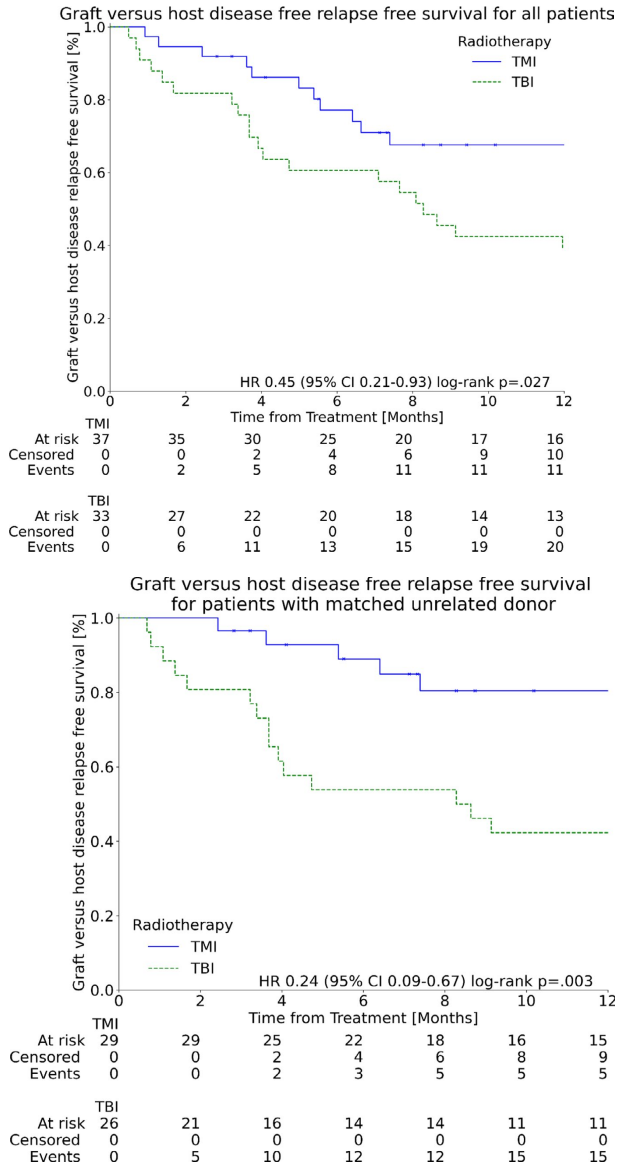


TABLE 3 [Graft-versus-host disease-free/relapse-free survival and graft-versus-host disease]: Regression for GRFS, acute GvHD and chronic GvHD, presented with hazard ratio (HR), confidence intervals (CI) and significance. The variables were Radiotherapy treatment type, total marrow or total body irradiation, Cytomegalovirus (CMV) serostatus (D-/R-), type of donor, matched unrelated (MUD) or matched related (MRD), if the donor was over 40, Hematopoietic Cell Transplantation-Comorbidity Index (HCT-CI). Numbers in bold was found significant $P < .05$. Multivariate analysis with all the corresponding dependent variables listed under the independent variable, four dependents for GRFS and acute GvHD, and three dependents for chronic GvHD, with independent variables in bold

	(N)	Univariable		Multivariable	
		HR (95% CI)	P	HR (95% CI)	P
GRFS (1 year)					
Radiation treatment type	TMI (37)	0.45 (0.21-0.93)	.03	0.39 (0.18-0.84)	.02
	TBI (33)				
Transplantation type	MRD (15)	2.29 (1.09-4.79)	.03	2.08 (0.98-4.38)	.05
	MUD (55)				
Disease stage	>CR1 (32)	1.78 (0.88-3.63)	.11	2.30 (1.10-4.79)	.03
	CR1 (38)				
Acute GvHD					
Radiation treatment type	TMI (37)	0.55 (0.16-1.92)	.35	0.49 (0.08-1.62)	.25
	TBI (33)				
Transplantation type	MRD (15)	1.70 (0.43-6.61)	.45	4.29 (0.68-27.06)	.12
	MUD (55)				
CMV serostatus status	D-/R- (15)	2.68 (0.76-9.09)	.13	7.25 (1.47-35.59)	.01
	<D-/R- (55)				
Donor age	cont.	1.06 (1.02-1.13)	.01	1.08 (1.04-1.12)	<.01
Chronic GvHD					
Radiation treatment type	TMI (37)	0.35 (0.10-1.30)	.11	0.33 (0.09-1.18)	.08
	TBI (33)				
Transplantation type	MRD (15)	4.54 (1.43-14.37)	.01	4.99 (1.44-17.35)	.01
	MUD (55)				
CMV serostatus status	D-/R- (15)	0.80 (0.18-3.52)	.76	1.66 (0.35-7.97)	.52
	< D-/R- (55)				

and transplantation type ($P = .13$) did not. Most notable, the pattern of acute GvHD differed between the two cohorts with more cases of lower GI involvement for patients receiving TBI, 4 with stage >2 in the TBI cohort, versus 2 with stage >2 in the TMI cohort. Hence, a regression for lower GI acute GVHD stage >2 as the dependent variable was performed but none of the independent variables was significant. Twelve patients in the TMI cohort fulfilled the new MAGIC criteria for mild acute GVHD with upper GI involvement stage 1, whereas only two were biopsy-verified with a typical histologic picture, thereby fulfilling the older modified Glucksberg criteria for this diagnosis.³¹ In the TBI cohort, only one patient was diagnosed with acute GVHD with upper gastrointestinal (GI) involvement according to older criteria. In an attempt to retrospectively re-evaluate the TBI cohort according to the modern MAGIC criteria, at least five more patients would have been scored with mild upper GI acute GVHD. There was one case of acute severe liver GvHD stage 4 in the TBI cohort, compared to one case with milder stage 2 liver engagement of acute GVHD in the TMI cohort.

3.5 | Radiation-induced normal tissue toxicity

The probability of radiation-induced normal tissue complication (NTCP) grade over stage II, as graded according to RTOG criteria, was calculated for TMI and TBI, respectively. Estimated glomerular filtration (eGFR) was lower after radiotherapy for the TBI group than for the TMI group, the difference was significant ($P = .020$) but too small to be clinically relevant, Table 5. With linear regression to predict eGFR, no significant regression equation was found ($P = .186$, $N = 44$), where a few patients lacked follow-up serum creatinine.

There was only one incident of IPS in each cohort, a grade 4 event from the TMI cohort versus a grade 5 event from the TBI group according to CTCAE v.5. Both patients were older, 45 and 47 years respectively, the TMI patient diagnosed with CML in a second chronic phase and the TBI patient with AML in second complete remission. There was no incident of hepatic sinusoidal obstruction syndrome (HSOS) in either cohort.

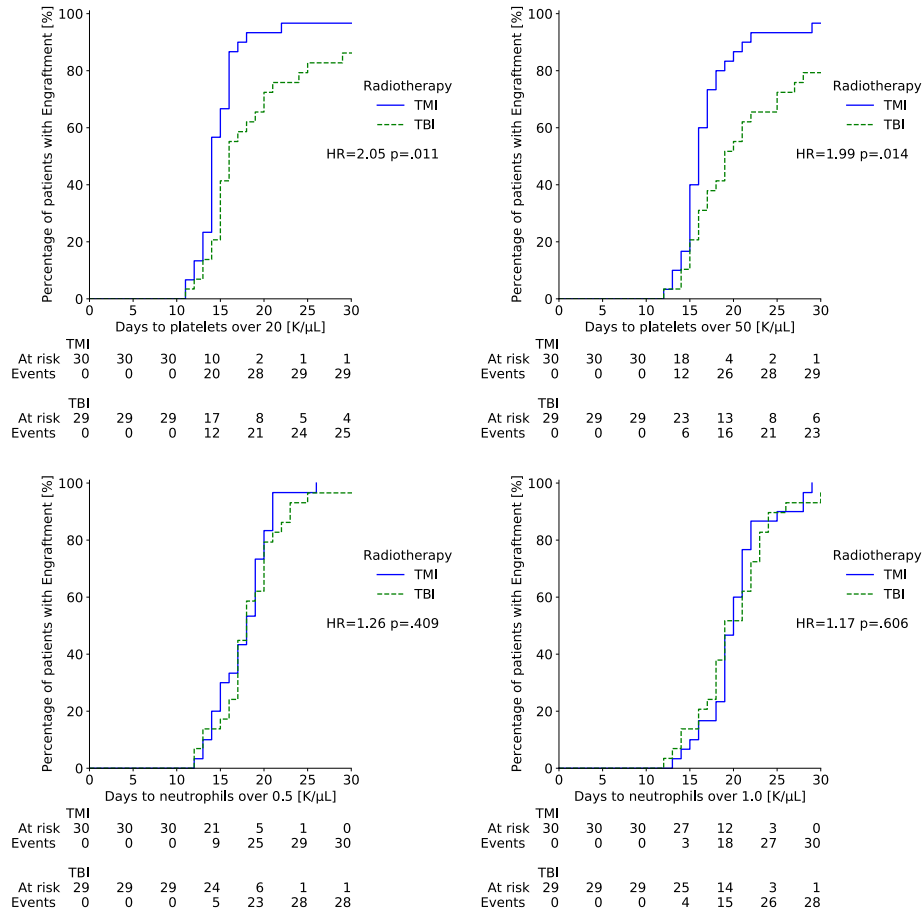


FIGURE 3 [Time to engraftment]. Cumulative time to engraftment comparing radiotherapy treatment type. Time to engraftment according to EBMT criteria plotted for patients transplanted from peripheral stem cells (PBSCs)

4 | DISCUSSION

The GRFS was significantly better for patients treated with TMI prior to HSCT than for patients irradiated with TBI when considering matched unrelated donors. The difference remained significant when modelled with multivariate logistic regression. This result strengthens the impression that conditioning with TMI generally results in a lower occurrence of toxicity, treatment-related mortality and GvHD. The treatment groups were very similar with regards to HCT-CI score, age, donor age, diagnosis, infused CD34+ cell count, and patients were given the same GvH prophylaxis and treatment

except for the radiotherapy technique. The TMI cohort had more patients in second complete remission or worse. One factor that could attribute to increased GRFS was the year of treatment, where the TMI cohort was treated more recently. GRFS has been shown to increase to some extent over time and Holtan et al¹⁷ stratified a number of variables related to HSCT and found in multivariate logistic regression that the period of treatment was significant with an RR of 0.8. This can be compared to the HR of a GRFS-related adverse event for our two cohorts of 0.24 in our study when considering only patients transplanted from a matched unrelated donor. Thus, post-treatment care and other factors that have improved over time

TABLE 4 [Engraftment data for days to platelet count over 20 K/ μ L and days to neutrophils over 1.0 K/ μ L]: The variables were radiotherapy treatment type, total marrow or total body irradiation, stem cell source bone marrow or PBSCs and donor age over or under 40. Numbers in bold was found significant $P < .05$. Independent variables in bold using all the dependent variables listed for multivariable regression. Higher hazard ratio (HR) should be interpreted in favour of faster engraftment

	N	Univariable		Multivariable	
		HR (95% CI)	P-value	HR (95% CI)	P-value
Days to platelets >20 [K/μL]					
Radiation treatment type	TMI (37)	1.61 (1.02-2.55)	.04	2.04 (1.28-3.23)	<.01
	TBI (33)				
Infused cell count CD34+	70	1.30 (1.10-1.53)	<.01	1.28 (1.02-1.61)	.03
Stem cell source	PBSC (59)	2.01 (1.33-3.05)	.01	2.12 (1.24-3.63)	<.01
	BM (11)				
Donor age	70	0.98 (0.96-1.01)	.14	0.97 (0.95-0.99)	.03
Days to neutrophils >1.0 [K/μL]					
Radiation treatment type	TMI (37)	1.29 (0.79-2.09)	.31	1.20 (0.72-1.98)	.49
	TBI (33)				
Infused cell count CD34+	70	0.95 (0.78-1.15)	.59	0.83 (0.63-1.07)	.15
Stem cell source	PBSC (59)	1.60 (0.83-3.10)	.16	2.46 (1.04-5.80)	.04
	BM (11)				
Donor age	70	0.99(0.97-1.02)	.66	0.98 (0.96-1.01)	.19

TABLE 5 [Outcome data] The median follow-up for the TMI cohort is 12 months and for TBI patients 60 months. Estimated glomerular filtration rate (eGFR), median difference between the pre-transplant measurement versus 12 months after HSCT. Acute graft-versus-host-disease (aGvHD) patients with symptoms over grade II and which organ, with some patients experiencing symptoms in several organs. Abbreviations: Idiopathic Pneumonia Syndrome (IPS) and Hepatic Sinusoidal Obstruction Syndrome (HSOS) and aGvHD according to the modified Glucksberg criteria (MG). FEV1 is presented as the difference versus pre-treatment FEV1. *Number of patients with chronic graft-versus-host disease for patients alive at day 100. †Significant difference ($p = .02$). **number of patients with aGvHD with the number of incidence at each site

	TMI (N = 37)	TBI (N = 33)
IPS incidence		
<Grade 4	0	0
Grade 4	1 (3%)	0
Grade 5	0	1 (3%)
eGFR difference (σ) [mL/min/1.73 m ²]	-8.6 (13.7) [†]	-9.8 (16.7) [†]
FEV1 3 mo difference, median (σ) [L]	0.0 (0.3)	0.0 (0.4)
FEV1 6 mo difference, median (σ) [L]	0.1 (0.4)	0.1 (0.7)
VOD incidence	0 (0%)	0 (0%)
cGvHD*, moderate to severe	3 (9%) (N = 35)	8 (25%) (N = 32)
AGvHD > grade 2**	4 (8%)	6 (18%)
Skin	3	3
Lower GI	2	4
Liver	0	1

could, to some extent, explain the improved GRFS. However, the difference we present is more prominent than shown in other publications attributed to the difference in time of treatment.

Limiting the dose to organs at risk and to a higher degree target the bone marrow with TMI will subsequently lower the dose to circulating blood. There have been speculations that circulating leukemic cells could increase the risk of relapse when decreasing the dose to non-stem cell sites. The follow-up is too short to assess

such a risk. Kim et al³² investigated patterns of relapse following TMI prior to HSCT and found no evidence of increased extramedullary relapse related to total marrow or total lymph node irradiation compared to published results of regimens with TBI, nor did they find any increased risk of relapse in part of the patients irradiated with over 10 Gy versus under 10 Gy. Similar, Stein et al³³ found no higher risk of extramedullary relapse with TMI as a radiotherapy technique prior to HSCT when compared to similar studies with TBI.

In addition, in a review of literature by Kogut et al,³⁴ including 246 patients, no risk of extramedullary relapse was found for patients that did not receive TBI.

Engraftment was significantly faster in the TMI group when measured by platelet count and with a lower incidence of both acute and chronic GVHD. This has previously only been found in pre-clinical trials,^{35,36} where both a dose distribution and dose rate have been found to correlate with engraftment. Hui et al³⁶ hypothesise that in TMI, compared to TBI, the reduced radiation dose to the non-skeletal organs results in a chemokine stromal-derived factor-1 (SDF-1) gradient facilitating donor stem cells engraftment in the bone marrow niche. This could explain the shorter engraftment times in our TMI cohort, though the engraftment time was adequate in the TBI group. Another factor that could affect the engraftment time is the radiotherapy dose rate. Increased dose rate has long been linked directly to cell kill.³⁷ In this study, the local dose rate, that is the instantaneous dose rate, was increased 30 times in TMI compared to TBI. The global dose rate, the fraction dose divided by the total treatment delivery time, was on the other hand decreased. We suggest the local, but not the global, dose rate to influence cell kill and thus toxicity, but this subject is partly uncharted in a clinical setting for TBI and TMI. In addition, there is a difference in dose coverage to the bone marrow of the ribs, in the lung shielded area between the two techniques. The effect is negligible when considering the total volume but may affect the cell kill from the radiotherapy treatment in that volume. Finally, differences and advances in care for HSCT patients have improved³⁸ and could contribute to the increased recovery. Which of these effects impacts the treatment, and to what extent, should be attributed to further studies.

The large difference in the mean dose and probability of complication to kidneys as calculated by NTCP did not translate to a large difference in renal dysfunction. Renal dysfunction after TBI and SCT has previously been reported for children,^{39,40} where 44.4% had impaired renal function or elevated creatinine levels at follow-up, and for adults⁴¹ where 5 out of 29 and 4 out of 64 adult patients in the respective study had elevated levels. Pulmonary toxicity has previously been found to correlate with radiotherapy, cyclophosphamide, the addition of busulphan⁴² and dose rate^{43,44} in total body irradiation using similar radiotherapy fractionation as the current study. The fractionation of 12 Gy TBI in 6 fractions was found to induce an IPS incidence of 6%-7% with lung shielding, which correlates well with this study. Since dose rate has been found to correlate with pulmonary toxicity, there was an a priori concern that a switch to TMI on TomoTherapy could increase the pulmonary toxicity. However, the occurrence of IPS was low in both study groups. Hence, no correlation could be found caused by increased local dose rate. A much larger cohort would be required to rule out any difference. The incidence of IPS that occurred was both in older patients, which actualise questions of reducing the prescribed radiation dose to patients past their forties, similar to what has been recommended previously.⁴⁵ For the TMI cohort, the follow-up time is yet too short to evaluate late toxicity. However, as early toxicity following radiotherapy is related to an increased risk of developing late toxicity, the low

incidence of radiotherapy-related early toxicity in the TMI cohort may be expected to also yield a lower risk of late side effects. This will be reported in later studies with longer follow-up for this group.

The incidence of chronic GVHD was lower in patients who received TMI prior to SCT than the control group that received TBI, but the difference was not found significant. The prevalence of GVHD has been found to correlate with dose distribution³⁶ in preclinical trials. The prevalence of moderate-to-severe GVHD of 9% was similar to other studies for TMI⁴⁶ in general, and more notable thus far no patients that were transplanted from MUD have developed severe or moderate chronic GVHD. The incidence of acute GVHD was, similar to chronic GVHD, lower in the TMI group as compared to the TBI group but not statistically significant. One hypothesis for the lower incidence is that TMI, compared to standard TBI, reduces the extent of damage to intestinal epithelial cells, a potential trigger of alloreactive T-cell reactions.^{47,48} This is important, since the early onset of acute GVHD has been found to correlate with an increased risk of extensive chronic GVHD and TRM.^{49,50}

Total marrow irradiation and TBI prior to HSCT have been studied in randomised trials. Paix et al⁵¹ reviewed the current literature in 2018. They concluded that Phase I and II trials have demonstrated the feasibility and tolerance of TMI and that the dose to organs at risk could be reduced. High-dose TBI of up to 14 Gy has been compared to standard regimen.³⁸ The authors found that the reduced relapse risk with higher doses was hampered by increased non-relapse mortality (NRM) and found no significant difference in OS. Dose escalation with TMI has been investigated from 12 Gy up to 15 Gy¹³ for patients with ALL. The authors concluded that dose escalation was feasible and that the doses were well tolerated. The authors concluded that research should focus on strategies to reduce TBI toxicity since radiotherapy clearly benefits disease control. TMI irradiation has also been investigated in patients with relapsed ALL³³ with doses of up to 20 Gy and had a relatively low occurrence of severe acute GVHD but many patients exhibited severe cGVHD, and with a 1-year OS of 55.5%. Further, Stein et al³³ concluded that TMI is feasible and was encouraged by the preliminary clinical response. Treatment and dose escalation with TMI prior to HSCT has been studied for a number of diseases such as multiple myeloma and ALL^{11,12,14} where the key takeaway was that TMI was found feasible, and CR rate was found encouraging. Jensen et al¹⁴ reported outcome and toxicity and compared transplant-related toxicity and mortality from other studies⁵²⁻⁵⁵ with FLU/MEL conditioning combined with TMI regimens and concluded that their patient's outcome compared favourably to those reported with chemotherapy-based conditioning alone. The lower toxicity in our study strengthens the perception that dose escalation using TMI is feasible, and patients previously ineligible for full-dose treatment could be eligible for radiotherapy thanks to organ-sparing radiotherapy.

This study compared two similar cohorts from the same clinic that received similar treatment in all regards except radiotherapy and time of treatment. The same GVH prophylaxis was used for both cohorts. Despite the large similarities in treatment, changes in care can to some extent influence the result of the comparison and we interpret the result with caution.

5 | Conclusion

Our early results indicate that organ-sparing radiotherapy with TMI as part of the myeloablative conditioning translates to a low occurrence of toxicity, a robust and fast engraftment, and a low degree of GvHD. GRFS was significantly higher with TMI compared to conditioning with TBI. The low number of adverse events for patients that received TMI prior to HSCT at our one-year follow-up shows promising results and that organ sparing TMI warrants further studies and further follow-up to assess long-term effects and survival.

ACKNOWLEDGEMENT

The authors want to sincerely thank Dr Susann Ullén (Clinical Studies Sweden—Forum South, Skane University Hospital, Lund, Sweden) for input and discussion regarding the statistical methodology and presentation.

CONFLICT OF INTEREST

Department of the corresponding author has an ongoing research agreement with Accuray Inc, which includes funding.

DATA AVAILABILITY STATEMENT

The data that support the findings of this study are available on request from the corresponding author.

ORCID

André Haraldsson  <https://orcid.org/0000-0002-1694-3738>

REFERENCES

- Adkins DR, DiPersio JF, Adkins DR. Total body irradiation before an allogeneic stem cell transplantation: is there a magic dose? *Curr Opin Hematol.* 2008;15:555-560. <https://doi.org/10.1097/MOH.0b013e32831188f5>
- Hartman A-R, Williams SF, Dillon JJ. Survival, disease-free survival and adverse effects of conditioning for allogeneic bone marrow transplantation with busulfan/cyclophosphamide vs total body irradiation: a meta-analysis. *Bone Marrow Transplant.* 1998;22:439-443. <https://doi.org/10.1038/sj.bmt.1701334>
- Peters C, Dalle J-H, Locatelli F, et al. Total body irradiation or chemotherapy conditioning in childhood ALL: a multinational, randomized, noninferiority phase III study. *J Clin Oncol.* 2020;39:295-307. <https://doi.org/10.1200/JCO.20.02529>
- Giralt SA, LeMaistre CF, Vriesendorp HM, et al. Etoposide, cyclophosphamide, total-body irradiation, and allogeneic bone marrow transplantation for hematologic malignancies. *J Clin Oncol.* 1994;12:1923-1930. <https://doi.org/10.1200/JCO.1994.12.9.1923>
- Cliff RA, Buckner CD, Appelbaum FR, et al. Allogeneic marrow transplantation in patients with chronic myeloid leukemia in the chronic phase: a randomized trial of two irradiation regimens. *Blood.* 1991;8:1660-1665.
- Giebel S, Mischczyk L, Slosarek K, et al. Extreme heterogeneity of myeloablative total body irradiation techniques in clinical practice: a survey of the Acute Leukemia Working Party of the European Group for Blood and Marrow Transplantation. *Cancer.* 2014;120:2760-2765. <https://doi.org/10.1002/cncr.28768>
- Hoeben BAW, Pazos M, Albert MH, et al. Towards homogenization of total body irradiation practices in pediatric patients across SIOPE affiliated centers a survey by the SIOPE radiation oncology

- working group. *Radiother Oncol.* 2020;155:113-119. <https://doi.org/10.1016/j.radonc.2020.10.032>
- Peñagaricano JA, Chao M, Rhee FV, Moros EG, Corry PM, Ratanatharathorn V. Clinical feasibility of TBI with helical tomotherapy. *Bone Marrow Transplant.* 2011;46:929-935. <https://doi.org/10.1038/bmt.2010.237>
- Nalichowski A, Eagle DG, Burmeister J. Dosimetric evaluation of total marrow irradiation using 2 different planning systems. *Med Dosim.* 2016;41:230-235. <https://doi.org/10.1016/j.meddos.2016.06.001>
- Shinde A, Yang D, Frankel P, et al. Radiation related toxicities using organ sparing total marrow irradiation transplant conditioning regimens. *Int J Radiat Oncol Biol Phys.* 2019;105(5):1025-1033. <https://doi.org/10.1016/j.ijrobp.2019.08.010>
- Somlo G, Spielberger R, Frankel P, et al. Total marrow irradiation: a new ablative regimen as part of tandem autologous stem cell transplantation for patients with multiple myeloma. *Clin Cancer Res.* 2011;17:174-182. <https://doi.org/10.1158/1078-0432.CCR-10-1912>
- Patel P, Oh AL, Saraf SL, et al. A phase 1 trial of autologous stem cell transplantation conditioned with melphalan 200 mg/m² and total marrow irradiation (TMI) in patients with relapsed/refractory multiple myeloma. *Leuk Lymphoma.* 2018;59:1666-1671. <https://doi.org/10.1080/10428194.2017.1390231>
- Wong JY, Forman S, Somlo G, et al. Dose escalation of total marrow irradiation with concurrent chemotherapy in patients with advanced acute leukemia undergoing allogeneic hematopoietic cell transplantation. *Int J Radiat Oncol Biol Phys.* 2013;85:148-156. <https://doi.org/10.1016/j.ijrobp.2012.03.033>
- Jensen LG, Stiller T, Wong JYC, Palmer J, Stein A, Rosenthal J. Total marrow lymphoid irradiation/fludarabine/melphalan conditioning for allogeneic hematopoietic cell transplantation. *Biol Blood Marrow Transplant.* 2018;24:301-307. <https://doi.org/10.1016/j.bbmt.2017.09.019>
- Haraldsson A, Engellau J, Lenhoff S, Engelholm S, Bäck S, Engström PE. Implementing safe and robust total marrow irradiation using helical tomotherapy - A practical guide. *Phys Med.* 2019;60:162-167. <https://doi.org/10.1016/j.ejmp.2019.03.032>
- Svahn-Tapper G, Nilsson P, Jönsson C, Alvegård TA. Calculation and measurements of absorbed dose in total body irradiation. *Acta Oncol.* 1990;29:627-633. <https://doi.org/10.3109/02841869009090064>
- Holtan SG, DeFor TE, Lazaryan A, et al. Composite end point of graft-versus-host disease-free, relapse-free survival after allogeneic hematopoietic cell transplantation. *Blood.* 2015;125:1333-1338. <https://doi.org/10.1182/blood-2014-10-609032>
- Bjork J, Grubb A, Sterner G, Nyman U. Revised equations for estimating glomerular filtration rate based on the Lund-Malmö Study cohort. *Scand J Clin Lab Invest.* 2011;71:232-239. <https://doi.org/10.3109/00365513.2011.557086>
- Przepiorka D, Weisdorf D, Martin P, et al. 1994 consensus conference on acute GVHD grading. *Bone Marrow Transplant.* 1995;15:825-828.
- Harris AC, Young R, Devine S, et al. International, multicenter standardization of acute graft-versus-host disease clinical data collection: a report from the Mount Sinai Acute GVHD International Consortium. *Biol Blood Marrow Transplant.* 2016;22:4-10. <https://doi.org/10.1016/j.bbmt.2015.09.001>
- Filipovich AH, Weisdorf D, Pavletic S, et al. National Institutes of Health consensus development project on criteria for clinical trials in chronic graft-versus-host disease: I. Diagnosis and staging working group report. *Biol Blood Marrow Transplant.* 2005;11:945-956. <https://doi.org/10.1016/j.bbmt.2005.09.004>
- Jagasia MH, Greinix HT, Arora M, et al. National Institutes of Health consensus development project on criteria for

- clinical trials in chronic graft-versus-host disease: I. The 2014 Diagnosis and Staging Working Group Report. *Biol Blood Marrow Transplant*. 2015;21(3):389-401.e1. <https://doi.org/10.1016/j.bbmt.2014.12.001>
23. Borg M, Hughes T, Horvath N, Rice M, Thomas AC. Renal toxicity after total body irradiation. *Int J Radiat Oncol Biol Phys*. 2002;54:1165-1173. [https://doi.org/10.1016/S0360-3016\(02\)03039-0](https://doi.org/10.1016/S0360-3016(02)03039-0)
 24. Panoskaltis-Mortari A, Griese M, Madtes DK, et al. An official American Thoracic Society research statement: noninfectious lung injury after hematopoietic stem cell transplantation: idiopathic pneumonia syndrome. *Am J Respir Crit Care Med*. 2011;183:1262-1279. <https://doi.org/10.1164/rccm.2007-413ST>
 25. Lyman JT. Complication probability as assessed from dose-volume histograms. *Radiat Res Suppl*. 1985;8:S13-S19.
 26. Emami B, Lyman J, Brown A, et al. Tolerance of normal tissue to therapeutic irradiation. *Int J Radiat Oncol Biol Phys*. 1991;21:109-122. [https://doi.org/10.1016/0360-3016\(91\)90171-y](https://doi.org/10.1016/0360-3016(91)90171-y)
 27. Cox JD, Stetz J, Pajak TF. Toxicity criteria of the Radiation Therapy Oncology Group (RTOG) and the European Organization for Research and Treatment of Cancer (EORTC). *Int J Radiat Oncol Biol Phys*. 1995;31:1341-1346. [https://doi.org/10.1016/0360-3016\(95\)00060-c](https://doi.org/10.1016/0360-3016(95)00060-c)
 28. Fine JP, Gray RJ. A proportional hazards model for the subdistribution of a competing risk. *J Am Stat Assoc*. 1999;94:496-509. <https://doi.org/10.2307/2670170>
 29. Python Software Foundation. Python Language Reference, version 3.6. <http://www.python.org>. 2019.
 30. Team RC. R: A Language and Environment for Statistical Computing. 2020.
 31. Schoemans HM, Lee SJ, Ferrara JL, et al. EBMT-NIH-CIBMTR Task Force position statement on standardized terminology & guidance for graft-versus-host disease assessment. *Bone Marrow Transplant*. 2018;53:1401-1415. <https://doi.org/10.1038/s41409-018-0204-7>
 32. Kim JH, Stein A, Tsai N, et al. Extramedullary relapse following total marrow and lymphoid irradiation in patients undergoing allogeneic hematopoietic cell transplantation. *Int J Radiat Oncol*. 2014;89:75-81. <https://doi.org/10.1016/j.ijrobp.2014.01.036>
 33. Stein A, Palmer J, Tsai NC, et al. Phase I trial of total marrow and lymphoid irradiation transplantation conditioning in patients with relapsed/refractory acute leukemia. *Biol Blood Marrow Transplant*. 2017;23:618-624. <https://doi.org/10.1016/j.bbmt.2017.01.067>
 34. Kogut N, Tsai N-C, Thomas SH, et al. Extramedullary relapse following reduced intensity allogeneic hematopoietic cell transplant for adult acute myelogenous leukemia. *Leuk Lymphoma*. 2013;54:665-668. <https://doi.org/10.3109/10428194.2012.720375>
 35. Glass TJ, Hui SK, Blazar BR, Lund TC. Effect of radiation dose-rate on hematopoietic cell engraftment in adult zebrafish. *PLoS ONE*. 2013;8:e73745. <https://doi.org/10.1371/journal.pone.0073745>
 36. Hui S, Takahashi Y, Holtan SG, et al. Early assessment of dosimetric and biological differences of total marrow irradiation versus total body irradiation in rodents. *Radiation Oncol*. 2017;12:468-474. <https://doi.org/10.1016/j.radonc.2017.07.018>
 37. Hall EJ, Brenner DJ. The dose-rate effect revisited: radiobiological considerations of importance in radiotherapy. *Int J Radiat Oncol Biol Phys*. 1991;21:1403-1414.
 38. Sabloff M, Chhabra S, Wang T, et al. Comparison of high doses of total body irradiation in myeloablative conditioning before hematopoietic cell transplantation. *Biol Blood Marrow Transplant*. 2019;25:2398-2407. <https://doi.org/10.1016/j.bbmt.2019.08.012>
 39. Watanabe Nemoto M, Isobe K, Togasaki G, et al. Delayed renal dysfunction after total body irradiation in pediatric malignancies. *J Radiat Res*. 2014;55:996-1001. <https://doi.org/10.1093/jrr/ru041>
 40. Esiashvili N, Chiang KY, Hasselle MD, Bryant C, Riffenburgh RH, Paulino AC. Renal toxicity in children undergoing total body irradiation for bone marrow transplant. *Radiation Oncol*. 2009;90:242-246. <https://doi.org/10.1016/j.radonc.2008.09.017>
 41. Kunkele A, Engelhard M, Hauffa BP, et al. Long-term follow-up of pediatric patients receiving total body irradiation before hematopoietic stem cell transplantation and post-transplant survival of >2 years. *Pediatr Blood Cancer*. 2013;60:1792-1797. <https://doi.org/10.1002/pbc.24702>
 42. Sampath S, Schultzeis TE, Wong J. Dose response and factors related to interstitial pneumonitis after bone marrow transplant. *Int J Radiat Oncol Biol Phys*. 2005;63:S0360-S0316.
 43. Kim DY, Kim IH, Yoon SS, Kang HJ, Shin HY, Kang HC. Effect of dose rate on pulmonary toxicity in patients with hematolymphoid malignancies undergoing total body irradiation. *Radiation Oncol*. 2018;13:180. <https://doi.org/10.1186/s13014-018-1116-9>
 44. Abugideiri M, Nanda RH, Butker C, et al. Factors influencing pulmonary toxicity in children undergoing allogeneic hematopoietic stem cell transplantation in the setting of total body irradiation-based myeloablative conditioning. *Int J Radiat Oncol Biol Phys*. 2016;94:349-359. <https://doi.org/10.1016/j.ijrobp.2015.10.054>
 45. Wong JYC, Filippi AR, Dabaja BS, Yahalom J, Specht L. Total body irradiation: guidelines from the International Lymphoma Radiation Oncology Group (ILROG). *Int J Radiat Oncol Biol Phys*. 2018;101:521-529. <https://doi.org/10.1016/j.ijrobp.2018.04.071>
 46. Corvò R, Zeverino M, Vagge S, et al. Helical tomotherapy targeting total bone marrow after total body irradiation for patients with relapsed acute leukemia undergoing an allogeneic stem cell transplant. *Radiation Oncol*. 2011;98:382-386. <https://doi.org/10.1016/j.radonc.2011.01.016>
 47. Perkey E, Maillard I. New insights into graft-versus-host disease and graft rejection. *Annu Rev Pathol*. 2018;13:219-245. <https://doi.org/10.1146/annurev-pathol-020117-043720>
 48. Nalle SC, Zuo L, Ong MLD, et al. Graft-versus-host disease propagation depends on increased intestinal epithelial tight junction permeability. *J Clin Invest*. 2019;129:902-914. <https://doi.org/10.1172/JCI98554>
 49. Ljungman P, Bregni M, Brune M, et al. Allogeneic and autologous transplantation for haematological diseases, solid tumours and immune disorders: current practice in Europe 2009. *Bone Marrow Transplant*. 2010;45:219-234. <https://doi.org/10.1038/bmt.2009.141>
 50. Ringden O, Labopin M, Sadeghi B, et al. What is the outcome in patients with acute leukaemia who survive severe acute graft-versus-host disease? *J Intern Med*. 2018;283:166-177. <https://doi.org/10.1111/joim.12695>
 51. Paix A, Antoni D, Waissi W, et al. Total body irradiation in allogeneic bone marrow transplantation conditioning regimens: a review. *Crit Rev Oncol Hematol*. 2018;123:138-148. <https://doi.org/10.1016/j.critrevonc.2018.01.011>
 52. Giral S, Thall PF, Khouri I, et al. Melphalan and purine analog-containing preparative regimens: reduced-intensity conditioning for patients with hematologic malignancies undergoing allogeneic progenitor cell transplantation. *Blood*. 2001;97:631-637. <https://doi.org/10.1182/blood.v97.3.631>
 53. Giral S, Aleman A, Anagnostopoulos A, et al. Fludarabine/melphalan conditioning for allogeneic transplantation in patients with multiple myeloma. *Bone Marrow Transplant*. 2002;30:367-373. <https://doi.org/10.1038/sj.bmt.1703652>
 54. Ritchie DS, Morton J, Szer J, et al. Graft-versus-host disease, donor chimerism, and organ toxicity in stem cell transplantation after conditioning with fludarabine and melphalan. *Biol Blood Marrow Transplant*. 2003;9:435-442.
 55. de Lima M, Anagnostopoulos A, Munsell M, et al. Nonablative versus reduced-intensity conditioning regimens in the treatment of acute myeloid leukemia and high-risk myelodysplastic syndrome: dose is relevant for long-term disease control after allogeneic



- hematopoietic stem cell transplantation. *Blood*. 2004;104:865-872. <https://doi.org/10.1182/blood-2003-11-3750>
56. Kyle RA, Rajkumar SV. Criteria for diagnosis, staging, risk stratification and response assessment of multiple myeloma. *Leukemia*. 2009;23:3-9. <https://doi.org/10.1038/leu.2008.291>
57. Hochhaus A, Baccarani M, Silver RT, et al. European LeukemiaNet 2020 recommendations for treating chronic myeloid leukemia. *Leukemia*. 2020;34:966-984. <https://doi.org/10.1038/s41375-020-0776-2>

How to cite this article: Haraldsson A, Wichert S, Engström PE, et al. Organ sparing total marrow irradiation compared to total body irradiation prior to allogeneic stem cell transplantation. *Eur J Haematol*. 2021;00:1-15. <https://doi.org/10.1111/ejh.13675>

SUPPORTING INFORMATION

Additional supporting information may be found online in the Supporting Information section.

Appendix



Appendix: Conference proceedings

Poster I: Dose-rate dependence in haematological recovery following total marrow irradiation compared to total body irradiation

Presented 2020 at *ESTRO 2020*. For further details refer to Paper Dose-rate dependence in haematological recovery following total marrow irradiation compared to total body irradiation and Sect. 5.



Dose-rate dependence in haematological recovery following total marrow irradiation compared to total body irradiation

André Haraldsson, Stina Wichert, Jacob Engellau, Stig Lenhoff, Sarah Warsi, Silke Engelholm, Sven Bäck, Per E. Engström. Skåne universitetssjukhus, Lunds universitet

- We conducted a prospective observational study on 29 patients that received organ sparing total marrow irradiation (TMI) prior to HSCT and compared this cohort to 34 patients that received total body irradiation (TBI) prior to hematopoietic stem cell transplantation
- A multi stage compartment model was adapted from literature to model the platelet reconstitution
- The compartment model was applied to both the TMI and TBI patients, with the dose rate modelled as a difference in the immunosuppressive effect on the bone marrow
- There were a significant difference between the engraftment when the TMI and TBI cohort was compared
- We found that the model did not support the hypotheses that the dose rate explains the difference in engraftment as measured with time to platelet count in blood over 50 [K/ μ L]

We retrospectively evaluate dose-rate dependent differences in haematological recovery and engraftment after allogenic stem-cell transplantation with organ sparing total marrow irradiation (TMI), as compared to historically data from our clinic for patients treated with total body irradiation (TBI).

Doses to organs at risk for TBI was estimated from central doses and anterior posterior measurements. Dose rate was <30 cGy/min at dose maximum for the TBI treatments, and approximately 850 cGy/min for the TMI treatments. Time to engraftment was assessed by thrombocytes count. Significance testing was done using Mann Whitney U-test. There was no difference between cell dose for the cohorts, TMI=5.6 (σ =1.8) 10^9 /L and TBI=5.8 (2.0) 10^9 /L, respectively.

For patients receiving PBSCT, mean time to engraftment as measured by thrombocytes over 50 [K/ μ L], was 19 and 16 days for TBI and TMI respectively, a significant difference (p =0.0006). Cox proportional model revealed an impact of number of transplanted CD34-cells, radiotherapy type and stem cell transplantation type. Further, there was a significant shorter time to thrombocytes >50 (p <0.01) for the TMI cohort compared to the TBI patients.

Subsequently, we adapted a compartment model from Ward et al. 2016 and Marciniak-Czochra et al. 2013, according to

$$\frac{dc_1}{dt} = (2a_{1,max}s - 1)p_1c_1 - d_1c_1$$

$$\dots$$

$$\frac{dc_i}{dt} = (2a_{i,max}s - 1)p_i c_i + 2(1 - a_{i-1,max}s)p_{i-1}c_{i-1} - d_i c_i$$

$$\frac{dc_n}{dt} = 2(1 - a_{n-1,max}s)p_{n-1}c_{n-1} - d_n c_n$$

and, $s = \frac{1}{1 + kc_n}$

Where $c(t)$ is the population cell density at time t , $s(t)$ the signalling molecules, $p(t)$ is the proliferation rate at t , and $a(t)$ the fraction of daughter cells that stays undifferentiated and death rate is denoted by $d(t)$. Parameters was adapted from Ward et al. and from Marciniak-Czochra et al and adapted to normal conditions. We used 6 compartments to model homeopathic stem cell to platelet progression, with the Megakaryocytes split to on average 3500 platelets. Cell dose (CD34 infusion) as well as transplantation type and radiotherapy type was modeled as a difference in initial uptake in the bone marrow of the infused CD34 cells, were the difference in dose rate was modeled as a scaled difference from log-cell kill, approximately 1.9 %, from Fowler et al. In addition, a random component was added to the initial uptake of transplanted cells.

The model was adapted to a TMI patient and correctly modeled the distribution of engraftment in the cohort apart from 1 outlier. The model does not predict the difference in engraftment between radiotherapy type, on the contrary, the higher average cell dose in the TBI dose would depict a slightly faster engraftment in the TBI cohort compared to TMI despite the 2% lower dose rate effect.

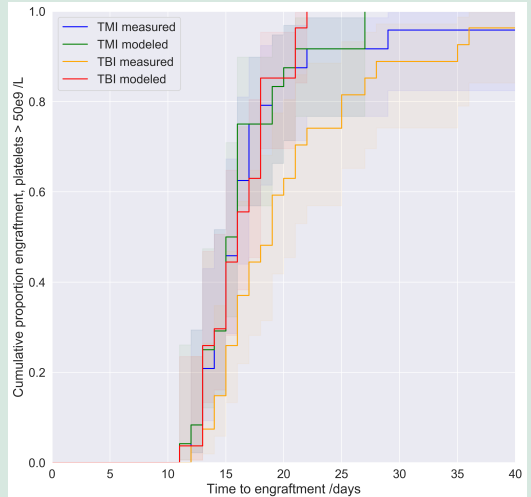


Figure 1: Time to engraftment for total marrow irradiation (TMI), Total body irradiation (TBI) as measure with platelet count over $50 \cdot 10^9$ per liter blood. The platelet reconstitution was modeled with a compartment model and varied with the transplanted CD34 cell dose count, transplantation type and a normal distributed random noise. The model parameter was adapted to one patient and applied to the cohorts with the difference in dose rate scaled to log cell kill as immunosuppressive, i.e less initial uptake of transplanted CD34 cells.

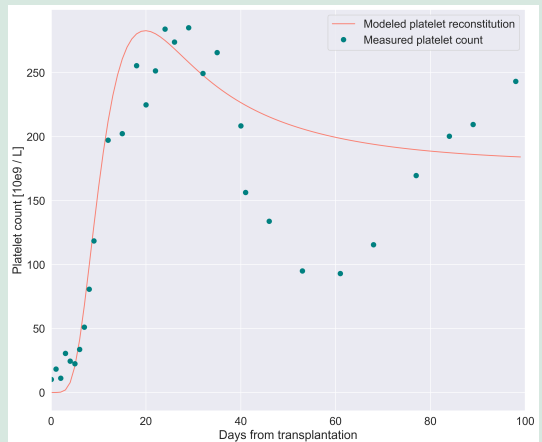


Figure 2: Platelet reconstitution after homeopathic stem cell transplantation (HSC) and radiotherapy for one patient that received total marrow irradiation prior to HSC. The model correctly depicts the initial recovery and max count but not the extra oscillation. The level for engraftment is 50 [10e9 platelets per liter blood, which makes the model sufficient for the current problem.



Poster II: OC-0461: Acute toxicity and recovery following total marrow irradiation compared to total body irradiation

Presented 2016 at *ESTRO 2016*. For further details refer to Paper OC-0461: Acute toxicity and recovery following total marrow irradiation compared to total body irradiation and Sect. 4.



Plan specific pitch values effect on gamma pass rate for patient QA measured with Scandidos Delta⁴ on Tomotherapy

Conclusion

An introduction of plan specific pitch values increases the pass rate of the patient QA significant when measured with Delta⁴.

Purpose/objective

The purpose of this study was to analyze if the change from standard pitch to individually optimized plan specific pitch values on our Tomotherapy plans had effect on the measured gamma pass rate for our patient QA. Tomotherapy is helically delivered with a pneumatic MLC where each leave is either closed or open. Pitch on Tomotherapy is the overlap each rotation has with the previous at isocenter; or rather, the couch distance traveled per gantry rotation, and is dependent of collimator width. Our hypothesis is that the change from fixed pitch values, 0.215, 0.287 and 0.43 for field width of 1.05, 2.5 and 5.02 cm respectively, to values calculated individually based on fraction dose, targets position relative to isocenter and field width, will increase the gamma pass rate due to less stress on the mlc.

Results

Our measurements are approximately truncated normally distributed, and with higher gamma pass rate on average after the introduction of plan specific pitch values (M=97.4%, SD=2.08), then with fixed values as used previously (M=95.1%, SD=3.67). As presented in table 1, we have an increase in pass rate over 90%, 95% and 100%. After the introduction of plan specific pitch values, we have no

Materials/Methods

At our clinic, all patients undergoing Tomotherapy are planned individually and approved plans are measured on the Tomotherapy with a Delta⁴ (Scandidos, Uppsala, Sweden), prior to treatment. Gamma pass/fail criteria is 90% at DTA: 2mm and DD: 3% when planned dose distribution is compared with measured. Recently, we started using individually optimized plan specific pitch values. These values are calculated using a program, based on the works of Chen M, Chen Y, Chen Q, et al. Med. Phys. (2011). The ripple effect, which is peak to through dose relative to average in longitudinal direction is caused by pitch when the target is not at isocenter. This puts stress on the mlc during delivery when the optimizing software tries to compensate the non-optimal overlap with mlc movement. A too low pitch also puts unnecessary stress on the mlc when the gantry rotations are low and thus increases the fraction of mlc movement that are close to mlc latency time, 20ms. A more careful selection of pitch should reduce the ripple effects and use an optimal gantry rotation period, around 20s, that in effect puts less stress on the mlc-pneumatics. We analyzed the difference in results of our measurements before and after we started using individually optimized plan specific pitch values.

reported plans with gamma pass rate under 90%. Mann-Whitney test indicate that we have a significant increase of gamma pass rate (DTA=2mm, DD=3%, global dose) after plan specific pitch values (Mdn=98.2%) then before plan specific pitch values (Mdn=96.6%) was introduced at our clinic, p=0.01.

TABLE 1: MEASURED GAMMA PASS RATE BEFORE AND AFTER INTRODUCTION OF PLAN SPECIFIC PITCH VALUES. DTA=2MM DD=3%.

	pre PSPV		post PSPV	
	Value	Cl _{.95}	Value	Cl _{.95}
NUMBER OF PLANS MEASURED	581		92	
FRACTION <u>100%</u> PASSRATE	0.04	.05-.02	0.13	.21-.06
FRACTION < <u>90%</u> PASSRATE	0.07	.09-.05	0.00	.01-.00
FRACTION ><u>95%</u> PASSRATE	0.66	.70-.62	0.82	.90-.73

Authors

André Haraldsson, Anna Karlsson Hauer, Lee Ambolt and Dr Per Engström

References

Chen M, Chen Y, Chen Q, et al. Theoretical analysis of the thread effect in helical Tomotherapy. Med Phys. 2011;38:5945–5960.



Some of the many involved in the installation and clinical use of the Radixact at Skåne university hospital in Lund. Standing left to right: Malin Spoelstra, Annika Jacobsson, Marie Rosén, Per E. Engström, Jenny Gorgisyan, Andreas Tofth, Hunor Benedek, Jacob Snäll. Sitting, from left: Marika Enmark, Anneli Edvardsson, André Haraldsson (author).

Helical tomotherapy for total marrow and total skin irradiation

Radiotherapy is a cornerstone in modern cancer therapy. Today, complicated treatments with intensity-modulated steep dose gradients increase the requirement to control uncertainties in planning and delivery. A TomoTherapy device (Accuray Inc., Madison, WI, USA) has a linear accelerator mounted on a slip-ring construction, giving it the ability to irradiate while continuously rotating around the patient. Since helical delivery with a TomoTherapy can entail long, complicated treatments, new radiotherapy treatment types targeting large parts of the body have emerged. Recurring blood cancers can be treated with radiotherapy and chemotherapy before hematopoietic stem-cell transplantation (HSCT). Lately, helical tomotherapy has been used to create targeted radiotherapy before stem cell transplantation for such disease, with reduced dose to organs at risk compared to the standard technique. In addition, helical tomotherapy of whole-body neoplastic skin lesions, such as mycosis fungoides, is an emerging technique. Delivering these treatments with intensity-modulated radiotherapy is complex but opens new possibilities. In this work, we demonstrated the implementation of such techniques and followed up on the outcome. Compared to previous technique, patients treated with helical tomotherapy as part of HSCT was found to have a significantly higher survival without severe complications at one-year follow-up.

